Dissertation zur Erlangung des Doktorgrades
der Fakultät für Chemie und Pharmazie
der Ludwig-Maximilians-Universität München

Development of bifunctional cancer-targeting antibody constructs for the local blockade of CD47/SIRPα immune checkpoint in acute myeloid leukemia and neuroblastoma

Siret Tahk (geb. Somarokov)
aus
Saku, Estland
2021

Erklärung

Diese Dissertation wurde im Sinne von § 7 der Promotionsordnung vom 28. November 2011 von Herrn Prof. Dr. Karl-Peter Hopfner betreut.

Eidesstattliche Versicherung

Diese Dissertation wurde eigenständig und ohne unerlaubte Hilfe erarbeitet.

München, den 17.02.2021

……..

Siret Tahk

Dissertation eingereicht am 22.02.21

1. Gutachter: Prof. Dr. rer. nat. Karl-Peter Hopfner

2. Gutachter: Prof. Dr. med. Marion Subklewe

Mündliche Prüfung am 15.04.21

This thesis has been prepared from September 2016 to February 2021 in the laboratory of Professor Dr. Karl-Peter Hopfner at the Gene Center of the Ludwig-Maximilians-Universität München.

Parts of this thesis have been submitted for publication:

Tahk S, Vick B, Schmitt S, Reischer A, Humpe A, Jeremias I, Subklewe M, Fenn NC, Hopfner K-P. Targeting CD123 in conjunction with CD47 blockade for enhanced clearance of AML-initiating cells by SIRPα-αCD123 fusion antibodies. *Submitted to Leukemia*.

Parts of this thesis have been presented at international conferences:

Tahk S, Schmitt S, Augsberger C, Vick B, Pascual Ponce L, Jeremias I, Subklewe M, Fenn NC, Hopfner K-P. Evaluation of the bifunctional SIRPα-anti-CD123 fusion antibody for the elimination of acute myeloid leukemia stem cells.
Progress and Challenges in Cancer Immune Therapy, European Training Network Immutrain, Spanish National Cancer Research Centre, July 23-26, 2019. Madrid, Spain.

Tahk S, Schmitt S, Augsberger C, Vick B, Pascual Ponce L, Jeremias I, Wittmann G, Fenn NC, Subklewe M, Hopfner K-P. Evaluation of a Bifunctional Sirpα-CD123 Fusion Antibody for the Elimination of Acute Myeloid Leukemia Stem Cells.
61st American Society of Hematology Annual Meeting & Exposition (ASH 2019). December 7-10, 2019. Orlando, FL, US.

Tahk S, Schmitt S, Vick B, Augsberger C, Pascual Ponce L, Jeremias I, Wittmann G, Subklewe M, Fenn NC, Hopfner K-P. Bifunctional SIRPα-CD123 fusion antibody for the elimination of acute myeloid leukemia stem cells
7th Immunotherapy of Cancer Conference (ITOC), October 2-3, 2020. Munich, Germany.

Table of contents

Summary 1
1. Introduction 3
1.1. Basic principles of the human immune system 3
1.2. Immune system in cancer 3
1.2.1. Immunosurveillance 3
1.2.2. Immune editing and escape 4
1.3. Cancer immunotherapy 6
1.3.1. Monoclonal antibodies 6
1.3.2. Success with CTLA4 and PD1/PDL1 blockade 9
1.4. The myeloid specific CD47/SIRPα checkpoint 11
1.4.1. General information about the CD47/SIRPα axis 11
1.4.2. Therapeutic targeting of the CD47/SIRPα axis 12
1.5. Acute myeloid leukemia 16
1.5.1. AML pathogenesis 16
1.5.2. Current therapy for AML 16
1.5.3. Leukemic stem cells 17
1.6. Neuroblastoma 18
2. Objectives 20
3. Materials and Methods 21
3.1. Generation of the bifunctional antibodies 21
3.1.1. αCD123 antibody constructs 21
3.1.2. CD123 extracellular domain construct 21
3.1.3. αGD2 antibody constructs 21
3.1.4. Generation of the plasmids 23
3.1.5. Protein purification using Expi293F cell expression system 24
3.2. Cell culture methods 26
3.2.1. Cultivation of cell lines 26
3.2.2. Healthy donor and AML patient-derived material 27
3.2.3. AML patient-derived xenograft material 28

3.2.4. Isolation of murine cells....29
3.3. Binding and interaction analysis....29
3.3.1. Flow cytometry....29
3.3.2. Detection of cell surface antigen expression....29
3.3.3. Quantification of cell surface antigen expression....30
3.3.4. Flow cytometry-based antibody binding....31
3.3.5. *K*D determination by surface plasmon resonance....31
3.3.6. K_D determination by flow cytometry....31
3.3.7. Competitive binding assay with RBCs....31
3.3.8. Hemagglutination assays....32
3.3.9. CD47-blocking assays....32
3.4. Functional *in vitro* assays....33
3.4.1. Antibody-dependent cellular phagocytosis of human cell lines....33
3.4.2. Antibody-dependent cellular phagocytosis of allogenic and autologous primary AML cells....33
3.4.3. Antibody-dependent cellular phagocytosis by mouse bone marrow-derived macrophages....34
3.4.4. NK cell-mediated antibody-dependent cellular cytotoxicity of leukemia cell lines 34
3.4.5. ADCC with AML PDX cells....35
3.5. *In vivo* engraftment studies....35
3.5.1. Study design....35
3.5.2. *Ex vivo* ADCC and engraftment....36
3.5.3. Evaluation of the results....36
3.6. Data plotting and statistical analysis....36
4. Results....37
4.1. SIRPα-αCD123 fusion antibodies targeting AML....37
4.1.1. Generation and purification of the SIRPα-αCD123 fusion antibodies....37
4.1.2. Binding of SIRPα-αCD123 fusion antibodies....38
4.1.3. Functional characterization of SIRPα-αCD123 fusion antibodies....42
4.2. αGD2-SIRPα fusion antibodies targeting neuroblastoma....54

4.2.1. Generation and purification of αGD2-SIRPα fusion antibodies 54
4.2.2. Binding of -SIRPα fusion antibodies to mouse and human cells 56
4.2.3. Functional characterization of αGD2-SIRPα fusion antibodies 60
5. Discussion 64
5.1. Rationale for the bifunctional SIRPα-antibody fusion molecules 64
5.2. SIRPα-antibody fusion constructs target AML and NBS but spare healthy cells 64
5.3. SIRPα-antibody fusion constructs enhance the elimination of cancer cells 65
5.4. SIRPα-αCD123 fusion antibodies specifically target LSCs 67
5.5. GD2-SIRPα fusion antibodies developed for the mouse NBS model 68
5.6. Advantages and limitations of the SIRPα-antibody fusion molecules 69
5.7. Future perspectives 72
6. References 74
7. List of Abbreviations 94
8. Acknowledgements 100

Summary

The importance of immune system's role in controlling or stimulating the progression of malignant diseases is well established. Cancer cells often take advantage of the natural pathways that dampen the immune response, such as immune checkpoints, to escape from immune surveillance. In recent years, the field of immuno-oncology has been revolutionized by utilizing blocking antibodies which target immune checkpoints programmed death-1 (PD1) and CTL associated protein 4 (CTLA4) and restore the antitumor immune response. Among others, the myeloid-specific cluster of differentiation 47 (CD47) and signal regulatory protein alpha (SIRPα) axis has emerged as a new therapeutic target in cancer immunotherapy. CD47 is expressed ubiquitously as a "don't eat me" signal, which negatively regulates clearance of cells by interacting with the SIRPα receptor on phagocytes. Activation of the immune system by blocking CD47 has shown encouraging results, but the ubiquitous expression of CD47 on healthy cells proposes potential limitations for such therapies.

Here, the targeted blockade of CD47 is tackled for acute myeloid leukemia (AML) and neuroblastoma (NBS). A considerable subset of people suffering from these diseases do not benefit from current treatments, highlighting the urgent need for novel therapies. Latest advances in the treatment of high-risk AML and NBS patients indicate that activating macrophages could improve the prognosis. The present work establishes bifunctional fusion antibodies that locally block the CD47/SIRPα checkpoint and boost the macrophage-mediated cancer clearance. The bifunctional fusion antibodies consist of an AML targeting αCD123 or NBS specific αGD2 antibody fused with the endogenous SIRPα domain. This format takes advantage of the naturally occurring weak binding of SIRPα, which is not efficient in targeting CD47 by itself. Thus, the CD47 blockade by the SIRPα-antibody fusion molecules relies on the cancer specific antibody moiety.

In AML, two versions of the fusion antibodies, 1×SIRPα-αCD123 and 2×SIRPα-αCD123, are investigated. A strong binding to cancer cells is observed for both of the SIRPα-αCD123 antibodies even in the abundance of CD47 positive healthy cells. The molecules effectively block CD47 and enhance phagocytosis of AML cell line MOLM-13. Moreover, SIRPα-αCD123 antibodies are potent stimulators of primary patient derived AML cell phagocytosis mediated by allogeneic and autologous macrophages. The fusion antibodies further induce high natural killer cell-mediated lysis of AML blasts. Importantly, the 2×SIRPα-αCD123 induces an extreme reduction of leukemic stem cells (LSC), which are the main cause for AML relapse. Collectively, the results establish the SIRPα-αCD123 antibodies as a promising approach for AML therapy as they minimize the risk of targeting healthy cells while efficiently eliminating AML LSCs.

Two conformations of fusion antibodies are evaluated for NBS, SIRPα-αGD2 and αGD2-SIRPα. Both molecules are generated for human and mouse. Although, species-specific

differences are observed for SIRPα domain binding, the αGD2-SIRPα fusion antibody demonstrates specific targeting of cancer cells in both human and mouse setting *in vitro*. αGD2-SIRPα molecules further exhibited a potent NBS cell phagocytosis and are thus proposed as highly promising candidates for future studies, including *in vivo* evaluation of the molecules.

1. Introduction

1.1. Basic principles of the human immune system

The primary role of the immune system is to protect the host against various potentially harmful external agents and endogenous perturbations of homeostasis. It is divided into innate and adaptive responses that are composed of a complex network of cells and soluble factors. The innate immune system includes cells such as macrophages, dendritic cells (DCs), neutrophils and innate lymphoid cells of which the most well-known are natural killer (NK) cells. Germline-encoded pattern recognition receptors are an integral part of the innate immunity [1-3]. They recognize invariant pathogen or damage-associated molecular patterns as danger signals to discriminate between self and non-self [2, 4, 5]. On the other hand, the adaptive immune system comprised of T and B lymphocytes can distinguish between a vast number of unique antigenic determinants through somatically diversified receptors and forms a highly effective immunological memory [6-8]. Synergy between the innate and adaptive immunity is essential for an intact, fully effective immune response. The innate immune system, namely macrophages and DCs, sense danger signals and acquire antigens to present them to T lymphocytes via the major histocompatibility complex (MHC) molecules to initiate the adaptive immune response [9]. Only properly stimulated T lymphocytes that have recognized the presented antigen by specific T cell receptors (TCRs) can acquire effector functions. Cluster of differentiation 8 (CD8) expressing cytotoxic T lymphocytes (CTL) kill antigen-expressing cells and CD4 positive T helper cells orchestrate humoral responses through B cells or modify the behavior of other cells like macrophages and neutrophils [9, 10]. Antibodies produced by B cells in turn opsonize invaders for macrophage-mediated antibody dependent cellular phagocytosis (ADCP) or NK cell-mediated antibody dependent cellular cytotoxicity (ADCC) via activation of receptors sensing the antibody's fragment crystallizable (Fc) domain. Macrophages also act as effector cells by inducing antimicrobial responses and both macrophages and NK cells recognize signals that represent missing-self and can mount a phagocytic and/or cytotoxic response, respectively [5, 11, 12]. Coordination of interactions between tissues, cells and soluble factors within the immune system is highly complex. Insights into the regulation of the immune system in health and disease have paved the way for developing new therapeutic interventions for conditions that are highly influenced by the immune system, such as cancer.

1.2. Immune system in cancer

1.2.1. Immunosurveillance

Cancer progression is a multistep process where genome instability, mutations and tumor-promoting inflammation enable the abnormal growth of tumor cells [13]. Already in the early 1900s Paul Ehrlich reasoned that cancer would be quite common in long-lived organisms if not

for the protective effects of immunity [14]. In 1960s, Macfarlane Burnet and Lewis Thomas further formulated the "cancer immunosurveillance" hypothesis suggesting that the immune system must be able to eliminate the majority of newly arising potentially dangerous mutant cells before clinically detectable cancers arise [15-19]. Nevertheless, it took years until experimental and clinical evidence confirmed the existence of cancer immunosurveillance [19]. In addition to fundamental insights derived from mouse studies, the hypothesis was further supported by observations that people with immune deficits have higher probability of developing cancer [20-23]. It was also noted that an increased number of lymphocytes within the tumor correlated with higher patient survival confirming their role in tumor progression control [24-33].

Both the innate and adaptive arms of the immune system participate in cancer immunosurveillance [19]. In early phases of the tumor progression, transformed cells are recognized by NK cells that detect the aberrant expression of surface proteins such as MHC class I chain-related protein A and B (MICA/B) [34, 35] or sense the loss of MHC class I as a signal of missing self [36, 37]. Activation of CTL relies on the expression of cancer specific immunogenic peptides, called neoantigens, induced by intrinsic genetic damage [38, 39]. Antigen presenting cells (APCs) take up debris from dying cancer cells and present the neoantigens to T cells through the MHC class I or MHC class II [40]. Importantly, APCs must also provide an additional co-stimulation that specifies immunity for a successful activation of T cells. It is proposed that the signals leading to the expression of co-stimulatory molecules on DCs, such as CD80/CD86, could be proinflammatory cytokines or factors released by dying tumor cells or by the gut microbiota [41]. When activated, CTLs can recognize the neoantigen - MHC class I complex via the TCR and subsequently kill the cancerous cell [41]. Tumor infiltrating lymphocytes additionally produce interferon-gamma (IFNγ) [42] which stimulates macrophages to induce cancer cell death [43-45]. Nevertheless, cancer cells exploit several mechanisms to overcome immune surveillance and thereby clinically detectable tumors can ultimately arise [19].

1.2.2. Immune editing and escape

The ability to survive an immune attack has been recognized as one of the major hallmarks of cancer [13]. Cancer cells do not just persist under immune surveillance but variants that are better suited to thrive are selected. This process is called immune editing and, eventually leads to immune escape of cancerous cells [19].

The traits that malignant cells acquire to escape from the immune system are various. For example, malignant cells downregulate their expression of MHC class I molecules to escape from CTL-mediated clearance [46-51]. Although NK cells specifically recognize the missing MHC class I molecules, cancer cells also evade recognition by modulating the expression of ligands to deactivate NK cells [52, 53]. Moreover, malignant cells tune the tumor

microenvironment by secreting immunosuppressive molecules, such as indoleamine 2,3-dioxygenase (IDO) which catabolizes tryptophan and suppresses T and NK cell functions [54-56].

Inhibitory immune cells, such as myeloid-derived suppressor cells (MDSC) and regulatory T cells (Treg), further contribute to the tumor permissive immune environment. MDSC are tumor-programmed immature myeloid cells that can suppress anticancer T cell activity by controlling the availability of arginine, which is needed for effector T cell proliferation, and promote Tregs [57, 58]. Tregs are crucial for maintenance of self-tolerance and control of inflammatory responses under normal circumstances [59]. In the tumor microenvironment Tregs suppress effector T cell functions through sequestering interleukin 2 (IL2), secreting immunosuppressive cytokines and constitutively expressing CTL associated protein 4 (CTLA4) [60]. The latter has been shown to participate in the Treg dependent downregulation of the co-stimulatory CD80/CD86 molecules on APCs which in turn leads to decreased CD28-mediated activation of CTLs [61].

Besides MDSC accumulation, tumors also promote tolerogenic environment by inducing tumor-associated macrophages (TAMs). Macrophages have the potential to attack and eliminate tumor cells, but TAMs exhibit many protumor roles that interfere with the function and proliferation of immune effector cells [62]. TAMs can have many phenotypes that fall along a continuum between tumor killing (M1) or tumor promoting (M2) subtypes. The M1 macrophages are functionally pro-inflammatory and cytotoxic whereas M2 macrophages act preferentially in anti-inflammatory responses and tissue repair [62]. The protumor TAMs suppress T cell activity by depleting of arginine in the tumor microenvironment [62]. TAMs, among other cells, express the ligands of the inhibitory receptors programmed cell death protein 1 (PD1) and CTLA4, leading to a negative regulation of NK cells and CTLs [62].

PD1 receptor is mostly known as an inhibitory receptor expressed on activated T cells [63]. PD1 interacts with its ligands PDL1 and PDL2 to prevent overreaction of the immune response and is thus called “immune checkpoint”. Cancer cells take advantage of this checkpoint and upregulate PDL1 and PDL2 to negatively regulate T cell function, promote their exhaustion and escape from immune recognition [64-66]. Furthermore, PDL1 is expressed on TAMs and DCs where it negatively regulates the immunosuppressive properties of tumor-specific T cells [67-69]. PD1 likewise does not only control the function of T cells but also negatively regulates the anticancer response of the innate immune system, such as macrophages, NK cells and group 2 innate lymphoid cells [70-72].

Another inhibitory checkpoint molecule expressed on tumor cells is the CD47 “don’t eat me” signal [73-76]. CD47 negatively regulates phagocytosis by interacting with the signal regulatory protein alpha (SIRPα) receptor on monocytes, macrophages and DCs [11, 73, 74]. These phagocytes function as APCs that present antigens from engulfed cells and thus, CD47

overexpression compromises the activation of both innate and adaptive antitumor immunity [77-79].

1.3. Cancer immunotherapy

The goal of cancer immunotherapy is to overcome the tumor induced evasion by (re)activating the immunity against cancer. In 1893, William Coley, a pioneer in the field of cancer immunotherapy, observed a regression of inoperable tumors after a bacterial infection and thereafter treated his patients by boosting their immune system with "Coley's toxin" [80]. Although this method was set aside when radiation therapy gained popularity, significant advances have later been made and cancer immunotherapy is now established as a fifth modality in cancer treatment besides surgery, radiation, chemotherapy and targeted therapies. The important role of the immune system in cancer treatment is illustrated by the fact that the efficacy of some chemotherapeutic drugs and radiotherapy depends at least in part on the immune response stimulated by the immunogenic death of cancer cells and does not only rely on the direct cytostatic/cytotoxic effects [81-83]. In the last decades, several novel strategies aiming to enhance the anticancer immune response have been developed, such as adoptive T cell therapy, monoclonal antibodies, cancer vaccines and immune system modulators. From these, monoclonal antibodies targeting the CTLA4 and PD1/PDL1 immune checkpoints have led the revolution of the immuno-oncology field [84-86].

1.3.1. Monoclonal antibodies

Antibodies, also called immunoglobulins (Ig), are proteins that are secreted by plasma cells as a part of the natural adaptive immune response. Plasma cells are terminally differentiated B cells that have recognized their cognate antigen and stimulated by T helper cells [87]. Antibodies are relatively large proteins composed of light and heavy chains that are connected by disulfide bonds [88]. The light (L) chain consists of one variable (V) and one constant (C) domain, whereas the heavy (H) chain has one V and several C domains (Figure 1) [87]. VH and VL domains determine the antigen to which the antibody is binding [89] and the heavy chain C regions establish the isotype of the immunoglobulin [87]. There are five main isotypes of different effector functions – IgA, IgD, IgE, IgG, IgM and two types of light chains called kappa (κ) and lambda (λ) [87]. Antibodies have been historically characterized based on the structural regions after treatment with the protease papain [90]. Upon cleavage of the IgG antibody by papain two fragments are formed. The antigen-binding fragment (Fab) contains VL-CL and VH-CH1 domains and the Fc contains the CH2-CH3 domains and binds to Fc receptors on effector cells (Figure 1).

The 12 domains of the IgG molecule are folded to a distinct structure called the immunoglobulin-fold (Ig-fold, Figure 1A). In this structure, antiparallel β-strands connected with flexible loops form two layers of β-sheets that are linked by a disulfide bond [87]. The

flexible loops of the outer edges of the V domains form the hypervariable antigen-binding site [87]. Each V domain has three hypervariable sequences that form a surface complementary to the antigen and are termed the complementarity-determining regions (CDRs) [87]. Both the CDRs from VH and VL domains contribute to the antigen-binding site and determine the final specificity [87, 89].

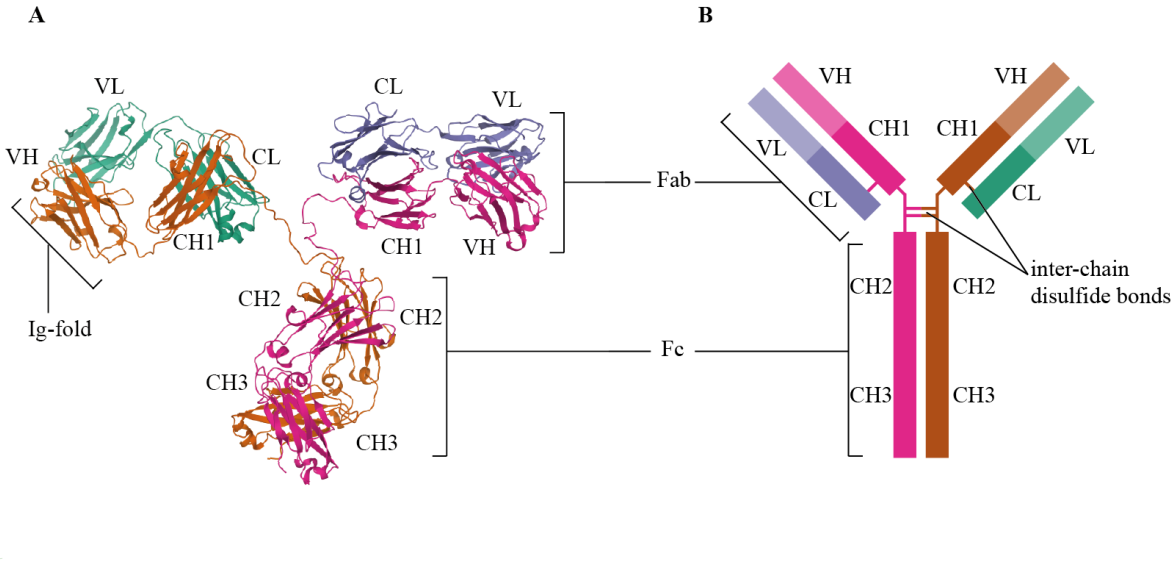

Figure 1. Crystal structure and schematic representation of an IgG antibody. (A) Crystal structure of an IgG1 monoclonal antibody (PDB 1IGT). Each domain in the antibody consist of a distinct Ig-fold structure. (B) Schematic representation of the antibody. IgG antibodies consist of two heavy (H) chains (pink and brown) and two light (L) chains (purple and green) stabilized by inter-chain disulfide bonds. Both light and heavy chain have a variable (V) region at the N-terminus followed by constant (C) domain(s). Antibodies can be further divided into antigen-binding fragment (Fab) and fragment crystallizable (Fc) regions.

The IgG isotype is the most prevalent antibody in the serum [87]. Human IgGs are further subdivided into four classes (IgG1, IgG2, IgG3, and IgG4) that have different binding affinities to activating and inhibiting Fc gamma receptors (FcγRs) or to the neonatal Fc receptor (FcnR) regulating antibody half-life [91, 92] (Table 1). There are four activating receptors (FcγRI/CD64, FcγRIIA/CD32A, FcγRIIC/CD32C, FcγRIIIA/CD16A) and one inhibitory receptor (FcγRIIB/CD32B). Activating FcγRs need the immunoreceptor tyrosine-based activation motifs (ITAMs) while the inhibitory FcγRIIB carries the immunoreceptor tyrosine-based inhibition motif (ITIM) that negatively regulates the effector functions [93, 94]. Antibody bound immune complexes stimulate tyrosine phosphorylation of FcγRs ITAMs by the Src family kinases leading to the activation of various downstream targets [95]. All IgG antibodies, except the IgG4, can also initiate the classical activation pathway of the complement when bound by the antigen to aid phagocytosis or to directly destroy pathogens [87].

Table 1. Affinity constants (K_A) for human IgG subclass binding to human FcγRs ($\times 10^5\ M^{-1}$). Adapted from Bruhns et al 2012.

Receptor	FcγRI	FcγRIIA*		FcγRIIB/C	FcγRIIC**	FcγRIIIA*	
		H131	R131			V158	F158
Function	Activation	Activation		Inhibition	Activation	Activation	
IgG1	650	52	35	1.2	1.2	2	11.7
IgG2		4.5	1.0	0.2	0.2	0.7	0.3
IgG3	610	8.9	9.1	1.7	1.7	98	77
IgG4	340	1.7	2.1	2.0	2.0	2.5	2.0

High-affinity binding is represented in pink. * For FcγRIIA variants H_{131}/R_{131} and FcγRIIIA variants F_{158}/V_{158} the mutation is in the extracellular domain of the receptor [91]. ** expressed in Fcgr2c-ORF persons [91].

1.3.1.1. IgG1 functions

IgG1 molecules can recruit the innate immune effectors such as NK cells, macrophages or DCs by the activating human FcγRs. NK cells express the FcγRIIIA that activate ADCC via release of cytolytic granules containing perforin and granzymes at the immunological synapse [96]. Macrophages are professional phagocytes that express activating receptors FcγRI, FcγRIIA and FcγRIIIA. These receptors can facilitate ADCP by engulfing the immune complex via remodeling of the actin cytoskeleton and subsequent degradation of the material in lysosomal compartments [91, 97]. Tumor cell clearance by therapeutic antibodies can be facilitated by TAMs via both ADCC or ADCP [98]. Macrophage-mediated and FcγR-dependent ADCP can also be the prominent mechanism for removal of tumor cells from the circulation and preventing metastatic dissemination [99]. DCs also participate in the uptake of antibody opsonized material through FcγRI and FcγRIIA which can lead to cross-presentation of cancer-derived peptides to CTLs through MHC class I molecules stimulating their anticancer effector functions [91, 100].

Due to their ability to induce effector functions, IgG antibodies have been generated for decades to be used as therapeutic approaches. In 1975, Milstein and Köhler produced hybrid cells termed hybridomas by fusing cells from an immunized mouse spleen with mouse myeloma cells [101]. These immortal cells could be used to produce predefined specific monoclonal antibodies (mAbs) from a single B cell clone in high quantities. The early clinical trials with murine anticancer mAbs were nevertheless disappointing as they yielded low IgG-mediated cellular effector responses [102]. The main reasons for this were immunogenicity, short half-life and depressed immune-mediated effector functions of murine mAbs in humans [103]. The use of chimeric, humanized or fully human mAbs has helped to overcome these limitations [102, 103]. Chimeric antibodies consist of a murine variable region fused to constant domains of a human antibody backbone while humanized antibodies contain the murine sequence only in CDRs that actually interact with the antigenic target [102]. The

majority of the antibodies currently used in anticancer therapy contain the human IgG1 heavy chain [102, 104]. Importantly, the therapeutic mAb-mediated activation of immune system via ADCP or ADCC is clinically validated to be an important component of the antitumor activity [105-109].

The ability to specifically target various surface antigens has warranted for the use of mAbs in various applications in addition to the FcγR-mediated mechanisms. For example, the IgG-mediated complement activation has been shown to play at least a partial role in the anticancer effect of the CD20-targeting antibody rituximab [110]. Some mAbs are directly blocking membrane receptors to inhibit tumor cells from receiving activation signals and many are used as carriers of toxins and radioactive elements providing a much more selective therapy than conventional chemo- or radiotherapy [109]. MAbs can also enhance the antitumor immune responses by directly targeting the immune cells. The most well-known are the CTLA-4 and PD1 mAbs that block T cell negative signaling and promote their effector functions [109].

MAbs are one of the fastest growing drug class to date and more than 60 antibody drugs are approved for clinical use, of which over half are for cancer therapy [104, 111]. Although mAbs have provided beneficial effects to date, novel antibody constructs are an area of great research to improve and broaden the effector functions. Recombinant DNA technology has enabled to move on from hybridomas to mammalian cell expression systems for the production of mAbs. This provides the possibility to produce humanized, bispecific antibodies and various other antibody-derivatives for therapeutic purposes.

1.3.2. Success with CTLA4 and PD1/PDL1 blockade

Both CTLA4 and PD1/PDL1 pathways act as immune checkpoints that limit the activity of self-reactive T cells. Unfortunately, this translates into a suppressed immune response within the tumor microenvironment [86]. Five blocking mAbs targeting PD1 (nivolumab, pembrolizumab, cemiplimab, sintilimab, toripalimab, camrelizumab), three targeting PDL1 (atezolizumab, avelumab, durvalumab) and one targeting CTLA4 (ipilimumab) are currently approved in clinics [112, 113]. These antibodies have provided substantial survival benefit with durable responses in many different tumor settings and have fundamentally changed cancer treatment [114-116].

CTLA4 is a negative regulator of T cells that have engaged their cognate antigen via TCR. When anti-CTLA4 mAbs bind to the receptor, they block its interaction with the CD80/CD86 on APCs which allows for the activating T cell receptor CD28 to bind CD80/CD86 instead [117, 118]. The exact mechanism of CTLA4-targeting antibodies is nevertheless under debate [119]. Recent evidence proposes an alternative mode of action where engagement of FcγRs contribute to the antitumor effects of anti-CTLA4 [120, 121]. Depletion of Tregs via ADCC or

ADCP has been suggested as some of the FcγR dependent mechanisms that contribute to the clinical effect of CTLA4-targeting antibodies [119, 122].

PD1 is best known for attenuating the activated T cell effector functions in the periphery through interacting with PDL1 and PDL2 on target cells or APCs [63, 65, 66]. PD1/PDL1-blocking antibodies disrupt the negative signaling through PD1 on T cells, revert their exhausted state and allow them to attack cancer cells [66, 123]. Recent studies have shown that the mechanism behind PD1/PDL1 blockade may, however, be more complex. PDL1 on APCs might play bigger role in regulating the antitumor T cell responses than previously thought [124, 125]. In addition to preventing T cell exhaustion, PD1/PDL1 axis blockade boosts APC-mediated T cell priming and expansion [126]. Furthermore, direct regulation of PD1 signaling on myeloid cells might be crucial for the success of anti-PD1 therapy. PD1 expression on macrophages inhibits phagocytosis and limits tumor control [72]. Preclinical data also indicates that PD1 blockade on myeloid cells induces a shift from immature MDSCs towards differentiated monocytes, macrophages and DCs that orchestrate an enchased T cell response against tumors [127].

As CTLA4 and PD1/PDL1 are crucial regulators of the immune system it is not surprising that blocking their function systemically causes serious immune-related adverse events that mostly manifest as autoimmune toxicities against self-tissues [112, 128]. New therapeutics that restrict the checkpoint blockade to the tumor site instead of systemic application have been proposed to tackle this issue [129]. It was recently reported that PD1/PDL1 blockade might play a more deceive role in the tumor draining lymph nodes than in the tumor [130] and corresponding therapeutic antibody formats could thereby provide more efficient and safer strategies in the future.

Still, anti-CTLA4 and anti-PD1/PDL1 have undoubtedly changed the field of immuno-oncology by inducing durable responses even in advanced cancer cases [84-86]. New strategies for cancer treatment are nevertheless sought as only a minority of people currently respond to the established immune checkpoint blockade therapy and a considerable population of patients suffers from dangerous adverse events [112, 131]. Big part of cancer immunotherapy has been focusing on enhancing T cell functions but innate cells, such as DCs, macrophages and NK cells, likewise play a key role in cancer immune surveillance. This is illustrated by the fact that the most successful immunotherapy in clinics to date, the PD1/PDL1 blockade, does not only directly regulate T cells but also the myeloid compartment. New therapies and combinations that take advantage of the full scope of the immune response and broaden the responsive patient subset are clearly needed.

1.4. The myeloid specific CD47/SIRPα checkpoint

1.4.1. General information about the CD47/SIRPα axis

CD47/SIRPα has emerged as a myeloid-specific axis that negatively regulates phagocytic clearance of cells. CD47 is a transmembrane protein composed of an extracellular N-terminal Ig V-like domain, five transmembrane domains and a carboxy-terminal cytoplasmic tail [132]. It is ubiquitously expressed across different cell types in the body [133]. CD47 was first described to activate and associate with certain integrins and was thus called integrin-associated protein (IAP) [134]. Later, it was demonstrated that the extracellular domain of CD47 interacts with other molecules such as thrombospondin-1 and, importantly, negatively regulates macrophage-mediated engulfment of cells through SIRPα receptor signaling [11, 135]. Modulation of CD47 expression has been subsequently shown to regulate the homeostasis of red blood cells (RBCs), platelets and hematopoietic stem cells (HSCs), among others [73, 74, 135, 136]. CD47 also seems to regulate anti-viral immune responses. Its analogues can be expressed on some viruses and upregulation of CD47 during viral infection has been demonstrated [79]. CD47 was first cloned from cells of an ovarian tumor and both solid and hematological malignancies exploit the CD47/SIRPα axis as an escape mechanism to avoid surveillance by the innate immune cells [73, 76, 137, 138].

SIRPα, known as CD172a, is an inhibitory member of the SIRP family (Figure 2) [139]. Other members include the activating SIRPβ and SIRPγ that have closely related extracellular regions but distinct cytoplasmic tails [139]. SIRPα and SIRPβ are expressed mainly by myeloid cells whereas SIRPγ is found on T cells and NK cells [140, 141]. The SIRPα ligand CD47 interacts with SIRPγ although the exact role of the interaction is not clear [140]. SIRPα contains one Ig V-like and two Ig C-like domains, a single transmembrane region, and a cytoplasmic region with inhibitory ITIM domain [140]. The recognition of the CD47 “don’t eat me” signal by the V-like domain of SIRPα leads to phosphorylation of ITIMs in the cytoplasmic domain by Src family kinases [139]. This mechanism of regulation is achieved by retaining SIRPα at the Src kinase-rich phagocytic synapse [142]. Phosphorylated SIRPα recruits the phosphatases Src homology region 2 domain-containing phosphatase 1 (SHP1) and SHP2, which dephosphorylate targets upstream of integrin activation and inhibit phagocytosis through mechanisms involving deactivation of myosin IIA [11, 142, 143].

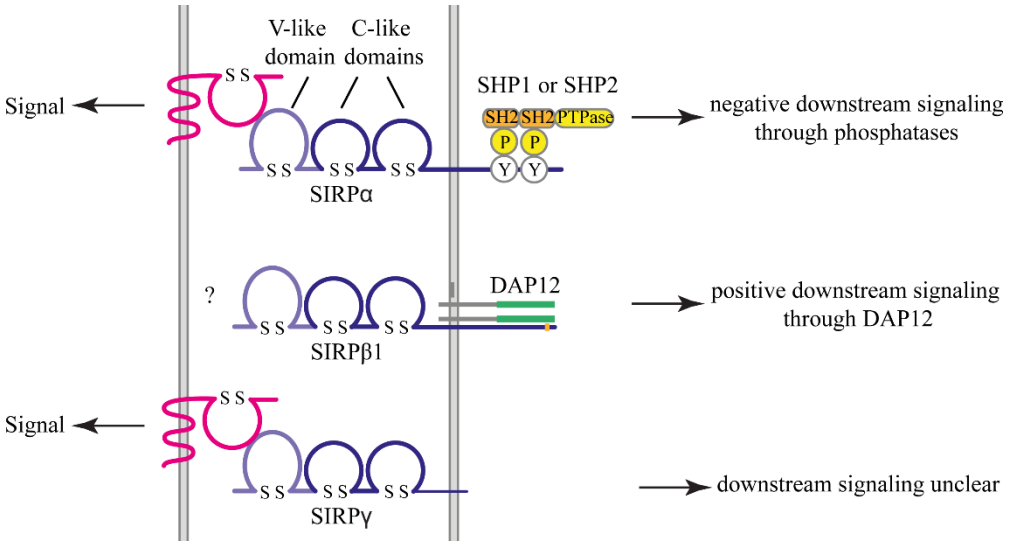

Figure 2. Schematic structures of SIRP family and signaling of SIRPα. SIRPα, SIRPβ1 and SIRPγ have been characterized in humans. The extracellular regions of SIRP receptors consist of one variable (V)-like and two constant (C)-like immunoglobulin (Ig) domains. CD47 is reported as a ligand for SIRPα and SIRPγ. SIRPβ1 ligand has not been identified. CD47 has one Ig-like domain. CD47 binding to SIRPα leads to tyrosine (Y) phosphorylation (P). Phosphorylated SIRPα recruits phosphatases (PTPase) SHP1 and SHP2 via their phosphobinding SH2 domains. Their activation leads to downstream regulation by the PTPase domain. SIRPβ1 signaling is mediated by DAP12. SIRPγ lacks cytoplasmic signaling motifs and the signaling mechanism remains unclear. CD47 does not have a substantial cytoplasmic signaling domain but has been shown to participate in signal transduction [144]. Figure adapted from Matozaki et al 2009.

The interaction of CD47/SIRPα is species-specific [145]. Human and mouse CD47/SIRPα interaction is generally not compatible with the exception of the non-obese diabetic (NOD) strain mice that express a variant of SIRPα that binds to human CD47 with especially high affinity (approximately 7.5 times more than human SIRPα) [146]. This makes the NOD mouse a particularly good host for engraftment of human cells as a strong “don’t eat me” signal is present [146, 147]. Nevertheless, caution must be exercised when using these mice to study the therapeutic effects of CD47/SIRPα interaction as its disruption could have a stronger impact. Cynomolgus monkey CD47 differs from human by 3 amino acids, none of which are present in the CD47/SIRPα interaction interface [148, 149] and they have been used to study effects of axis blockade on healthy cells such as RBCs [149, 150]. Although both mouse and human IgV-like domain of SIRPα is highly polymorphic, there is not much intraspecies variation at the CD47 interaction site [147, 151, 152]. CD47 is essentially nonpolymorphic [152].

1.4.2. Therapeutic targeting of the CD47/SIRPα axis

Cancer cells exploit the CD47/SIRPα axis to avoid surveillance by the innate immune system and the therapeutic targeting of this checkpoint is intensely investigated. Elevated levels of CD47 have been observed in several malignancies including non-Hodgkin lymphoma (NHL),

acute myeloid leukemia (AML), melanoma, glioblastoma in addition to ovarian, breast, colon, bladder, hepatocellular, prostate and small-cell lung cancers [73, 75, 76, 153, 154]. The feasibility of targeting the CD47/SIRPα axis was first verified preclinically using the anti-human CD47 blocking antibody B6H12 which successfully boosted the clearance of tumor cells [73, 75, 76]. These advances led to the development of a first-in-class CD47-blocking antibody magrolimab (Hu5F9-G4) that is currently being evaluated in various clinical trials [150, 155].

The disruption of the CD47/SIRPα axis alone is not enough and pro-phagocytic signals are needed for an efficient phagocytosis of tumor cells (Figure 3) [75, 153, 156-158]. These positive signals can include expression of calreticulin and opsonization of target cells by antibodies or complement components [159, 160]. On the other hand, SIRPα receptor signaling is sufficient to counteract the positive pro-phagocytic signals (Figure 3A) [160]. B6H12 is a murine IgG1 antibody that has limited potential to bind the human activating FcγRIIA and can thus provide some activating signals in addition to CD47 blockade [161]. Accordingly, its Fab domain only blocks CD47 but does not induce tumor cell clearance alone [157, 162]. Magrolimab is a human IgG4 class antibody that can bind FcγRI and, thus, activate macrophages to some degree [91, 92]. Although magrolimab monotherapy has shown some evidence of anticancer activity in AML phase 1 clinical trial, it has not been further developed as a single agent [158, 163, 164]. In contrast, human IgG1 antibodies can engage different types of activating FcγR receptors and are known to be good stimulators of the immune system effector functions [91, 92]. Combining human IgG1 with CD47 blockade can provide a strong positive signal for effector cells and simultaneously remove the inhibiting “don’t eat me” signal (Figure 3C). To achieve this synergy in humans, magrolimab has been combined in clinical trials with the IgG1 class antibodies rituximab, cetuximab and avelumab in addition to the calreticulin-inducing azacitidine, which all provide a strong pro-phagocytic signal [155, 158, 165-167]. The combination of a cancer specific IgG1 and CD47 blockade seems to be highly beneficial at least in some indications. In a phase 1b trial of rituximab and magrolimab combination where 95% of B-cell NHL patients were refractory to rituximab, 50% were reported to reached objective response (OR) and 36% complete response (CR) upon receiving the combination therapy [167]. Synergy between cancer-specific antibodies and CD47 blockade has been also demonstrated by using the recombinantly expressed high affinity SIRPα domain CV1 in preclinical studies [149, 153]. A phase 1 clinical study combining the high affinity SIRPα domain as CD47 blocker (ALX148) in combination with standard anticancer antibodies and chemotherapy is ongoing [168].

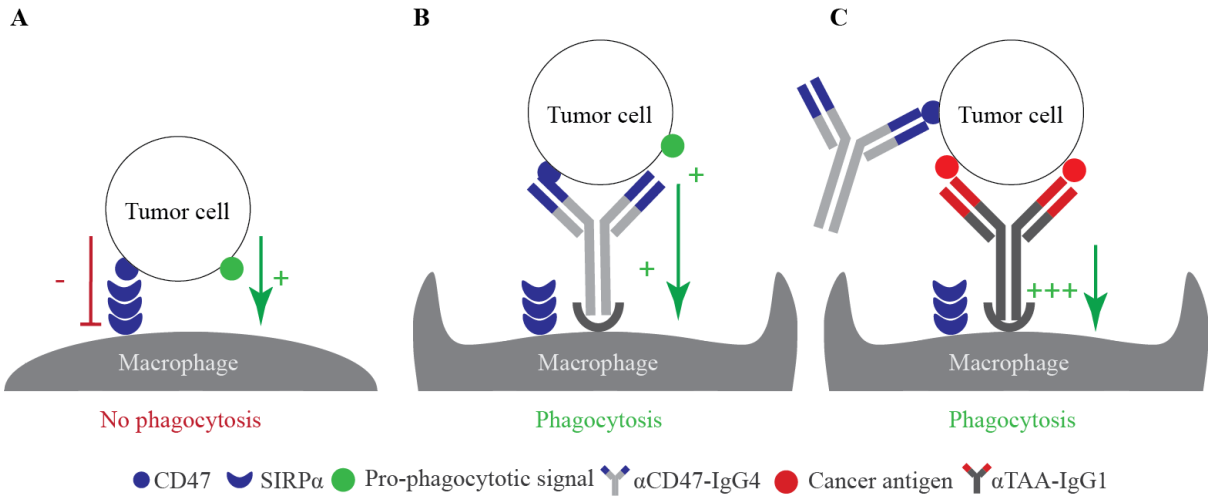

Figure 3. Blocking the inhibitory CD47 signaling boosts phagocytosis. (A) CD47/SIPRα interaction inhibits phagocytosis (-) even in the presence of a pro-phagocytic signal (+). (B) Human IgG4 αCD47 antibodies, such as magrolimab, block CD47 and activate FcγR to some extent but phagocytosis is more efficient in the presence of an additional pro-phagocytic signal, such as calreticulin [160]. (C) Cancer antigen specific human IgG1 antibodies provide a strong FcγR activation and synergize with CD47 blockade despite the lack of an additional pro-phagocytic signal.

Macrophage-mediated phagocytosis is the most extensively studied mechanism of action that promotes effects observed in tumor control upon CD47/SIRPα pathway inhibition. Anti-CD47 treatment has been described to enhance the phagocytosis of tumor cells by both M1 and M2 macrophage subtypes in xenograft mouse models of glioblastoma [169]. Furthermore, anti-CD47 treatment led to a shift towards M1 subtype which also exhibited a higher phagocytosis rate [169]. Besides macrophages, neutrophils express SIRPα and can be stimulated via the CD47/SIRPα blockade to facilitate ADCC [156, 162]. A growing body of evidence further indicates that the adaptive immune system and especially the activation of CTLs contributes to elimination of cancer cells upon CD47 blockade as a result of improved antigen presentation by APCs [77, 78, 170]. Macrophages that phagocytose target cells in the presence of anti-CD47 antibody were shown to enhance the antigen specific T cell-mediated killing of cancer cells [77]. In other studies, DCs, rather than macrophages, were suggested to be the APCs responsible for activating T cells when CD47 on target cells is blocked [78, 137]. The anti-CD47 antibodies were shown to enhance the DC antigen cross-presentation via activation of cyclic GMP-AMP synthase (cGAS) and stimulator of interferon genes (STING) pathway [137, 171]. The preclinical studies therefore clearly indicate that activation of the adaptive immunity by CD47/SIRPα pathway inhibition is expected, but the exact nature of APC activation in humans needs further investigation.

Using high affinity CD47-targeting approaches nevertheless has its drawbacks. As mentioned earlier, blocking CD47 alone should not lead to clearance of tumor cells without a strong pro-phagocytic signal, but RBCs are still readily removed by the splenic pulp macrophages when CD47 is blocked [135]. Correspondingly, unspecific blockade of CD47 has been shown to

cause severe anemia in both preclinical studies with cynomolgus macaques as well as in the phase 1 clinical trials [149, 150, 167]. In addition, the ubiquitously expressed CD47 acts as an antigen sink and lowers the effective dose of the drug [133, 135]. Other on-target off-tumor toxicities beyond RBC targeting are also plausible due to the broad expression and functions of CD47. CD47 activates some intracellular signaling pathways and it has been described to regulate various cellular processes [144]. For example, targeting CD47 has been shown to impair human T cell activation, proliferation, and endothelial transmigration all of which can negatively impact tumor control [172].

Novel protein formats have been developed to focus the disruption of CD47/SIRPα axis selectively on tumor cells. The endogenous extracellular domain of SIRPα binds to CD47 with approximately 100 times lower affinity than the mAbs targeting CD47 [146, 148, 173]. SIRPα domain has been thus utilized as a CD47-blocking moiety to overcome binding to healthy cells expressing low levels of CD47. SIRPα-hIgG1 and hIgG4-derived Fc-fusion proteins TTI-621 and TTI-622 should target only tumor cells with high CD47 expression and are reported not to bind to CD47 on human RBCs [174, 175]. Among others, Ponce et al. developed a more targeted approach by fusing the αCD33 antibody with the SIRPα domain [176, 177]. These antibodies specifically bind to antigen-positive tumor cells but not to RBCs present in high excess [176, 177]. Moreover, the CD33 expressing malignant cells were readily killed by NK cells and, importantly, phagocytosis was boosted [177]. In another study, CD20-targeting constructs were fused with the SIRPα domain leading to a reduced tumor burden and prolonged survival of human cancer-bearing NOD *scid* gamma (NSG) mice [176]. The authors hypothesized this effect was derived from enhanced phagocytosis of malignant cells *in vivo* [176]. Some approaches have combined the CD20, CD19 or mesothelin-targeting antibodies with a low affinity anti-CD47 domain instead of SIRPα to specifically address the antigen-positive cancer cells [173, 178]. Furthermore, two anti-CD47 antibodies named lemzoparlimab and AO-176, which spare RBCs, have been developed to target cancer cells with higher preference [179, 180]. Finally, besides targeting CD47, blocking SIRPα is also being investigated in combination with tumor-opsonizing antibodies [156, 162, 181, 182].

In summary, blocking the CD47/SIRPα axis has great potential to contribute to tumor control by directly stimulating the effector functions of macrophages and activating adaptive immunity through enhancing the role of APCs. Furthermore, novel strategies that confine the site of intervention to the tumor microenvironment can provide an improved tumor control while restraining the side effects to healthy tissues.

1.5. Acute myeloid leukemia

1.5.1. AML pathogenesis

AML is a hematological malignancy characterized by clonal expansion of poorly differentiated myeloid precursors with bone marrow infiltration and impaired hematopoiesis [183]. Clinical symptoms include leukocytosis and signs of bone marrow failure such as anemia and thrombocytopenia [184]. The acquisition of genetic lesions over time leads to leukemic transformation of the preleukemic cells, which arise when HSC clones accumulate somatic DNA mutations long before clinical manifestation of the disease [185, 186]. Next generation sequencing has enabled to realize that AML is a heterogenic disease with several genetically defined subtypes. While some mutations are shared by few subgroups and some co-occur, others are not usually found in the same clone [187, 188]. Some of the most commonly mutated genes in AML include *DNA methyltransferase 3A* (*DNMT3A*), *Wilms' tumor protein* (*WT1*), *isocitrate dehydrogenase 1/2* (*IDH1/2*), and *ten-eleven translocation 2 TET2* and together are observed in ~50% of AML cases while 30% of patients carry mutations in the *FMS-like tyrosine kinase 3* (*FLT3*) or *nucleophosmin 1* (*NPM1*) gene [189-191]. Immunophenotyping the expression of cell-surface markers further provides information about classification of the AML, aids diagnosis and helps to evaluate the expression of therapeutic targets [192].

1.5.2. Current therapy for AML

AML is an aggressive disease. Patients will die within months of diagnosis when left untreated and the average 5-year survival rate of all patients is a mere 24% [193]. AML incidence increases with age with the median age at diagnosis being 68 years based on the Surveillance, Epidemiology, and End Results (SEER) data from 2011-2016 [193]. The standard treatment for AML patients who are medically fit consist of cytotoxic induction chemotherapy with 3 days of anthracycline and 7 days of cytarabine (7+3 regimen) which impair DNA and RNA synthesis [194, 195]. With this intensive treatment, 60% to 80% of younger adults and in 40% to 60% of older adults (60 years or above) reach CR [194]. For patients who achieve remission, the relapse rate is nevertheless approximately 50% [196]. Post remission consolidation strategies such as chemotherapy or allogeneic hematopoietic stem cell transplantation (HSCT) are administered to reduce potential relapses [194]. Patients with advanced age or poor performance status are often not treated with intensive chemotherapy due to concerns regarding treatment-related morbidity and mortality or inherent biologic disease resistance to cytotoxic therapy [194, 197]. For those patients, low-dose cytarabine and the hypomethylating agents (HMAs), such as azacitidine (AZA) and decitabine, have been used [198, 199]. In a phase 3 trial including treatment-naive AML patients who were either elderly or otherwise ineligible to receive intensive chemotherapy, CR was achieved in 17.9% of the patients with AZA alone and in 36.7% of the patients with AZA and venetoclax (VEN) combination [200]. These results are likely to establish AZA+VEN as new standard of care for unfit AML patients [201]. Despite efforts in treatment, AML is still cured in

only 35 to 40% of younger adults and in 5 to 15% of older adults [194]. Since 2017, novel targeted therapies, such as FLT3 inhibitors and chemotherapy delivery via gemtuzumab ozogamycin, an anti-CD33 antibody-drug fusion, have been approved by the United States Food and Drug Administration (FDA) and might provide therapeutic benefit to some AML subgroups [190, 202].

AML, harbor multiple mechanisms to evade the immune system. Several mAbs and cellular therapies are being investigated either alone or in combination with chemotherapies to overcome the immune evasion and harness the full power of the immune system [203]. Interestingly, a number of immune-related genes increase their expression upon exposure to HMAs, including AZA [203]. This has been exploited in several combination studies. PD1 blockade with nivolumab has shown some promising results when used with AZA in AML patients with a relapsed or refractory disease. CR was achieved in 6% of patients and an overall response rate (ORR) of 33% was observed for the combination [204]. When ipilimumab-mediated CTLA4 blockade was added to AZA and nivolumab therapy, CR was 4% and ORR reached 44% [204]. Importantly, CD47 blockade has emerged as a promising novel approach in modulating immune response against AML. The combination of magrolimab and AZA demonstrate a CR of 44% and ORR of 64% in the latest update of the phase 1b trial including previously untreated AML patients unfit for chemotherapy [205]. Patients with a high-risk myelodysplastic syndrome (MDS), a clonal myeloid neoplasm which frequently progresses into AML, established furthermore a CR of 42% and ORR of 91% upon magrolimab and AZA combinatorial treatment [155, 206]. Importantly, CD47 is highly upregulated on leukemic stem cells (LSCs) where it functions as a strong “don't eat me” signal [11, 73, 74].

1.5.3. Leukemic stem cells

The persistence of chemoresistant LSCs is considered as the main reason for AML relapse [207, 208]. In 1990s, AML LSCs were first described by John Dick and co-workers [209, 210]. Besides providing the first empirical evidence of LSCs in patients, these experiments laid the ground for wider cancer stem cells research. LSCs can arise from preleukemic cells derived from HSCs or, alternatively, from cells in later stages of the hematopoietic hierarchy [211-216]. There is evidence that the early mutations acquired by preleukemic cells enhance or provide potential for their self-renewal and impair differentiation [217, 218]. Furthermore, these early mutated clones that carry increased numbers of LSCs can survive chemotherapy leading to restoration and new propagation of the malignancy and ultimately serves as a resource for relapse [207, 219, 220]. LSCs are thereby considered as a major and highly relevant clinical target in AML.

The interleukin-3 receptor alpha chain (IL3Rα, CD123) is an established marker of AML LSCs [221]. CD123 expression is associated with increased proliferation of AML cells and higher CD123 levels correlate with poor prognosis [222-224]. In addition, the majority of AML blasts

also express CD123 [225, 226], while normal HSCs show low or barely detectable levels of CD123 [221, 226, 227]. In 2018, the first drug targeting CD123-positive cells, SL-401 (Elzonris, tagraxofusp), was granted approval by the FDA for the treatment of a rare malignancy called blastic plasmacytoid dendritic cell neoplasm (BPDCN), which has morphologic and molecular similarities to AML and MDS [228]. SL-401 is composed of a recombinant IL-3 fused to a truncated diphtheria toxin [228]. The effect of SL-401 for the treatment of AML is still under investigation [229-231]. Flotetuzumab, a dual-affinity re-targeting (DART) T cell engager with an antibody-based CD123 and CD3ε recruiting domains, represents another advanced CD123-targeting approach [232]. A phase 1/2 study including patients with refractory or relapsed AML, flotetuzumab mediated an ORR of 30% [232].

1.6. Neuroblastoma

Neuroblastoma (NBS) is a solid tumor most frequently discovered in pediatric patients with the median age of diagnosis being 17 months [233]. It is a tumor of the autonomic nervous system which is thought to form from developing and incompletely committed precursor cells derived from neural-crest tissues [234]. The tumors typically arise in the adrenal medulla or paraspinal ganglia [235]. The disease has a heterogeneous clinical presentation ranging from a mass that causes no symptoms to metastatic disease that is refractory to therapy [235]. There has been a tremendous success in the treatment of NBS over the years with the 5-year relative survival increasing from 54% among patients diagnosed between 1975 and 1984 to 80.4% for those diagnosed between 2010 and 2016 [236]. Nevertheless, only a subset of the patients benefits from the advances. Diagnosis is good for the low-risk and intermediate-risk patients with only surgery alone or in combination with chemotherapy [237]. At the same time, 50% of the patients belong to the high-risk group and approximately 50% of them experience a relapse [238]. The treatment for high-risk patients includes induction chemotherapy, surgical resection, radiotherapy, high-dose chemotherapy with autologous hematopoietic stem-cell transplantation and differentiating agent isotretinoin [239]. Importantly, immunotherapy with anti-GD2 mAb dinutuximab has emerged as a novel strategy to improve the outcome for high-risk patients. Dinutuximab combined with granulocyte-macrophage colony stimulating factor (GM-CSF) and IL2 was shown to increase the overall survival (OS) at 2 years from 75.5% to 86% when compared to standard therapy and is now commonly used in maintenance treatment [240, 241].

GD2 has been the primary molecular target in NBS immunotherapy research as all human neuroblastomas are characterized by high levels of GD2 expression [242, 243]. Furthermore, GD2 is a diagnostic marker which can help to discriminate NBS from other related tumors [244]. A limited GD2 expression is observed on normal tissues [245]. GD2 belongs to a group of glycolipids found on the outer cell membrane called gangliosides [246]. The ganglioside is synthesized in a stepwise process of adding glucose, galactose and N-acetylgalactosamine to

ceramide and then linking sialic acids to the galactose [246]. NBS cells are reported to have high levels of GD2 synthase which produces the GD2 from precursor gangliosides GD3/GM3 [247]. Besides being actively overexpressed, GD2 can be shed from tumor cells and both forms of it modulate the function of normal cells in the tumor microenvironment [248, 249]. Importantly, tumor-derived gangliosides suppress immune cell functions [250].

Dinutuximab is a chimeric monoclonal antibody composed of the variable heavy- and light-chain regions of the murine anti-GD2 mAb 14.18 and the constant regions of human IgG1 and is also called as ch14.18 [251]. The effector mechanism of dinutuximab was shown to be granulocyte and NK cell-mediated ADCC [252-254].

TAMs are abundant in NBS [255] and can acquire M1 antitumor or M2 protumor phenotypes [256]. Reprogramming macrophages into an immunostimulatory phenotype has gained attention as a mechanism of improving the efficacy of NBS therapy [257]. The histone deacetylase inhibitor vorinostat, for example, promotes M1 repolarization and shows synergy with anti-GD2 immunotherapy [258]. Blocking the inhibitory CD47 “don’t eat me” signal has been shown to increase the numbers of the antitumor M1 subtype TAMs [169]. NBS patient samples have ubiquitous expression of CD47 [259]. Activation of macrophage-mediated immune response via CD47 blockade could thus have a considerable impact in improving the survival of high-risk NBS patients.

2. Objectives

The aim of this thesis was to generate and preclinically characterize bifunctional fusion antibodies that block the CD47/SIRPα checkpoint locally on cancer cells and mediate their specific elimination. To this end, the endogenous SIRPα domain was fused to antibodies targeting CD123 on AML LSCs or GD2 on NBS, respectively. The physiological interaction of the SIRPα and CD47 is much weaker than the affinity of a mAb for its target [146, 148]. SIRPα-antibody fusion molecules are thereby expected to primarily attach to the surface of cancer cells and subsequently block CD47. The presence of a simultaneous pro-phagocytic signal, such as IgG1 opsonization, is crucial for the therapeutic effect of CD47 blockade [158]. The SIRPα-antibody molecules generated in this study carry the Fc region of the human IgG1 isotype, which provides a strong pro-phagocytic signal [91]. The bifunctional SIRPα-antibodies can thus provide the needed second stimulation in addition to the CD47 blockade. SIRPα-antibody fusion molecules can even further amplify the anticancer immune response as IgG1 antibodies stimulate the activation NK cells [260]. The reduced on-target off-tumor side effects and broad immune cell activation via IgG comprise two of the main objectives of the bifunctional SIRPα-antibody fusion molecules and support the rationale of combining CD47 blockade and FcγR stimulation in one molecule.

In the first part of this study, bifunctional fusion antibodies consisting of αCD123 and endogenous SIRPα domain were generated to confine the CD47 blockade and to specifically target AML LCSs. LSCs are the major cause of AML relapse and new therapies targeting these cells are particularly needed [194, 207, 208]. The novel SIRPα-αCD123 molecules were expressed, purified and biochemically characterized. The biological functionality was evaluated *in vitro* using cell lines and primary AML patient samples. In collaboration with Binje Vick[1], the specific targeting of AML LSCs was finally analyzed by *in vivo* engraftment studies.

The second part of this thesis focused on targeting NBS, a solid pediatric tumor with a high myeloid cell infiltration where high-risk group patients do not benefit from current treatment options [238]. Here, the SIRPα domain was fused to the αGD2 antibodies and both human and mouse formats of the bifunctional antibodies were expressed, purified and biochemically characterized. The biological functionality of the molecules was analyzed *in vitro* using human and mouse cell lines in collaboration with Renske van den Bijgaart[2] to lay the ground for future *in vivo* studies.

[1] Research group of Irmela Jeremias, Helmholtz Zentrum München, Germany
[2] Research group of Gosse Adema, Laboratory of Radiotherapy and Oncoimmunology, Radboud University Medical Centre, Nijmegen, Netherlands.

3. Materials and Methods

Unless otherwise stated, all chemicals were purchased from Carl Roth, Merck or Sigma–Aldrich. All primers were obtained from Metabion. Cell culture media and supplements were obtained from Thermo Fisher Scientific and cell culture supplies from Sarstedt and VWR unless otherwise indicated.

3.1. Generation of the bifunctional antibodies

3.1.1. αCD123 antibody constructs

To generate anti human CD123 antibodies (αCD123), pFUSE-123-LC and pFUSE-123-HC plasmids were constructed using molecular cloning techniques. To this end, the VL and VH sequences of talacotuzumab [261] (Table 2) were inserted into human light chain (LC) and heavy chain (HC) expression plasmids, respectively (Table 2). The LC plasmid pFUSE2-CLIg-hK and the HC plasmid pFUSE-CHIg-hG1 (both InvivoGen) contain the Igκ leader sequence for protein secretion. For 1×SIRPα-αCD123 and 2×SIRPα-αCD123 antibodies, pFUSE-SIRPa-123-LC and pFUSE-SIRPa-SIRPa-123-LC vectors were generated by subcloning the VL and VH sequences of talacotuzumab into previously described constructs that carry one or two N-terminal SIRPα immunoglobulin V-like domains (accession number NP_542970, amino acids 31-149, Table 2) in the N-terminus of the light chain [177]. The SIRPα domain sequence in these plasmids is separated from the antibody light chain and from each other by poly-glycin-serine $(Gly_4Ser)_4$ linkers (Table 2). The αCD19 LC and HC plasmids based on the clone 4G7 were similarly cloned to generate the control molecules.

3.1.2. CD123 extracellular domain construct

The DNA sequence for the CD123 extracellular domain (CD123ex, amino acids 19-307, Table 2) was amplified by PCR from complementary DNA (cDNA) of L428 cells and subcloned into pSecTag2/HygroC containing a His_6-tag plasmid (Thermo Fisher Scientific) for expression. L428 cells were kindly provided by Marion Subklewe[3]. For L428 RNA extraction, TRIzol Reagent (Invitrogen) was used according to manufacturer's instructions. The centrifugation step was carried out with Phase Lock Gel tubes (5Prime). cDNA synthesis was performed with SuperScript III First Strand kit (Invitrogen).

3.1.3. αGD2 antibody constructs

For the human αGD2 antibody plasmids, V_L and V_H sequences of the αGD2 clone 14g2a were cloned into the respective αCD123 antibody vectors to generate pFUSE-GD2-LC, pFUSE-GD2-HC and pFUSE-SIRPα-GD2-LC constructs. The VL and VH sequences of the 14g2a (Table 2) were kindly provided by Sebastian Kobold[4]. The pFUSE-GD2-HC-SIRPα was

[3] Gene Center Munich, LMU München, Germany
[4] Clinical Pharmacology, Department of Internal Medicine IV, Klinikum der LMU München, Germany

cloned by fusing the SIRPα to the C terminus of pFUSE-GD2-HC via a $(Gly_4Ser)_8$ linker. The mouse IgG2a isotype corresponds to human IgG1 and thus the mouse αGD2 antibody coding plasmids pFUSE-GD2-LC-m and pFUSE-GD2-HC-m were generated by inserting the VL and VH sequences of the 14g2a into expression plasmids pFUSE2-CLIg-mK or pFUSE-CHIg-mG2a (InvivoGen), which contain the Igκ leader sequence (Table 2). The mouse SIRPα (amino acids 31 – 150) from strain 129 was respectively fused to the N-or C-terminus of the αGD2 antibody light chain to form the pFUSE-SIRPa-GD2-LC-m and pFUSE-GD2-LC-SIRPa-m similar to human constructs.

Table 2. Amino acid sequences of antigen-binding domains, the SIRPα domain, linkers and the leader sequence of the antibody DNA plasmids.

	Sequence
αCD123 VL	DIVMTQSPDSLAVSLGERATINCESSQSLLNSGNQKNYLTWYQQKPG QPPKPLIYWASTRESGVPDRFSGSGSGTDFTLTISSLQAEDVAVYYCQ NDYSYPYTFGQGTKLEIKR
αCD123 VH	EVQLVQSGAEVKKPGESLKISCKGSGYSFTDYYMKWARQMPGKGL EWMGDIIPSNGATFYNQKFKGQVTISADKSISTTYLQWSSLKASDTA MYYCARSHLLRASWFAYWGQGTMVTVSS
αGD2 VL	DILLTQTPLSLPVSLGDQASISCRSSQSLVHRNGNTYLHWYLQKPGQS PKLLIHKVSNRFSGVPDRFSGSGSGTDFTLKISRVEAEDLGVYFCSQST HVPPLTFGAGTKLELKR
αGD2 VH	EVKLQQSGPSLVEPGASVMISCKASGSSFTGYNMNWVRQNIGKSLEWI GAIDPYYGGTSYNQKFKGRATLTVDKSSSTAYMHLKSLTSEDSAVYYC VSGMEYWGQGTSVTVSS
Human SIRPα	EEELQVIQPDKSVLVAAGETATLRCTATSLIPVGPIQWFRGAGPGREL IYNQKEGHFPRVTTVSDLTKRNNMDFSIRIGNITPADAGTYYCVKFR KGSPDDVEFKSGAGTELSVRAKPS
Mouse SIRPα	GKELKVTQPEKSVSVAAGDSTVLNCTLTSLLPVGPIKWYRGVGQSRLL IYSFTGEHFPRVTNVSDATKRNNMDFSIRISNVTPEDAGTYYCVKFQK GPSEPDTEIQSGGGTEVYVLAKPS
$(Gly_4Ser)_4$ linker	GGGSGGGGSGGGGSGGGGS
$(Gly_4Ser)_8$ linker	GGGSGGGGSGGGGSGGGGSGGGGSGGGGSGGGGSGGGGS
Igκ leader	METDTLLLWVLLLWVPGSTG
CD123ex-Gly_4Ser-His_6	KEDPNPPITNLRMKAKAQQLTWDLNRNVTDIECVKDADYSMPAVNNS YCQFGAISLCEVTNYTVRVANPPFSTWILFPENSGKPWAGAENLTCWIH DVDFLSCSWAVGPGAPADVQYDLYLNVANRRQQYECLHYKTDAQGTR IGCRFDDISRLSSGSQSSHILVRGRSAAFGIPCTDKFVVFSQIEILTPPNMT AKCNKTHSFMHWKMRSHFNRKFRYELQIQKRMQPVITEQVRDRTSFQL LNPGTYTVQIRARERVYEFLSAWSTPQRFECDQEEGANTRAWRTSGGG GSHHHHHH

3.1.4. Generation of the plasmids

3.1.4.1. Preparation of DNA fragments

To clone the aforementioned plasmids, pFUSE2-CLIg-hK and pFUSE-CHIg-hG1were linearized and amplified by polymerase chain reaction (PCR) using the Phusion Flash High-Fidelity PCR Master Mix (Thermo Fisher Scientific). 50 µl PCR reactions contained 10 ng of DNA template and 0.5 µM of each primer. Details of the PCR program are in Table 3. The insert of interest was similarly amplified by PCR. PCR products were incubated with FastDigest DpnI (Thermo Fisher Scientific) for 30 min at 37°C to remove template DNA. The amplified and DpnI-digested DNA was separated by agarose gel electrophoresis and subsequently extracted from the gel using the NucleoSpin Gel and PCR clean-up kit (Macherey-Nagel).

Table 3. PCR reaction program

	Temperature	Time
Initial denaturation	98°C	30 s
Denaturation Annealing Extension (20-30 cycles)	98°C T_a 72°C	30 s 30 s 15- 30 s/kb
Final extension	72°C	5 min
Hold	16°C	

Annealing temperature (T_a) was calculated using the Thermo Scientific Tm Calculator[5].

3.1.4.2. Molecular cloning

Purified DNA fragments were joined by Gibson assembly according to Gibson et al. [262]. Briefy, 10-100 ng of the PCR-linearized vector was mixed with 3-5-fold excess of the insert and incubated for 1 hour at 50°C in the presence of 0.004 U/µL T5 exonuclease (New England Biolabs), 0.025 U/µL Phusion DNA polymerase and 4 U/µL Taq ligase in a final volume of in 10 µl. The Gibson assembly reaction was then transformed into chemically competent XL1 blue *Escherichia coli* cells (Stratagen) [263]. For transformation, 2-3 µl of the reaction was mixed with 100 µl of XL1 blue and incubated for 15 min on ice. Cells were heat-shocked for 45 sec at 42°C followed by a 2 min recovery on ice. 300 µl of lysogeny broth (LB) medium (10 g/l tryptone, 5 g/l yeast extract, 5 g/l NaCl, 1.3 ml/l NaOH) was added to the cells and incubated at 37°C for 1 h at constant shaking at 600 revolutions per minute (rpm) on a ThermoMixer C (Eppendorf). The transformed cells were plated onto LB agar (LB-Lennox medium with 15 g/l agar) plate supplemented with 100 µg/ml ampicillin for the pSecTag2/HygroC and 100 µg/ml blasticidine (InvivoGen) or 25 µg/ml zeocine (Thermo Fisher Scientific) for LC or HC pFUSE vectors, respectively. After an overnight (ON) incubation at 37°C, single colonies were selected and cultured in 3-5 ml LB medium containing

[5] https://www.thermofisher.com/de/de/home/brands/thermo-scientific/molecular-biology/molecular-biology-learning-center/molecular-biology-resource-library/thermo-scientific-web-tools/tm-calculator.html

the corresponding antibiotic at 37°C with constant shaking. Plasmid DNA was isolated from the cultures using NucleoSpin Plasmid EasyPure kit (Macherey-Nagel).

3.1.4.3. Final preparations for plasmid DNA

Kozak sequence was inserted to all constructs by using site-directed mutagenesis PCR as described in 3.1.3.1. Final sequencing of all generated DNA vectors was performed at Eurofins Genomics and large-scale plasmid purification was performed with Nucleobond Xtra Midi kit (Macherey-Nagel).

3.1.5. Protein purification using Expi293F cell expression system

3.1.5.1. Protein expression

In order to express the antibody molecules, Expi293F cell expression system (Thermo Fisher Scientific) was used. The cells were co-transfected with LC and HC plasmids according to the manufacturer's instructions. Briefly, for a standard expression of 30 ml, 25.5 ml of cells were adjusted to 2×10^6 live cells/ml one day before transfection. Live cell numbers were determined by using a Countess automated cell counter and trypan blue exclusion stain (0.4%) (both Thermo Fisher Scientific). On the day of transfection, 1.5 ml Opti-MEM reduced serum medium (Thermo Fisher Scientific) was mixed with 30 µg of DNA (Table 4) and 80 µl of ExpiFectamine, respectively. After 5 min incubation, at RT, the Opti-MEM mixtures were combined and further incubated for 20 min at RT. The transfection mix was added dropwise to the cells. 16 to 18 h post transfection, 150 µl of Enhancer 1 and 1.5 ml of Enhancer 2 were added to boost transfection, cell viability, and protein expression.

Table 4. Heavy and light chains for all antibodies.

Antibody	Heavy chain (HC)	Light chain (LC)	H to L ratio
αCD123	pFUSE-123-HC	pFUSE-123-LC	1 to 8
1xSIRPα-αCD123	pFUSE-123-HC	pFUSE-SIRPα-123-LC	1 to 4
2xSIRPα-αCD123	pFUSE-123-HC	pFUSE-SIRPα-SIRPα-123-LC	1 to 4
αGD2(h)	pFUSE-GD2-HC	pFUSE-GD2-LC	1 to 1
SIRPα-αGD2(h)	pFUSE-GD2-HC	pFUSE-SIRPα-GD2-LC	1 to 1
αGD2-SIRPα(h)	pFUSE-GD2-HC-SIRPα	pFUSE-GD2-LC	1 to 1
αGD2(m)	pFUSE-GD2-HC-m	pFUSE-GD2-LC-m	1 to 1
SIRPα-αGD2(m)	pFUSE-GD2-HC-m	pFUSE-SIRPα-GD2-LC-m	1 to 1
αGD2-SIRPα(m)	pFUSE-GD2-HC-SIRPα-m	pFUSE-GD2-LC-m	1 to 1

3.1.5.2. Protein A affinity chromatography

After five to seven days, cells were pelleted by centrifugation at 500 g for 10 min and the supernatant containing the antibody constructs was harvested. The supernatant was

subsequently incubated with 250 µl of Protein A Sepharose 4FF beads (GE Healthcare) at 4°C on a rotating wheel. After an ON incubation, the beads were collected by centrifugation (500 g, 10 min, 4°C) and loaded onto a Bio-Spin chromatography column (Thermo Fisher Scientific). Beads were first washed with 4 column volumes of wash buffer [50 mM tris(hydroxymethyl)aminomethane-HCl (Tris-HCl) pH 7.0], before antibodies were eluted with 6 column volumes of elution buffer (0.1 M citrate pH 3.0) into separate fractions. All elution fractions were eluted into neutralization buffer (1 M Tris-HCl pH 9.0) to adjust the pH to 7.0.

The wash and elution fractions were analyzed by sodium dodecyl sulfate polyacrylamide gel electrophoresis (SDS-PAGE) and Coomassie Brilliant Blue staining. To this end, protein samples were incubated in the presence of 1×Laemmli buffer [0.11 M Tris base (pH 6.8), 16% /v/v) glycerol, 4% (w/v) SDS, 5% (v/v) β-mercaptoethanol, 0.05% (w/v) bromophenol blue] for 5 min at 95°C and loaded into RunBlue SDS-PAGE Gel System 4-20% Bis-Tris gels (Expedeon) in 20×SDS Running Buffer (0.01% SDS, 8.95 g/l triethanolamine, 7.17 g/l tricine). After electrophoresis, gels were stained with Coomassie staining solution [50% (v/v) ethanol, 7% (v/v) acetic acid, 0.2% (w/v) Coomassie Brilliant Blue R250] or InstantBlue (Expedeon). PageRuler Unstained Protein Ladder (Thermo Fisher Scientific) was included to all gels as size standard. Protein A affinity chromatography fractions that contained antibodies were pooled and concentrated at (1000 g, 15 min, 4°C) using Amicon spin concentrators (Merck Millipore).

3.1.5.3. Size exclusion chromatography

On the same day with Protein A affinity chromatography, size exclusion chromatography (SEC) was performed. Hence, the Superdex 200 Increase 10/300 GL column (GE Healthcare) was used with Aekta Purifier 100 (GE Healthcare) with phosphate buffered saline (PBS, 8 g/L NaCl, 0.2 g/L KCl, 1.44 g/L Na2HPO4x2H2O, 0.2 g/L KH2PO4, pH 7.4) as running buffer. SEC fractions containing the antibodies were pooled, analyzed by SDS-PAGE and concentrated to approximately 1-3 µg/µl. In routine purifications, only the final purified protein, and not SEC fractions, were analyzed by SDS-PAGE. Protein concentration was measured with a spectrophotometer Nanodrop ND-100 (Peqlab Biotechnologies GmbH). Antibody aliquots were frozen in liquid nitrogen and stored at -80°C.

3.1.5.4. Thermal stability measurements

The thermal stability of final purified proteins was measured by using nano differential scanning fluorimetry (nanoDSF) with Tycho NT.6 (NanoTemper Technologies) which analyses the temperature-dependent changes in the intrinsic fluorescence of tryptophane and tyrosine residues. 1 µM of protein in PBS was used to determine the changes in fluorescence signal upon transitions in the folding state of the proteins. The temperatures at which a transition occurred are named as inflection temperatures (T_i) [264].

3.1.5.5. CD123ex purification

For the purification of His-tagged CD123ex, Expi293F culture supernatants were incubated with nickel nitrilotriacetic acid (Ni-NTA) agarose beads (Qiagen) on a rotation device for at least 2 h at 4°C. The beads were centrifuged (500 g, 10 min, 4°C), transferred to a Bio-Spin chromatography column and washed with 4 column volumes of wash buffer (PBS, 10 mM Imidazole) followed by elution with 6 column volumes of elution buffer (1×PBS + 200 mM Imidazole, pH 7.4). All further steps were performed as described for the antibody constructs in 3.1.5.3.

3.2. Cell culture methods

3.2.1. Cultivation of cell lines

Expi293F cells were maintained at 37°C, 5% CO_2 in shaking incubator (Multitron) at 125 rpm between 0.5-6×10^6 cells/ml in Expi293 Expression Medium using 125 ml Erlenmeyer flasks (Corning). The AML cell line MOLM-13 was purchased from the Deutsche Sammlung von Mikroorganismen und Zellkulturen (DSMZ) and cultured in Roswell Park Memorial Institute (RPMI) 1640 + GlutaMAX medium supplemented with 20% fetal bovine serum (FBS). The lymphoma cell line Raji was kindly provided by Prof. Marion Subklewe. The cells were cultured in RPMI 1640 + GlutaMAX supplemented with 10% FBS (full RPMI medium). Flp-INTM-Chinese hamster ovary (CHO) cells were obtained from Thermo Fisher Scientific and cultured in Ham's F-12 medium (Biochrom) supplemented with 10% FBS. Flp-INTM-CHO cells were stably transfected with human CD47 or CD33 (assigned as CHO^{CD47+} and CHO^{CD47}) by Nadine Magauer[6] and Monika Herrmann[6], respectively and cultivated in Ham's F-12 supplemented with 10% FBS and 500 µg/mL hygromycin B Gold (InvivoGen).

Human NBS cell lines SK-N-AS, IMR-32 and Shep2 were kindly provided by Gosse Adema[7]. SK-N-AS and Shep2 cell lines were maintained in Dulbecco's Modified Eagle Medium (DMEM) + GlutaMAX supplemented with 10% FBS, 1% minimum essential medium (MEM) non-essential amino acids (NEAA), 1% Penicillin/Streptomycin, 2 mM L-Glutamine and 1 mM sodium pyruvate. IMR-32 cells were cultured in RPMI 1640 + GlutaMAX supplemented with 20% of FBS and 1% MEM NEAA.

Mouse NBS cell lines Neuro2a, 9464D, 9464D-OVA and 9464D-GFP were provided by Gosse Adema. 9464D cells (from Dr. Orentas, National Institutes of Health, Bethesda) and Neuro-2a cells (American Type Culture Collection, ATCC) were cultured in DMEM + GlutaMAX medium containing 10 % FBS (Greiner Bio-One), 1% MEM NEAA, 50 µM β-mercaptoethanol (Sigma-Aldrich) and 1% antibiotic–antimycotic solution (Thermo Fisher Scientific). 9464D cells that were transfected with green fluorescent protein (GFP)-Ires-Luciferase sequence

[6] Research group of Karl-Peter Hopfner, Gene Center, Munich, Germany
[7] Laboratory of Radiotherapy and Oncoimmunology, Radboud University Medical Centre, Nijmegen, Netherlands

under the control of a cytomegalovirus (CMV) promoter (9464D-GFP) were generated previously and were cultured in the same medium as 9464D cells and supplemented with 1 mg/ml G418 [265]. The 9464D-OVA cells were stably transfected with the chicken ovalbumin (OVA) model antigen by Michiel Kroesen[8] and cultured in the same medium as 9464D-luc-GFP cells. Panc02 were provided by Sebastian Kobold and maintained in DMEM + GlutaMAX medium supplemented with 10% FBS.

3.2.2. Healthy donor and AML patient-derived material

After written informed consent in accordance with the Declaration of Helsinki and approval by the Institutional Review Board of the Ludwig-Maximilians-Universität, peripheral blood or bone marrow material was collected from healthy donors (HDs) and AML patients. AML samples were provided by and analyzed at the Laboratory for Leukemia Diagnostics of the Klinikum der Universität München[9]. The characteristics of AML patients used as target cells in ADCP assays are displayed in Table 5. Cells from patients 1- 4 were used in allogenic ADCP assays and cells from patients 5-9 in autologous ADCP assays.

3.2.2.1. PBMC isolation

Peripheral blood mononuclear cells (PBMC) were isolated from heparinized whole blood from HDs or from residual cells from leukoreduction chambers obtained from the Department of Transfusion Medicine of the Klinikum der Universität München [10]. Depending on the source, PBMC isolation was performed in two ways. For the isolation of PBMCs from whole blood, 15 ml of Biocoll solution (Biochrom) was preloaded to a 50 ml Leucosep tube (Greiner Bio-One) and subsequently centrifuged for 1 min at 1000 g. The heparinized whole-blood was diluted 1 to 1 with Dulbecco's PBS (DPBS, Thermo Fisher Scientific) and 30 ml of the dilution was gently pipetted on top of the Leucosep tube membrane. The Leucosep tubes were centrifuged for 10 min at 1000 g at room temperature with low acceleration and no breaking. For the leukoreduction chamber material, 15 ml of Biocoll solution was slowly added to a 50 ml tube. The leukoreduction chamber material was diluted 1 to 3 with DPBS and pipetted gently on top of the Biocoll solution. The tubes were centrifuged for 30 min at 818 g at room temperature with low acceleration and no breaking. Buffy coats containing the PBMCs were collected and washed twice by adding 45 ml DPBS followed by centrifugation (8 min, 300 g, RT). PBMCs were finally re-suspended in a magnetic-activated cell sorting (MACS) buffer (Miltenyi) for further use.

[8] Research group of Gosse Adema, Laboratory of Radiotherapy and Oncoimmunology, Radboud University Medical Centre, Nijmegen, Netherlands.
[9] University Hospital, Ludwig-Maximilians-Universität München, Munich, Germany.
[10] Department of Transfusion Medicine, Cellular Therapy and Hemostaseology, University Hospital, Ludwig-Maximilians-Universität München, Munich, Germany.

3.2.2.2. RBC isolation

To obtain RBCs, heparinized peripheral or fingerprick blood from HDs was centrifuged at 700 g 5 min and washed twice with DPBS.

Table 5. Characteristics of AML patient material used in ADCP assays

Patient	Age	Sex	Material	Disease status	Karyotype	ELN genetic group	*FLT3*-ITD	*NPM1*
1	29	F	PBMC	ID	aberrant	adverse	wt	wt
2	52	M	BMMC	ID	aberrant	intermediate	wt	wt
3	74	M	PBMC	ID	46XY	intermediate	wt	wt
4	54	M	PBMC	Relapse	normal	intermediate	wt	wt
5	49	F	PBMC	ID	complex	adverse	mut	mut
6	85	M	PBMC	ID	aberrant	adverse	wt	wt
7	30	F	BMMC	ID	aberrant	favorable	wt	wt
8	20	M	BM	ID	aberrant	intermediate	wt	wt
9	56	F	PBMC	ID	aberrant	favorable	wt	wt

European LeukemiaNet (ELN), initial diagnosis (ID), wild type (wt), mutated (mut), female (F), male (M).

3.2.3. AML patient-derived xenograft material

To obtain patient-derived xenograft (PDX) cells, AML patient cells were serially transplanted in NOD *scid* gamma (NOD.Cg-Prkdc^{scid} IL2rg^{tm1Wjl}/SzJ, NSG) mice in the research group of Irmela Jeremias as previously described [266, 267]. The PDX cells were lentivirally transduced with codon-optimized form of firefly luciferase and mCherry constructs for bioluminescence imaging and flow cytometry, respectively [266]. For *ex vivo* experiments, PDX cells were grown in StemPro-34 medium with Nutrient supplement, 2% FBS, 2 mM L-Glutamine and 1x Penicillin-Streptomycin (Gibco) and 0.01 µg/ml of recombinant human IL3 (rhIL3), rh thrombopoietin (rhTPO), rh stem cell factor (rhSCF, all Peprotech) and rhFLT3-ligand (R&D Systems). Available information about the patients is summarized in Table 6.

Table 6. Characteristics of AML-PDX cell donors

Patient	Age	Sex	Disease status	Karyotype	ELN genetic group	*FLT3*-ITD	*NPM1*
AML-491 [267]	53	F	Relapse	del(7)(q2?1)	adverse	wt	wt
AML-579 [267]	51	M	Relapse	normal	adverse	Mut, LOH	mut
AML-640	79	M	Relapse	t(11;15)	intermediate	mut	mut
AML-979	56	F	Relapse	normal	n. a.	wt + mut subclone	mut

Not available (n. a.).

3.2.4. Isolation of murine cells

Mouse bone marrow cells and RBCs were isolated by Renske van den Bijgaart in the laboratory of ROI. Bone marrow cells were isolated from femurs and tibiae of 6-10 weeks old female C57BL/6 mice (Charles River, Germany). A terminal blood collection was performed via cardiac puncture from C57BL/6 mice using heparin. RBCs were centrifuged at 700 g for 5 min and washed twice with DPBS.

3.3. Binding and interaction analysis

3.3.1. Flow cytometry

For flow cytometry, 0.8-1×10^5 cells were transferred per well to a 96-well plate with conical bottom. Cells were centrifuged (3 min at 500 g), supernatant was discarded and pellets were resuspended in 50 µl antibody solution in flow cytometry buffer [PBS with 1% (v/v) FBS, 1 mM ethylenediaminetetraacetic acid (EDTA)]. Cells were incubated for 30 min at 4°C in the dark. After staining, cells were washed twice by adding 200 µl of flow cytometry buffer and centrifuged (3 min, 500 g). If secondary antibody was used, cells were incubated in 50 µl of fluorochrome-labeled antibody solution in flow cytometry buffer for 30 min at 4°C in the dark. After this, cells were again washed twice by adding 200 µl of FC buffer and centrifuged (3 min, 500 g). Cells were finally resuspended in 200 µl flow cytometry buffer and analyzed using the Guava easyCyte 6HT (Merck Millipore) or FACSVerse (mouse NBS cell line experiments, BD Biosciences). To evaluate the antibody specificity, isotype controls were included. Antibody binding was determined by the median fluorescence intensity (MFI) ratio which was calculated by dividing the MFI of the tested antibody by the MFI of the corresponding isotype.

3.3.2. Detection of cell surface antigen expression

The expression of cell surface antigens was analyzed by flow cytometry as described in 3.3.1 using antibodies in Table 7.

Table. 7. Antibodies used for flow cytometry-based surface antigen expression analysis.

Antigen	F	R	Isotype	Clone	D / Ct	Company	Cells
CD123	PE	Human	Mouse IgG1, κ	6H6	1:20	Biolegend	Primary AML, macrophages
CD123	APC	Human	Mouse IgG1, κ	6H6	1:20	Biolegend	AML PDX
CD47	PE	Human	Mouse IgG1, κ	CC2C6	1:50	Biolegend	Primary AML, macrophages, human NBS cell lines
CD47	FITC	Human	Mouse IgG1, κ	B6H12	1:20	eBioscience	AML PDX
CD16	PE	Human	Mouse IgG1, κ	3G8	1:100	Biolegend	Primary AML, macrophages
CD32	APC	Human	Mouse IgG2b, κ	FUN-2	1:50	Biolegend	Primary AML, macrophages
CD64	APC	Human	Mouse IgG1, κ	10.1	1:50	Biolegend	Primary AML, macrophages
GD2	APC	Human/ mouse	Mouse IgG2a, κ	14G2a	1:50, 1:20	Biolegend	Human NBS cell lines, Raji, Panc02
CD47	APC	Mouse	Rat IgG2a, κ	MIAP-301	1:20, 1:10	Biolegend	Raji, Panc02
GD2	-	Human/ mouse	Mouse IgG1, κ	14G2a	100 nM	In house	Mouse NBS cell lines
IgG	PE	Mouse	Goat	Poly4053	1:200	Biolegend	Mouse NBS cell lines
CD47	-	Mouse	Rat IgG2a, κ	MIAP-301	100 nM	Biolegend	Mouse NBS cell lines
IgG	APC	Rat	Goat	Poly4054	1:400	Biolegend	Mouse NBS cell lines

Fluorochrome (F), Reactivity (R), Dilution (D), Concentration (Ct).

3.3.3. Quantification of cell surface antigen expression

Surface antigen density on different cell lines was quantified using the QIFIKIT (Dako) assay following the manufacturer's instructions. Antibody incubations were performed as described in 3.3.1. First, saturating concentrations (10 μg/ml) of unconjugated primary mouse anti human CD123 (clone 6H6), CD47 (clone B6H12), CD19 (clone HIB19, all from Biolegend) and GD2 (produced in house) were used. A secondary FITC-labeled anti mouse IgG antibody provided in the QIFIKIT was used in 1:50 dilution to detect primary antibody binding. After 45 min

incubation at 4°C in the dark, cells were washed and analyzed by flow cytometry as in 3.3.1. Calibration beads with a defined antigen expression provided by the kit were used to generate a standard curve to quantify the unknown surface antigen expression on cell lines.

3.3.4. Flow cytometry-based antibody binding

To investigate the binding of SIRPα-antibody fusions and control antibodies, flow cytometry measurement was performed as described in 3.3.1. To this end, target cell lines were incubated with 100 nM of unconjugated constructs or human IgG1 (QA16A12, Biolegend) or mouse IgG2a (MG2a-53, Biolegend) isotype controls. The primary staining was followed by a secondary antibody incubation with FITC-coupled αhuman IgG Fc (clone HP6017, 1:100, Biolegend) or PE-coupled αmouse IgG (clone Poly4053, 1:200).

3.3.5. K_D determination by surface plasmon resonance

For equilibrium binding constant (K_D) assessment by surface plasmon resonance (SPR) Biacore X100 system (GE Healthcare) was used. First, CM5 chip (GE Healthcare) was coated with an αhuman IgG Fc capture antibody (GE Healthcare) that reacts with the chip's amino groups at a level of around 8000 response units (RU). The ligands αCD123, 1xSIRPα-αCD123 or 2xSIRPα-αCD123 were immobilized on the chip at a level of 100 RU. The extracellular domain of CD123 then ran over the antibody-coated chip at concentrations of 3.91, 7.31, 15.62, 31.25, 62.5, 125, 250, 500 and 1000 nM with an association time of 180 s and a dissociation time of 600 s. K_D were calculated from the ratio of the association rate constant (k_{on}) and the dissociation rate constant (k_{off}) of the multi cycle kinetics measurements.

3.3.6. K_D determination by flow cytometry

To determine K_D values of αCD123, 1×SIRPα-αCD123 and 2×SIRPα-αCD123 by flow cytometry, MOLM-13 cells were incubated with various concentrations of the antibodies and analyzed as described in 3.3.1. and 3.3.4. For evaluation, the minimum MFI was set to 0% and maximum to 100% and all data points were normalized accordingly. The data was fitted with a non-linear regression curve using a one-site specific binding model.

3.3.7. Competitive binding assay with RBCs

To analyze the competitive binding of antibodies to cancer cells in the presence of RBCs, flow cytometry based binding analysis was performed as described in 3.3.1. and 3.3.4. Before the assay, RBCs were stored for a maximum of 1 day and washed with RBC buffer (21 mM Tris, 4.7 mM KCl, 2 mM $CaCl_2$, 140.5 mM NaCl, 1.2 mM $MgSO_4$, 5.5 mM glucose, 0.5% bovine serum albumin, pH 7.4) according to [268].

For the competitive binding assay with αCD123 antibodies, 0.15×10^5 MOLM-13 cells per well were stained with the membrane dye PKH26 (Sigma-Aldrich) according to the manufacturer's protocol. PKH26-labeled MOLM-13 cells were then mixed with a 20-fold excess of RBCs in

a round-bottom 96-well plate. Cells were incubated with 100 nM of αCD123, 1×SIRPα-αCD123, 2×SIRPα-αCD123 or αCD47 (clone B6H12, eBioscience) antibodies, washed twice with 200 µl flow cytometry buffer and centrifuged (5 min, 700 g). The supernatant was discarded and binding of the antibodies was detected with a secondary staining using APC-coupled αhuman IgG Fc (clone HP6017, 1:100, Biolegend) or APC-coupled αmouse IgG (clone HP6017, 1:100, Biolegend) as described in 3.3.1. The percentage of MOLM-13 cells ($PKH26^+$) or RBCs ($PKH26^-$) within the antibody-bound cells was determined using Guava easyCyte 6HT.

To analyze the competitive binding of human and mouse αGD2 antibody constructs, 0.25×10^5 human or mouse NBS cells per well were stained with 0.6 µg/ml Calcein acetoxymethyl (AM, Thermo Fisher Scientific) according to manufacturer's instructions. Labelled target cells were mixed with a 20-fold excess of human or mouse RBCs, respectively. The cells were then incubated with 100 nM of either human or mouse αGD2 antibodies followed by washing and labelling with APC-coupled anti human IgG Fc (clone HP6017, 1:100), APC-coupled anti mouse IgG (polyclonal, 1:400, BD Pharmigen). Additionally, human cells were incubated with αCD47(h) (clone B6H12) and mouse cells with αCD47(m) (clone MIAP301, Biolegend) followed by APC-coupled anti mouse IgG (polyclonal, BD Pharmingen) or APC-coupled anti rat IgG (Poly4054, 1:200). The percentage of labelled target cells or unlabeled RBCs within the antibody-bound cells was determined using Guava easyCyte 6HT (human cells) or FACSVerse (mouse cells).

3.3.8. Hemagglutination assays

RBC binding by the SIRPα-antibody fusion constructs was also analyzed by hemagglutination. To this end, 4×10^6 RBCs from human or mouse donors were incubated with various concentrations of species specific αGD2 antibodies or αCD47 on a round-bottom 96-well plate at room temperature (RT) ON. Images of the plates were captured as unmodified images the next day. Hemagglutination was defined as red flocculation in the supernatant from the images.

3.3.9. CD47-blocking assays

Flow cytometry was used to investigate CD47-blocking by the SIRPα domain in the fusion constructs as described in 3.3.1. MOLM-13 or NBS cells were first incubated with 100 nM concentration of SIRPα-antibody constructs followed by a second staining step with a FITC-conjugated anti human CD47 (clone B6H12) or APC-conjugated anti mouse CD47 (clone MIAP301) antibodies. CD47 blockade was normalized so that the isotype control was set to 0%.

CD47-blocking by the human αCD47 B6H12 or mouse αCD47 MIAP301, was also studied. To this end, human Raji and mouse Panc02 cells were incubated with different concentrations of αCD47 antibodies followed by a second incubation with human or mouse αGD2-SIRPα

antibody construct, respectively. Finally, a staining step with FITC-coupled αhuman IgG Fc (clone HP6017, 1:100) or FITC-coupled αmouse IgG (clone Poly4060, 1:200, Biolegend) was performed and cells were analyzed as described in 3.3.1.

3.4. Functional *in vitro* assays

3.4.1. Antibody-dependent cellular phagocytosis of human cell lines

Flow cytometry-based ADCP assay was performed to study the effect of SIRPα-antibody fusion constructs on macrophage-mediated phagocytosis. To this end, monocytes were enriched from human PBMCs by MACS using the classical monocyte isolation kit (Miltenyi) following the manufacturer's instructions. 2×10^4 monocytes per well of a flat-bottom 96-well plates (Nunclon Delta Sufrace, Thermo Fisher Scientific) were differentiated into macrophages in 100 µl of full RPMI medium containing 100 ng/ml macrophage colony-stimulating factor (MCSF, Biolegend). After 5 to 7 days of differentiation, macrophages were labeled with 0.5 µg/ml Calcein AM (Thermo Fisher Scientific) for 5 min at 37°C according to manufacturer's instructions. Next, macrophages were washed twice with medium and mixed with 2×10^4 target cells labeled with 5 µg/ml CellTrace Calcein red-orange AM (Thermo Fisher Scientific) for 20 min at 37°C. The macrophage and target cell mixture were incubated in the presence of 50 µl of antibody solution in full RPMI medium at 37°C for 3 h in the experiments with MOLM-13 cells and 1 h with human NBS cells. Human IgG1 isotype and αCD47 (B6H12) were used as controls. The suspension cells were removed after the incubation and macrophages detached with DPBS containing 4 mg/ml lidocain-HCl (Sigma-Aldrich) and 5mM EDTA for 10 min at 37°C. Finally, target cells and macrophages were pooled, centrifuged at 500 g for 3 min and resuspended in cold flow cytometry buffer immediately before analysis. Samples were measured by flow cytometry using either Guava easyCyte 6HT or Cytoflex LX (Beckman Coulter). Phagocytosis was quantified as the percentage of Calcein AM positive macrophages that have engulfed Calcein red-orange AM target cells. The phagocytosis of all conditions was normalized to the isotype control. In case MOLM-13 cells were used as target cells, the isotype control was set to 0% phagocytosis rate. In case human NBS cells were used, the isotype control was set to 0% and the condition showing the highest phagocytosis rate was set to 100%. The normalized results and their mean values from each experiment are shown.

3.4.2. Antibody-dependent cellular phagocytosis of allogenic and autologous primary AML cells

Macrophages were differentiated from monocytes isolated from HDs for allogenic ADCP assays. In autologous ADCP, AML target cells from initial diagnosis were used together with macrophages which were differentiated from monocytes of the same AML patients in remission. All AML target cells were cryo-preserved in 90% FBS and 10% dimethyl sulfoxide (DMSO, Sigma-Aldrich) in liquid nitrogen. On the day of the assay, patient AML target cells

were gently thawed and labelled with Calcein Red Orange AM and ADCP assays were performed using 50 nM antibody concentration as described in above with MOLM-13 cells. Samples were measured by flow cytometry using Guava easyCyte 6HT.

3.4.3. Antibody-dependent cellular phagocytosis by mouse bone marrow-derived macrophages

Mouse bone marrow-derived macrophages (BMDMs) were generated by Renske van den Bijgaart. Briefly, 4×10^6 bone marrow cells were cultured in a 10 cm^2 Petri dish in RPMI medium, 10% FBS, 1% L-alanyl-L-glutamine, 0.1% β-mercaptoethanol and 1% antibiotics/antimycotics, supplemented with 20 ng/ml mouse MCSF (Peprotech). On day 3 and 6, fresh MCSF was added to the culture. On day 7, the non-adherent cells were discarded and adherent cells were harvested using cold 1.5 mM EDTA in DPBS. BMDMs were labeled with 5 µg/ml CellTrace Calcein Red Orange AM for 5 min at 37°C and target cells were labeled with 0.6 µg/ml Calcein AM for 5 min at 37°C according to manufacturer's instructions. Target cells were first incubated with 50 nM antibody solution in full RPMI medium at 37°C for 15 min and washed once with the medium. Mouse IgG2a isotype and αCD47 (MIAP301) were used as controls. 3×10^4 pre-incubated target cells were mixed with 3×10^4 monocytes after which the cells were incubated at 37°C for 2.5 h. After the incubation, suspension cells were removed and rest of the cells detached with trypsin. All cells were pooled, centrifuged at 500 g for 3 min and resuspended in cold flow cytometry buffer immediately before flow cytometry analysis. Samples were measured by flow cytometry using the FACSVerse instrument. ADCP was measured as double-positive cells from macrophages. Results were normalized by setting the isotype control as 0% and maximum phagocytosis value to 100%.

3.4.4. NK cell-mediated antibody-dependent cellular cytotoxicity of leukemia cell lines

To study the NK cell-mediated lysis of cells, ADCC assay was performed. Accordingly, NK cells were enriched from human PBMCs using the NK cell isolation kit (Miltenyi) following manufacturer's instructions. NK cells were used on the same day or cryo-preserved in 90% FBS and 10% DMSO in -150°C until usage. 1×10^4 target cells per round-bottom 96-well plate were labeled with 16.6 µg/ml Calcein AM for 30 min at 37°C according to manufacturer's instructions. Labeled target cells were subsequently mixed with 5×10^4 NK cells in the presence of antibodies at different concentrations in a total volume of 200 µl of full RPMI medium for 4 h at 37°C at a 5:1 E:T ratio. In the competitive ADCC assay, NK cells were incubated with labeled MOLM-13 or Raji cells mixed with unlabeled Raji or MOLM-13 cells, respectively, at a 5:1:1 E:T:T ratio. Target cells were incubated in the presence of 2.5% Triton X-100 (Sigma-Aldrich) to establish the maximum lysis signal. Fluorescence intensity (FI) from Calcein AM release was measured with an Infinite M100 plate reader (TECAN) and lysis was calculated as

follows: $specific\ lysis\ [\%] = 100 \times \frac{FI(antibody\ stimulation) - FI(untreated)}{FI(\max) - FI(target)}$. Data were fitted to four-parameter dose-response curve.

3.4.5. ADCC with AML PDX cells

The cryo-preserved AML PDX cells derived from patients AML-491, AML-979, AML-640 and AML-579 were thawed according to Bonnet *et al.* 2008 [269] one to two days days prior the ADCC assay and cultivated in StemPro-34 medium described in 3.2.3. 1×10^4 AML cells per round-bottom 96-well plate were incubated with 5×10^4 NK cells and 100 nM antibodies for 20 h at 37°C in 200 µl of StemPro-34 medium. Cells were labeled with LIVE/DEAD Fixable Aqua (Thermo Fisher Scientific). The number of live mCherry$^+$ cells was determined by flow cytometry using the Cytoflex LX. Results were normalized to the isotype control which was set to 100% indicating no specific killing.

3.4.5.1. Detection of the CD34$^+$ CD38$^-$ leukemic stem cell population

To analyze the specific killing of LSCs, AML-491 and AML-579 cells were stained for the stem cell markers CD34 and CD38 after ADCC. PE/Cy7-conjugated αCD34 (clone 561, Biolegend) and Brilliant Violet-conjugated 421 αCD38 (clone HB-7, Biolegend) were used at a dilution of 1:20. For compensation of the fluorochromes, single staining controls were included. The samples were analyzed by flow cytometry within a fixed acquisition time of 60 sec using the Cytoflex LX. As the Cytoflex LX has a peristaltic pump-based fluidics system, it is possible to measure the absolute number of events without the addition of counting beads. The number of mCherry$^+$ CD34$^+$ CD38$^-$ cells was determined and normalized to the isotype control which was set to 100%.

3.5. *In vivo* engraftment studies

3.5.1. Study design

To evaluate the targeting of AML cells with leukemia initiating properties, an *ex vivo* NK cell-mediated ADCC was performed with the 2×SIRPα-αCD123 fusion antibody and the surviving cells were used in an *in vivo* engraftment experiment. This type of engraftment assay is highly sensitive and takes advantage of the ability of the leukemia-initiating cells (LICs) to regenerate leukemia in immunocompromised animals [270, 271]. All animal studies were performed in accordance with the current ethical standards of the official committee on animal experimentation (written approval by Regierung von Oberbayern, ROB-55.2Vet-2532.Vet_02-16-7 and ROB-55.2Vet-2532.Vet_03-16-56). Mouse studies were dome in cooperation with Binje Vick, who conducted the cell sorting, handling and injection of the mice, bioluminescence imaging (BLI) and data analysis.

3.5.2. *Ex vivo* ADCC and engraftment

PDX AML-491 and AML-579 were freshly isolated from NSG mice on the same day of the ADCC assay. 1×10^5 AML were incubated with 5×10^5 HD-derived NK cells and 100 nM antibodies for 20 h at 37°C on a round-bottom 96-well plate in StemPro-34 medium described in 3.2.3. After the ADCC, $mCherry^+$ PDX cells were separated from NK cells by fluorescence-activated cell sorting (FACS) with FACSAria III (BD Biosciences) and counted. Ebinger et al. determined that the LIC frequency was one in 1799 for AML-491 cells and one in 351 for AML-579 [267]. Correspondingly, 18 000 (10×LIC) or 180 000 (100×LIC) residual cells of the AML-491 isotype control treatment were injected intravenously into five male 10 to 12-week-old mice. Equal volumes of residual cells from αCD123 and 2xSIRPα-αCD123 treatments were similarly injected into five mice. For AML-579, 5000 (14×LIC) and 50 000 (140×LIC) residual cells of the isotype control treatment were injected intravenously into two to four female 10 to 12-week-old mice. Equal volumes of AML-579 residual cells from αCD123 and 2xSIRPα-αCD123 treatments were injected into same number of mice.

3.5.3. Evaluation of the results

Positive AML engraftment was analyzed by *in vivo* BLI, and total flux was quantified as described previously [266]. Mice showing total flux above 5×10^7 photons per second were classified as positive engraftment; mice showing no positive imaging signal within 28 weeks upon transplantation were classified as negative engraftment. Mice showing any clinical signs of illness or end stage leukemia according to Vick *et al.* 2015 (total flux $>2\times10^{10}$ photons/s; human $CD33^+$ cells in peripheral blood > 50%) were sacrificed [266]. Three mice died in narcosis during imaging and were counted as positive according to the last imaging signal or were excluded if not engrafted. Ratio of BLI positive animals to all animals was used to calculated LIC frequency using the extreme limiting dilution analysis (ELDA) software [272].

3.6. Data plotting and statistical analysis

Statistical evaluation was performed using GraphPad Prism versions 6.07 and 8.1.2 (GraphPad). Data sets were analyzed using one-way analysis of variance (ANOVA) including a test to determine equal variances within the groups and correction for multiple testing by Holm-Sidak's test. A Kaplan-Meier plot was generated to show AML engraftment and survival by treatment group and significance was assessed by log-rank Mantel-Cox test. Results were considered statistically significant at values and marked in figures as follows: p-value < 0.05 (*), < 0.01 (**), < 0.001 (***), < 0.0001 (****).

4. Results

4.1. SIRPα-αCD123 fusion antibodies targeting AML

4.1.1. Generation and purification of the SIRPα-αCD123 fusion antibodies

1×SIRPα-αCD123 and 2×SIRPα-αCD123 fusion antibodies were generated to boost the clearance of AML LSCs. The fusion antibodies were formed by genetically joining the human IgG1 αCD123 antibody with the N-terminal immunoglobulin V-like domains of the SIRPα (Figure 4). αCD123 was connected with the SIRPα domain with $(Gly_4Ser)_4$ linkers to provide flexibility between the binding modules. To evaluate the effects from the SIRPα domains alone, respective control fusion antibodies were generated with αCD19 or αGD2 (data not shown).

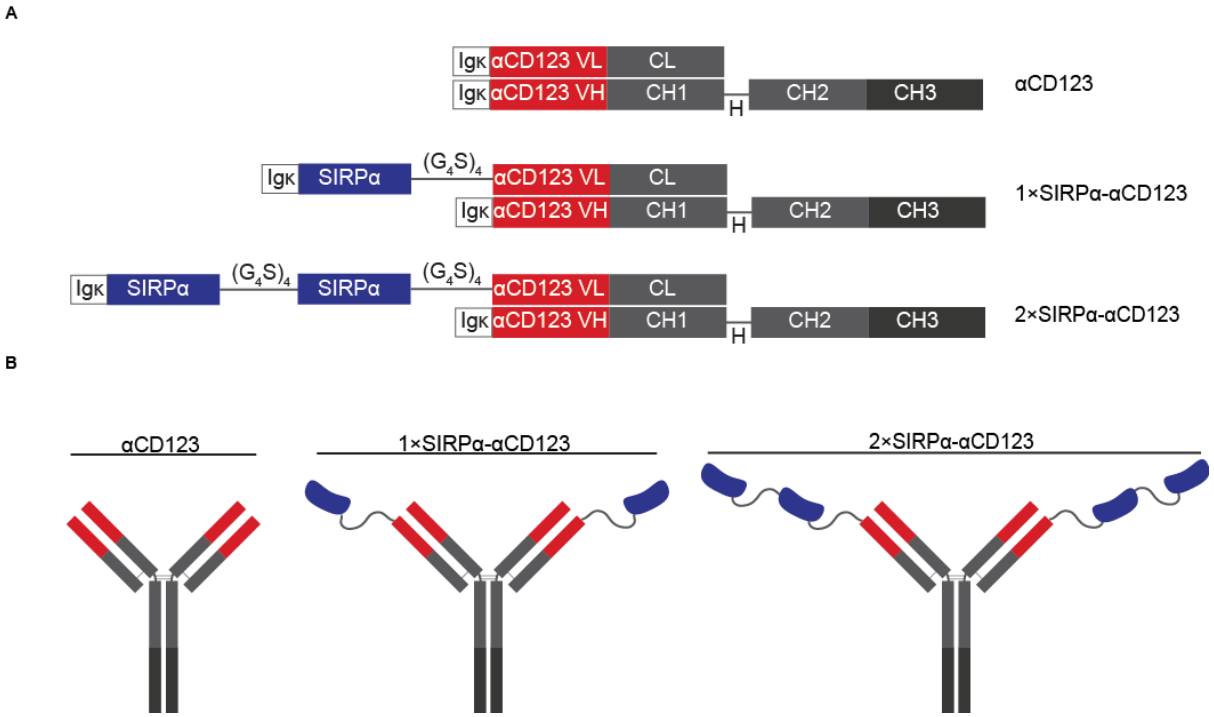

Figure 4. Schematic representation of αCD123 and SIRPα-αCD123 fusion antibodies. (A) The encoding DNA constructs. Igκ leader sequence (Igκ) is cleaved from the protein chain. VL – variable light, CL – constant light, VH – variable heavy, CH1 – constant heavy 1, CH2 – constant heavy 2, CH3 – constant heavy 3, H – hinge region. The N-terminal SIRPα immunoglobulin V-like domain is fused to the αCD123 via a $(G_4S)_4$ linker. (B) Schematic drawings of the fusion antibody proteins.

All antibodies were produced in Expi293F cells, purified from the cell culture supernatant by protein A affinity chromatography and preparative SEC (Figure 5A). A single SEC peak was observed for all antibodies demonstrating an absence of visible aggregations, degradation products or contaminating proteins. The αCD123 antibody eluted at around 12.8 ml while 1×SIRPα-αCD123 and 2×SIRPα-αCD123 antibodies eluted at around 11.6 ml and 10.8 ml, respectively. This coincides with their bigger size due to additional SIRPα domains. The non-reduced antibodies and their reduced heavy and light chains of the purified proteins corresponded to the computed masses with no detectable unspecific protein bands based on the

SDS-PAGE analysis (Figure 5B). Thermal stability of the antibodies was assessed by measuring changes in the intrinsic tryptophan or tyrosine fluorescence of the proteins using nanoDSF. The thermal unfolding profiles and T_i, which represent the unfolding events, are shown in figure 5C. The single or double SIRPα fusion did not influence thermal stability of the antibodies compared to αCD123.

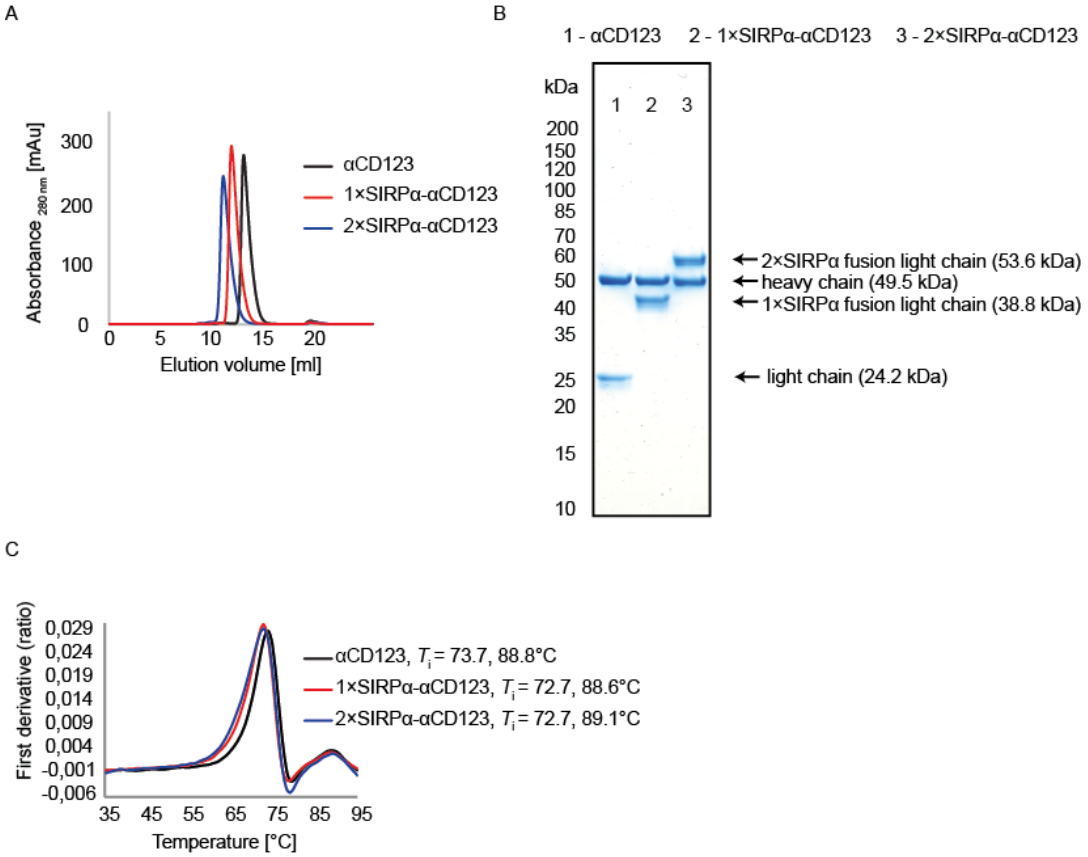

Figure 5. Purification and thermal stability of αCD123 and SIRPα-αCD123-fusion antibodies. (A) SEC chromatograms of preparative antibody purifications. A single peak was observed for all antibodies. (B) SDS-PAGE of the purified antibodies under non-reducing and reducing conditions. Computed masses of antibodies and the polypeptide chains are indicated. (C) Thermal stability of antibodies was determined by nanoSDF. The measured *T*i values are indicated, n=2.

4.1.2. Binding of SIRPα-αCD123 fusion antibodies

4.1.2.1. Binding to CD123 and CD47

The αCD123 binder used in this study has been shown to have a high binding affinity for the extracellular domain of CD123 [273]. To evaluate whether the affinity is influenced by the N-terminal fusion of the SIRPα domain, the K_D was measured by SPR for both αCD123 and SIRPα-αCD123 fusion antibodies (Figure 6A). The K_D values measured were not higher for the SIRPα-αCD123 fusion antibodies and therefore, the fusion of the SIRPα did not affect the affinity of αCD123 for CD123ex (Table 8). The binding of the antibodies was further analyzed using a flow cytometry-based assay where MOLM-13 cells were incubated with increasing

antibody concentrations up to saturation and K_D values were determined as an indication of avidity binding (Figure 6B). The K_D values of the SIRPα-αCD123 binding were significantly lower than for the αCD123 and thus, the avidity binding is increased due to the addition of the SIRPα domain (Table 8).

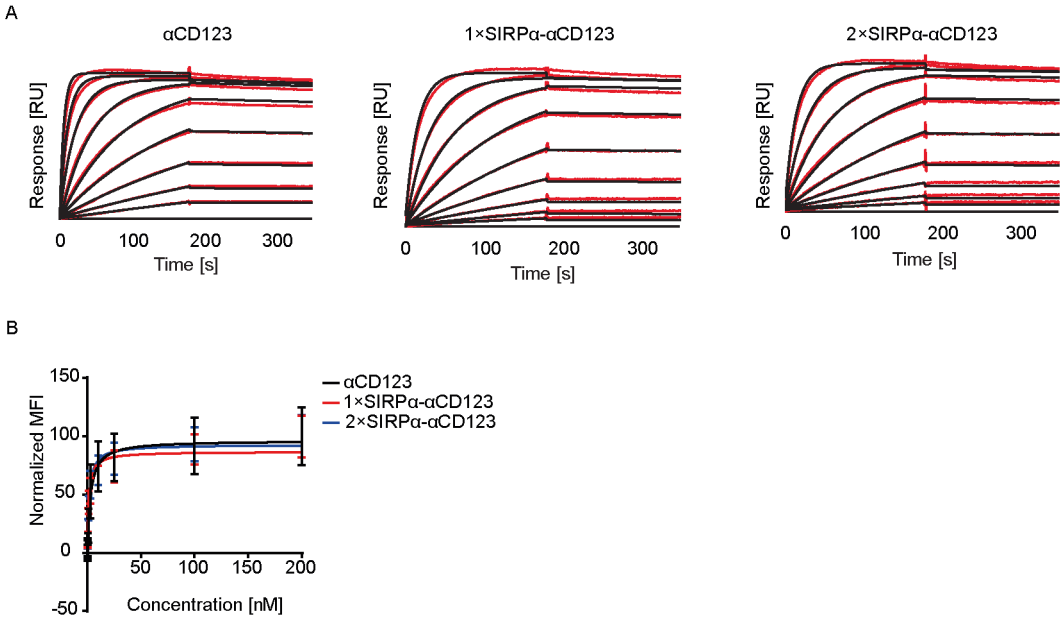

Figure 6. K_D measurements of αCD123 and SIRPα-αCD123-fusion antibodies. (A) Representative SPR profiles from 1 out of 3 Biacore measurements. Different concentrations of CD123 extracellular domain were used as an analyte binding to the antibodies. Raw data are in red; black curves were fitted to 1:1 interaction. (B) Flow cytometry based K_D measurements using MOLM-13 cells that were incubated with increasing concentrations of antibodies.

Table 8. K_D values measured by SPR and flow cytometry.

	αCD123	**1×SIRPα-αCD123**	***p***	**2×SIRPα-αCD123**	***p***
SPR	1.20 ± 0.59 nM	2.74 ± 1.1 nM	ns	2.34 ± 1.1 nM	ns
Flow cytometry	2.90 ± 0.46 nM	1.39 ± 0.38 nM	**	1.72 ± 0.30 nM	*

Mean ± standard deviation (SD) of n=3 experiments. Statistical differences were determined in comparison to αCD123.

Flow cytometry-based studies were performed to characterize the binding properties of the SIRPα-αCD123 fusion antibodies. Two CHO based cell lines were used to evaluated the functionality of the SIRPα domain within the fusion antibodies. The CHO^{CD47+} cells are stably transfected and express high levels of human CD47 whereas the control cells CHO^{CD47-} are negative (Table 9). As expected, 1×SIRPα-αCD123 and 2×SIRPα-αCD123 bound to CHO^{CD47+} cells but not to CHO^{CD47-} cells indicating that the SIRPα domain is able to target CD47 when fused to the αCD123 antibody (Figure 7).

Table 9. Average surface antigen expression levels per cell.

Cells	CD123	CD47	CD19
CHO^{CD47+}	104 ± 68	1 424 894 ± 329 869	n. d.
CHO^{CD47-}	159 ± 50	532 ± 35	n. d.
MOLM-13	13 723 ± 1 108	67 703 ± 3 784	30 ± 2
RBC	106 ± 33	33 841 ± 2 221	n. d.
Raji	94 ± 95	170 868 ± 37 029	141 688 ± 19 997

Expression levels were determined by QIFIKIT. Data are means ± standard error of the mean (SEM, *n*=2 - 3). Not determined (n. d.).

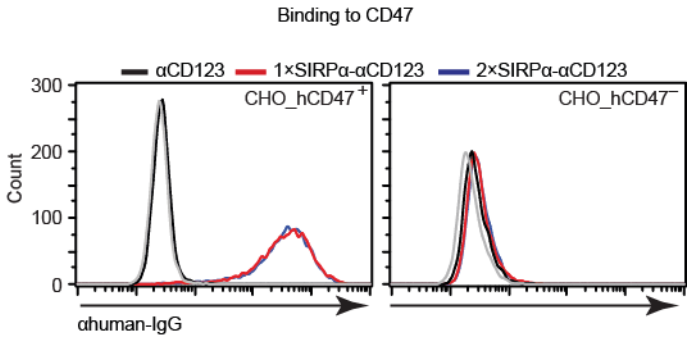

Figure 7. CD47 binding by the SIRPα-αCD123-fusion antibodies. Binding of antibodies to CHO^{CD47+} and CHO^{CD47-} cells was measured by flow cytometry. Grey line indicates unspecific staining of the isotype control and secondary antibody. Histograms show 1 of 3 experiments with similar results.

4.1.2.2. Binding to target cell line MOLM-13

The AML cell line MOLM-13 expresses both CD47 and CD123 and was selected as a target cell line for functional studies (Table 9). Flow cytometry was used to analyze the binding of SIRPα-αCD123 fusion antibodies to MOLM-13 cells. In agreement with increased avidity (Table 8), 1×SIRPα-αCD123 and 2×SIRPα-αCD123 showed higher overall binding to MOLM-13 cells than the αCD123 antibody indicating a contribution by the SIRPα domain (Figure 8A). MOLM-13 cells do not express CD19 (Table 9) and thus, αCD19 based SIRPα fusion antibodies were used as controls. The 1×SIRPα analogue did not bind to MOLM-13 cells and the 2×SIRPα fusion demonstrated only a low level of binding which is most likely facilitated through the four SIRPα domains.

The physiological interaction of the SIRPα domain and CD47 is about 100-fold weaker than the affinity of the αCD123 antibody for CD123 [146, 148]. Preferential binding to $CD123^{+}$ $CD47^{+}$ leukemic cells in the presence of $CD123^{-}$ $CD47^{+}$ healthy cells is therefore hypothesized

for the SIRPα-αCD123 fusion antibodies due to the high affinity αCD123 domain. RBCs are highly abundant healthy $CD47^+$ cells that are readily targeted by the CD47 targeting agents such as αCD47 antibodies [149, 167, 274]. To investigate whether SIRPα-αCD123 fusion antibodies selectively target AML cells, MOLM-13 cells were mixed with 20-fold excess of RBCs in a competitive binding assay and the percentage of either cell type bound by the antibody was analyzed. A strong preferential binding to MOLM-13 cells was observed with the αCD123 and 1×SIRPα-αCD123 antibodies (Figure 8B). The preferential binding to MOLM-13 cells was less pronounced with the 2×SIRPα-αCD123. In contrast, the high affinity αCD47 antibody (B6H12), demonstrated a substantial on-target off-leukemia effect and bond primarily to RBCs. Binding of the antibodies was also analyzed by MFI ratio on both the MOLM-13 and RBC population (Figure 8C and D). Surprisingly, the MFI ratio for αCD123 antibody binding to MOLM-13 cells was slightly below the binding threshold in the presence of 20-fold excess of RBCs while both of the SIRPα-αCD123 antibodies bound well. The measured MFI ratio was highest for the αCD47 antibody. Nevertheless, the RBCs did not bind αCD123 and 1xSIRPα-αCD123 antibodies and the little binding observed for 2×SIRPα-αCD123 was very weak falling far below the threshold. αCD47 antibody bound to RBCs similar what was observed for MOLM-13. In summary, the results of the competitive binding assay show that although the additional SIRPα domains increase the competition between MOLM-13 cells and RBCs, the αCD123 still guides the SIRPα-αCD123 antibodies preferentially to $CD123^+$ cells.

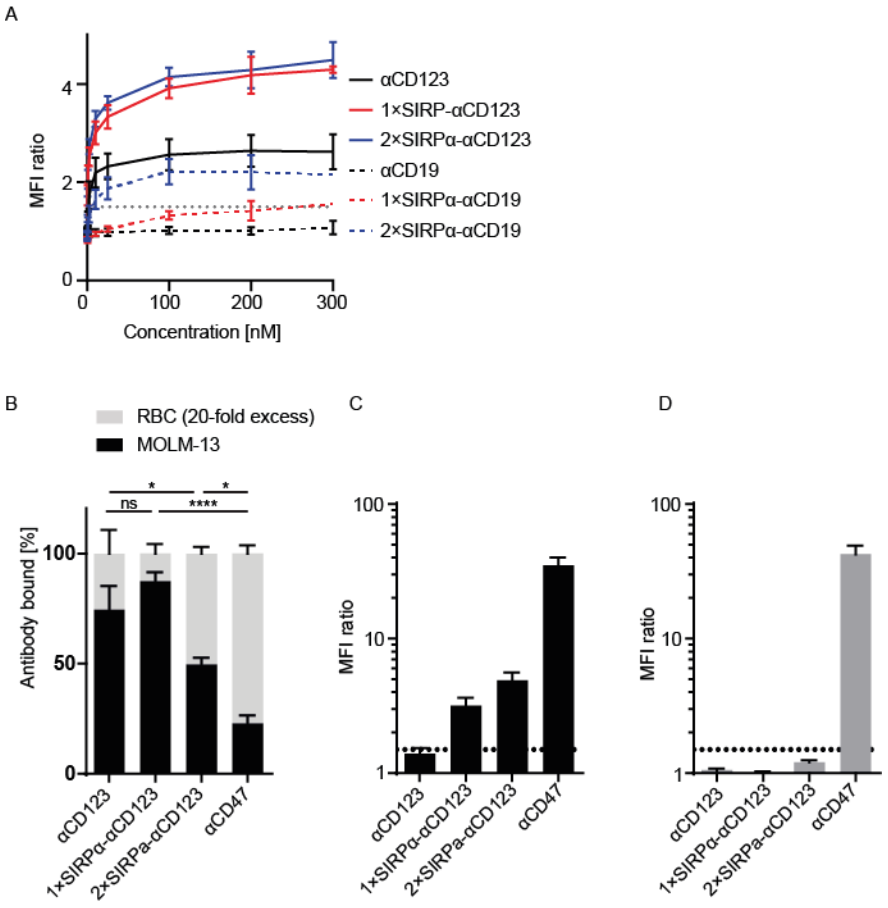

Figure 8. Competitive binding of SIRPα-αCD123-fusion antibodies to MOLM-13 in the presence of RBCs. (A) Binding of αCD123, 1×SIRPα-αCD123 and 2×SIRPα-αCD123 or respective αCD19 control antibodies to MOLM-13 cells was measured by flow cytometry. Shown are mean values from *n*=3 experiments (*n*=2 for 2×SIRPα-αCD19) ± SEM. (B) Percentage of 100 nM antibodies bound to MOLM-13 or RBCs measured by flow cytometry. Shown are results from *n*=4 RBC donors ± SEM. (C) Binding of the antibodies to only MOLM-13 cells in 20-fold excess of RBCs. (D) Binding of the antibodies to RBCs in the same conditions. *n*=4. Dotted line indicates MFI ratio of 1.5 as cut-off for positive expression.

4.1.3. Functional characterization of SIRPα-αCD123 fusion antibodies

4.1.3.1. SIRPα-αCD123-mediated CD47 blockade on AML cells

SIRPα-αCD123 fusion antibodies were designed to interfere with the CD47/SIRPα axis locally on $CD123^{+}$ cells. To measure the blocked CD47 sites due to SIRPα-αCD123 fusion antibody binding, a flow cytometry-based detection of labeled αCD47 antibodies that interfere with the binding of SIRPα was performed using MOLM-13 cells. The 1×SIRPα-αCD123 and 2×SIRPα-αCD123 were able to block a significant amount of CD47 molecules on MOLM-13 cells and, not surprisingly, a maximum blockade was seen with the high affinity αCD47 antibody (Figure 9A). In comparison, the αCD19 control molecule with 1×SIRPα did not block CD47 on MOLM-13 cells and although the 2×SIRPα control showed some blockade, it was lower than for the 2×SIRPα-αCD123 antibody (Figure 9A). The 1×SIRPα-αCD123 likewise did not block CD47 on $CD123^{-}$ Raji cells and the 2×SIRPα-αCD123 blocked significantly less CD47 than

the respective αCD19 control molecule that do bind to $CD19^+$ Raji cells (Table 9, Figure 9B). These results indicate that the high affinity αCD123 moiety is essential for an efficient disruption of the CD47/SIRPα axis on $CD123^+$ target cells.

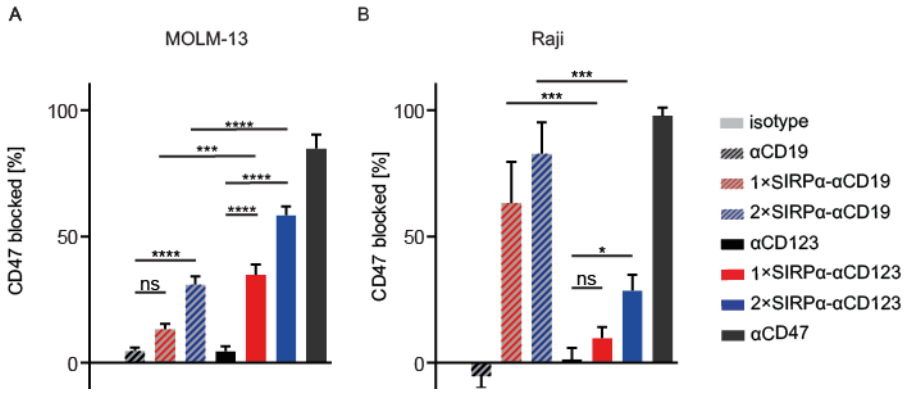

Figure 9 Blockade of CD47 on $CD123^+$ MOLM-13 and $CD123^-$ Raji cells. (A) CD47 blockade on MOLM-13 cells with 100 nM antibodies was determined by FITC αCD47 binding using flow cytometry. Mean ± SEM of *n*=4 experiments are shown. (A) CD47 blockade on $CD123^-$ $CD19^+$ Raji cells. Mean ± SEM of *n*=3 experiments are shown.

4.1.3.2. Phagocytosis of MOLM-13 cells induced by the SIRPα-αCD123 antibodies

The major goal for the SIRPα-αCD123 antibodies is to boost the macrophage-mediated immune control of AML. Phagocytosis of MOLM-13 cells by HD-derived macrophages was thereby analyzed using flow cytometry. 50 nM concentration was first chosen based on preclinical studies with αCD47 antibodies B6H12 and Hu5F9-G4 [73, 274]. 1×SIRPα-αCD123 and 2×SIRPα-αCD123 both induced significantly higher phagocytosis compared to αCD123 (Figure 10A). The αCD47 induced the highest phagocytosis alone and this was not boosted by combining it with the αCD123 antibody. Surprisingly, the corresponding αCD19 controls, induced similar phagocytosis levels as the SIRPα-αCD123 fusion antibodies. When analyzing a 1000-fold lower concentration, 1×SIRPα-αCD123 significantly enhanced the phagocytosis compared to αCD123 (Figure 10B). Similarly, 2×SIRPα-αCD123 induced higher phagocytosis, albeit it was not statistically significant. αCD19 controls and the αCD47 could not stimulate phagocytosis in the lower concentration, demonstrating a therapeutic window for the beneficial effect of local CD47 blockade on AML cells by SIRPα-αCD123 fusion antibodies. The selective phagocytosis induced by SIRPα-αCD123 antibodies over unspecific SIRPα binding was further confirmed when target cells were incubated with 1 nM concentration of antibodies prior the ADCP assay. This experiment demonstrated that the 1×SIRPα-αCD123 induced a clearly higher phagocytosis than the respective SIRPα binding control antibody (Figure 10C).

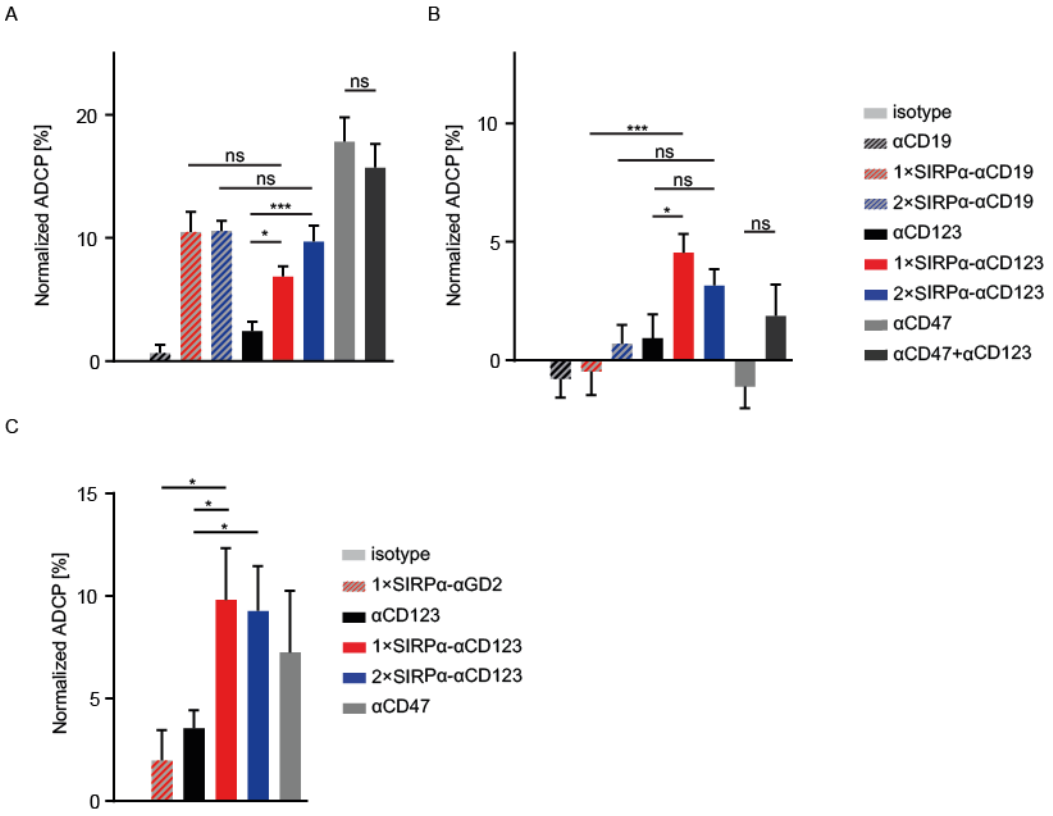

Figure 10. Phagocytosis of MOLM-13 cells. (A) ADCP of MOLM-13 cells at 50 nM concentration. Shown are mean ± SEM from experiments with *n*=6-11 different macrophage donors. (B) ADCP of MOLM-13 cells at 50 pM concentration. Shown are mean ± SEM from experiments with *n*=5-7 macrophage donors. (C) ADCP of MOLM-13 cells after incubation with 1 nM antibody concentration. Shown are mean ± SEM from experiments with 6 macrophage donors.

4.1.3.3. SIRPα-αCD123-mediated phagocytosis of primary AML cells

Patient-derived AML blasts were next used as targets cells and allogeneic HD macrophages as effectors to investigate the effect of the SIRPα-αCD123 fusion antibodies in an AML patient setting. Significantly higher ADCP was observed with both the 1×SIRPα-αCD123 and 2×SIRPα-αCD123 fusion antibodies compared to the αCD123 (Figure 11A). Importantly, these results were confirmed in an autologous setting where AML target cells and effector macrophages were derived from the same patient (Figure 11B). Phagocytosis mediated by 1×SIRPα-αCD123 and 2×SIRPα-αCD123 was significantly higher than observed for the αCD123. αCD47 alone and in combination with αCD123 antibody did not induce more phagocytosis than the SIRPα-αCD123 fusion antibodies with both allogeneic and autologous macrophages. Taken together, the bifunctional SIRPα-αCD123 antibodies induce potent macrophage-mediated ADCP of primary AML patient samples *in vitro* due to simultaneous targeting of $CD123^{+}$ cells and CD47 blockade.

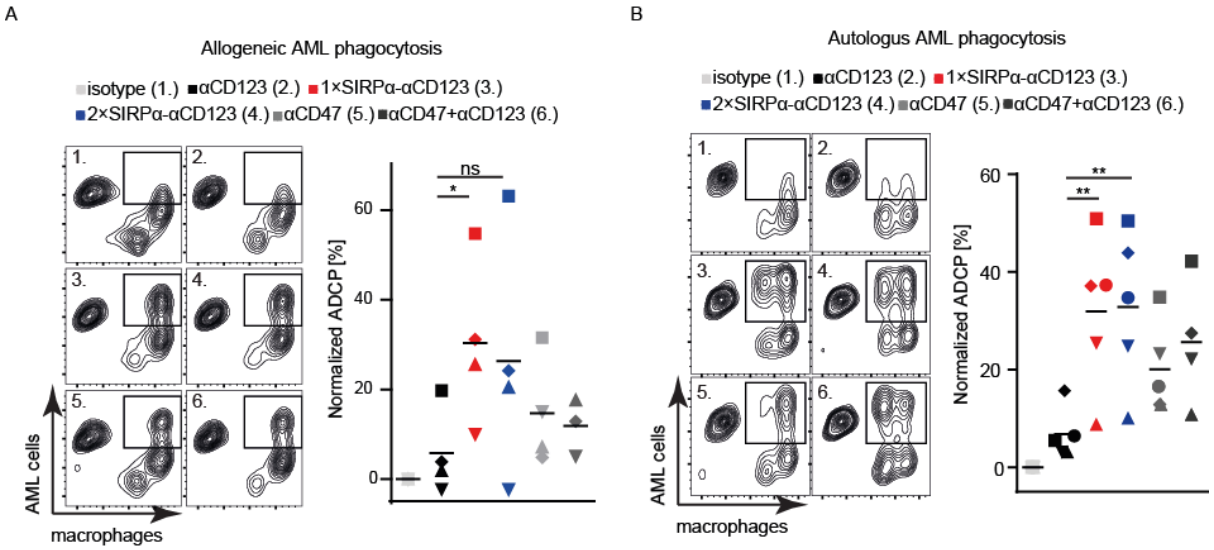

Figure 11. Phagocytosis of AML patient cells. (A) Phagocytosis of AML patient cells by allogeneic macrophages (*n*=3-4). (B) Phagocytosis of AML patient cells by autologous macrophages (*n*=4-5). On the left are examples of flow cytometry plots of raw data where ADCP is the % of double positive cells (gated) from all macrophages. On the right is the mean of normalized results of independent experiments with individual patients represented by different symbols.

A higher overall phagocytosis was observed with primary AML cells compared to MOLM-13 cells. An analysis of cell surface marker expression revealed that although both the cell line and primary AML cells express CD123 and CD47, MOLM-13 differ from the primary cells cells by having higher levels of the SIRPα as well as by expressing the FcγRII, known as CD32, which might interfere with the fusion antibody binding (Figure 12A and B). Both HD and AML patient-derived macrophages were positive for CD47, CD16 (FcγRIII), CD32, CD64 (FcγRI) and SIRPα (Figure 12C and D). CD123 was not expressed on HD and patient-derived macrophages whereas the AML target antigen CD33 was highly expressed.

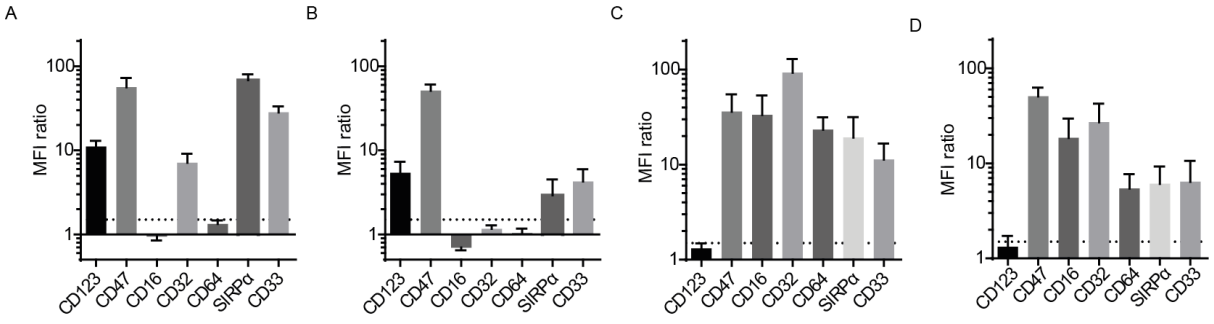

Figure 12. Expression of cell surface antigens. MFI ratios were calculated from flow cytometry measurements. (A) MOLM-13 cells (*n*=5-9). (B) Primary AML blasts (*n*=5-8). (C) HD-derived macrophages (*n*=4-5). (D) AML patient-derived macrophages (*n*=4-5). Dotted line indicates MFI ratio of 1.5 as cut-off for positive expression.

4.1.3.4. SIRPα-αCD123 antibody-mediated cytotoxic lysis of AML cells

In addition to ADCP, IgG1 antibodies facilitate NK cell-mediated ADCC, which is one of the main mechanisms by which antibody-bound cancer cells are eliminated by the immune system

[260]. The specific lysis induced by SIRPα-αCD123 antibodies was thereby analyzed by measuring the release of Calcein AM induced by HD-derived NK cells. αCD123 induced a moderate dose-dependent lysis of MOLM-13 with 20% of lysis in the highest concentration (Figure 13A). 1×SIRPα-αCD123 and 2×SIRPα-αCD123 were more potent in inducing cell death reaching higher maximum lysis of approximately 40% (Figure 13A). The respective αCD19 controls killed MOLM-13 cells only at high concentrations (Figure 13A). This is attributed to autonomous targeting of CD47 by the fused SIRPα domains and corresponds to a more prominent effect seen with the 2×SIRPα αCD19 control molecule which carries more SIRPα domains. A specific αCD123-facilitated cytotoxicity is nevertheless demonstrated for the SIRPα-αCD123 fusion antibodies as the 50% effective concentration (EC_{50}) was considerably lower for the 2×SIRPα-αCD123 (19.1 pM) compared to the 2×SIRPα αCD19 analogue (192.1 pM).

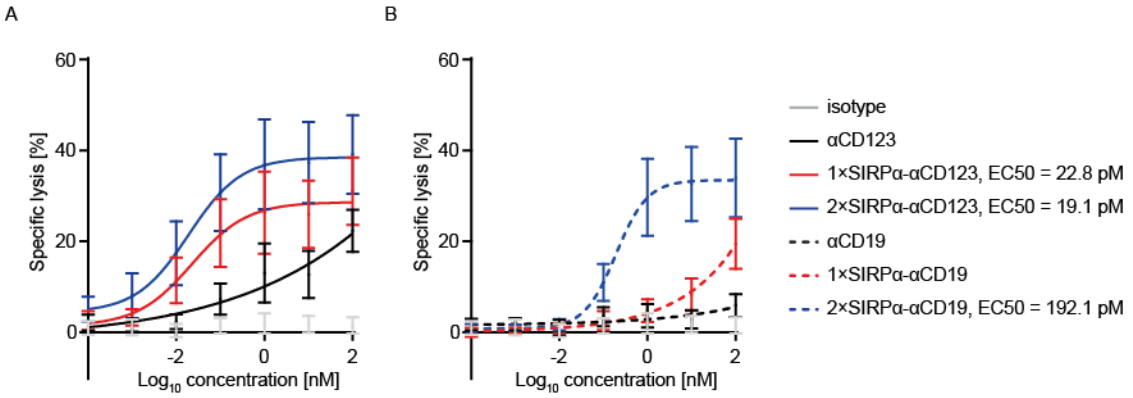

Figure 13. NK cell-mediated lysis of MOLM-13 cells. αCD123, 1xSIRPα-αCD123 and 2xSIRPα-αCD123 antibodies (A) or respective αCD19 controls (B) in a dose-dependent lysis assay of MOLM-13 cells measured by Calcein AM release. Shown are mean values ± SEM of *n*=6 different NK cell donors. EC50 values were calculated where possible.

As SIRPα-αCD123 can bind to both CD123 and CD47, a more efficient targeting of $CD123^+$ $CD47^+$ double positive cells over $CD47^+$ single positive cells are expected from the fusion antibodies. In order to evaluate this, ADCC assay with a 1:1 mixed population of $CD123^+$ MOLM-13 and $CD123^-$ Raji cells was performed. In this setting, MOLM-13 were lysed efficiently by SIRPα-αCD123 antibodies, whereas Raji cells were not lysed by the 1×SIRPα-αCD123 and 2×SIRPα-αCD123 induced lower lysis only at high concentrations (Figure 14). These results suggest that SIRPα-αCD123 preferentially induce killing of $CD123^+$ AML cells and not healthy cells.

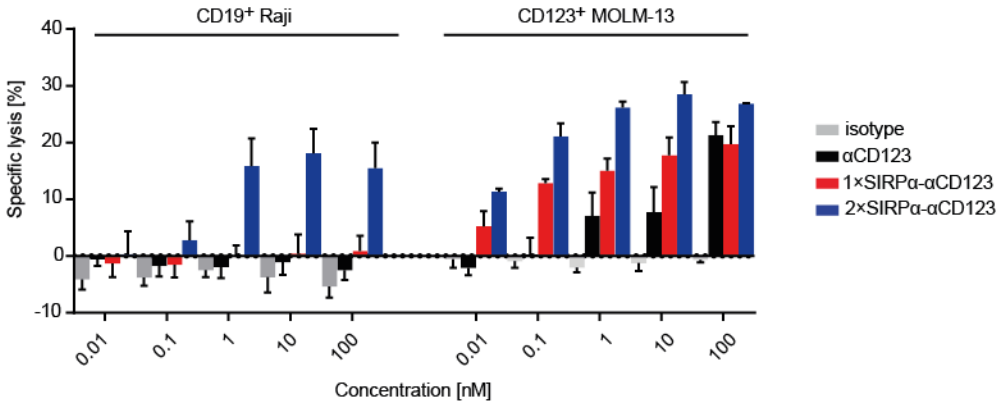

Figure 14. NK cell-mediated lysis of CD123$^+$ MOLM-13 or CD123$^-$ Raji cells in a competitive ADCC assay. (A) Dose-dependent lysis of either MOLM-13 or Raji cells in a 1:1 mixture of both measured form the indicated cell line by Calcein AM release. Shown are mean values ± SEM from experiments with *n*=2 NK cell donors for MOLM-13 and *n*=3 for Raji.

4.1.3.5. Cytotoxic lysis of AML patient-derived cells

The ability to specific lysis induced by SIRPα-αCD123 antibodies was further investigated using AML PDX cells. The cells were established in the laboratory of Irmela Jeremias by injecting primary AML patient cells into immunocompromised mice and selecting for samples capable of serial transplantation, a characteristic of an aggressive disease [266, 267]. The PDX cells were genetically engineered to express firefly luciferase for bioluminescence imaging *in vivo* and mCherry for flow cytometry analysis [266]. 57% and 18% of live AML cells could be detected after the ADCC with 1×SIRPα-αCD123 and 2×SIRPα-αCD123, respectively (Figure 15). Thus, both of the molecules induced a dramatic lysis of AML PDX cells which was significantly higher than the lysis mediated by αCD123 antibody.

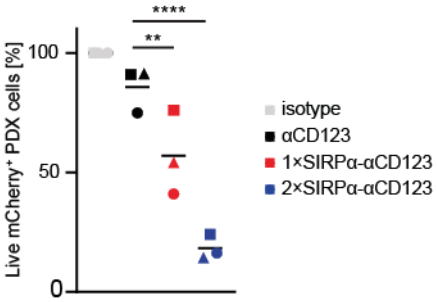

Figure 15. NK cell-mediated lysis of patient derived xenograft (PDX) cells. The percentage of live PDX cells was measured after an ADCC assay with αCD123, 1xSIRPα-αCD123 and 2xSIRPα-αCD123 antibodies. Results from *n*=3 AML patient samples, represented by different symbols, and their mean values are shown.

The lysis of PDX cells was demonstrated with three AML PDX samples (AML-491, AML-797, AML-640) using NK cells from a single HD. To evaluate the killing by NK cells from different donors, two AML PDX patient samples were chosen for further analysis. AML-491 and AML-579 both express high levels of CD123 and CD47 (Figure 16A). A pronounced lysis

of the PDX cells compared to the isotype control was observed for αCD123, but the SIRPα fusion antibodies induced a significantly higher lysis than αCD123 (Figure 16B and C).

The major goal in AML therapy is to target LSCs to prevent relapse and enhance the rate and duration of response in patients. As AML LSC express high levels of both CD123 and CD47 [73, 221], SIRPα-αCD123 fusion antibodies are expected to specifically target the LSC population. LSCs are considered to reside within the $CD34^{+}/CD38^{-}$ cell fraction [210, 275] and the prevalence of this population was analyzed by flow cytometry after ADCC with SIRPα-αCD123 fusion antibodies. The number of $CD34^{+}/CD38^{-}$ PDX cells greatly decreased after the ADCC and 2×SIRPα-αCD123 reduced the number of LSCs significantly more than the αCD123 antibody (Figure 16C and D).

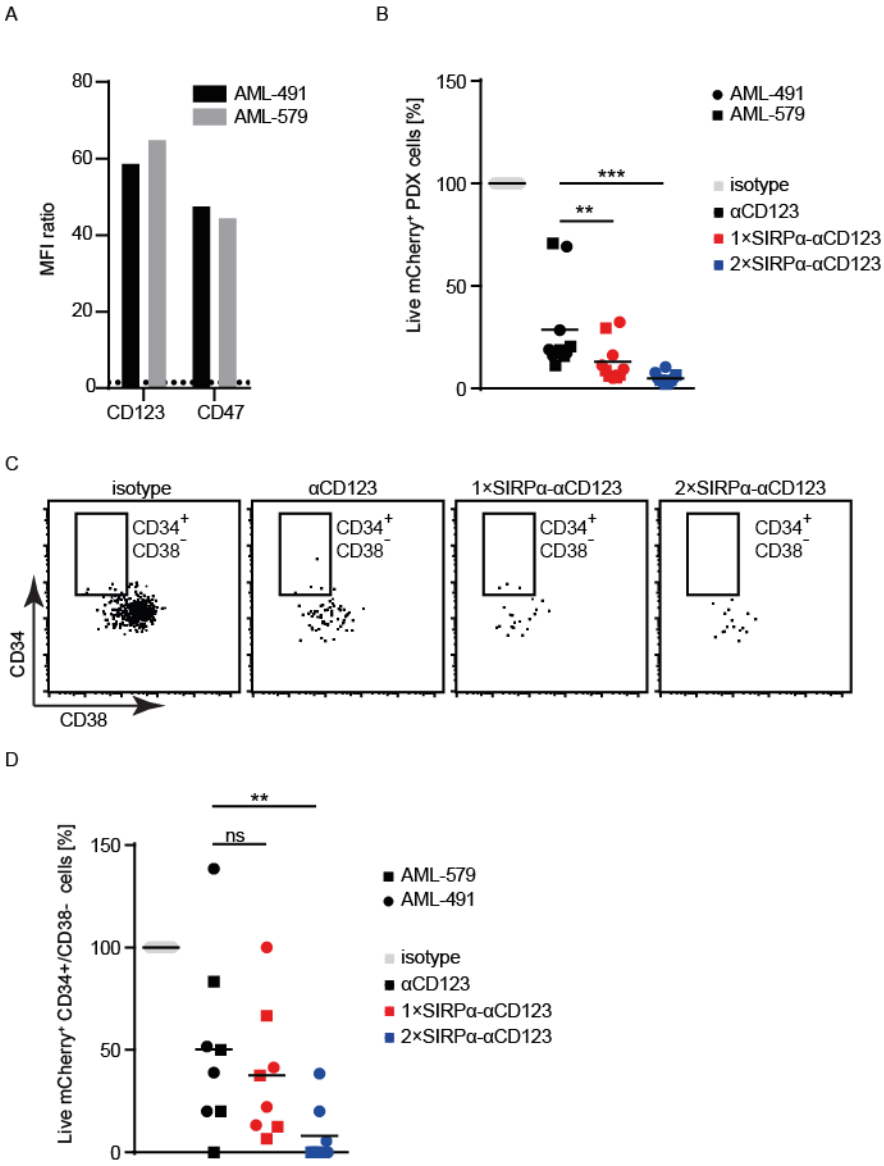

Figure 16. NK cell-mediated lysis of AML PDX cells and the $CD34^{+}/CD38^{-}$ population. (A) Phenotype of AML-491 and AML-579 PDX cells. (B) The number of live PDX cells was measured after an ADCC assay. Results from *n*=5 HD NK donors for both AML-579 and AML-491 patient samples. (C) Representative flow cytometry plots of $mCherry^{+}$ AML-PDX $CD34^{+}/CD38^{-}$ leukemic

stem cells after the ADCC assay. (D) The count of $CD34^+/CD38^-$ cells from all live $mCherry^+$ cells are normalized to isotype control. *n*=4 HD NK donors for both AML-579 and AML-491 patient samples

4.1.3.6. Selective targeting of AML stem cells by the SIRPα-αCD123 fusion antibodies

Despite the promising results regarding LSCs targeting by the SIRPα-αCD123 fusion antibodies observed in ADCC assays *in vitro*, the numbers of $CD34^+/CD38^-$ cells were generally low in all samples. This is a feature of the PDX cells that has been observed by others as well [267] and makes the analysis of the data complicated. Therefore, the activity of LSCs was further analyzed in a functional *in vivo* engraftment assay using a xenograft mouse model [266]. These assays have been widely used to investigate LIC population as a surrogate for LSCs [275-277]. To evaluate the impact of our antibodies on targeting LICs, an *ex vivo* ADCC was performed with AML-491 and AML-579 PDX cells. Next, the surviving PDX cells were separated from NK cells by FACS and injected into NSG mice at two doses corresponding to 10/14×LIC and 100/140×LICs (Figure 17A). The LIC frequencies in these samples have been previously determined [267]. AML engraftment was analyzed by BLI (Figure 17A). The *in vivo* experiment was performed in collaboration with Binje Vick from the laboratory of Irmela Jeremias.

2×SIRPα-αCD123 was chosen from the SIRPα fusion antibodies, as AML PDX cells and, importantly, the $CD34^+/CD38^-$ population was targeted most efficiently by this molecule (Figure 15, Figure 16B-D). Similar to previously observed results, PDX cells were potently lysed by the 2×SIRPα-αCD123 antibodies in the *ex vivo* ADCC assay (Figure 17B). Of note, slightly more AML-579 than AML-491 cells were viable in the 2×SIRPα-αCD123 condition (Figure 17B).

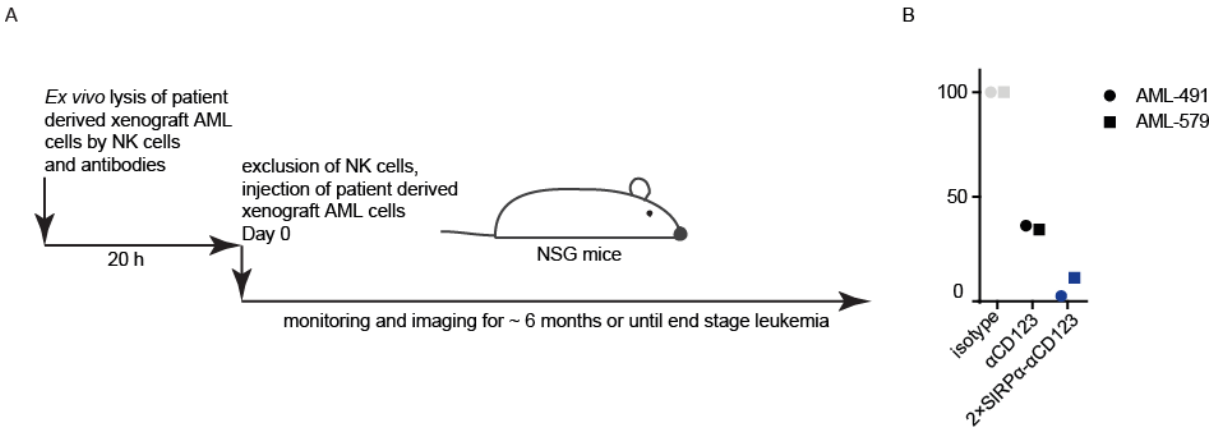

Figure 17. *Ex vivo* NK cell-mediated lysis of AML-491 and AML-579 PDX cells. (A) Setup of the engraftment assay. (B) Percentage of live PDX cells was measured by FACS after an ADCC assay with isotype control, αCD123 and 2×SIRPα-αCD123 antibodies before *in vivo* engraftment.

For analyzing the LIC targeting in AML-491 patient sample, 5 mice were injected with 10×LIC and 100×LIC doses of the isotype control treated cells. Respective volumes of αCD123 and

2×SIRPα-αCD123 antibody treated cells were both injected to 5 mice. Three mice died in narcosis during imaging and were counted as positive according to the last imaging signal or were excluded if not engrafted. As shown in Figure 18 A-B and Table 10, all mice that received isotype control treated AML-491 cells showed PDX engraftment soon after transplantation. Treatment with the αCD123 antibody delayed time to positive engraftment and, strikingly, residual cells from 2×SIRPα-αCD123 cultures showed nearly no engraftment capacity (Figure 18A-B, Table 10). In Figure 18C-D representative images of the BLI analysis from day 62 are shown. In Figure 18E, the analysis of engraftment probability confirmed a statistically significant difference between the αCD123 and 2×SIRPα-αCD123 treatments. Correspondingly, all mice with positive engraftment reached end stage leukemia fast (Figure 18F).

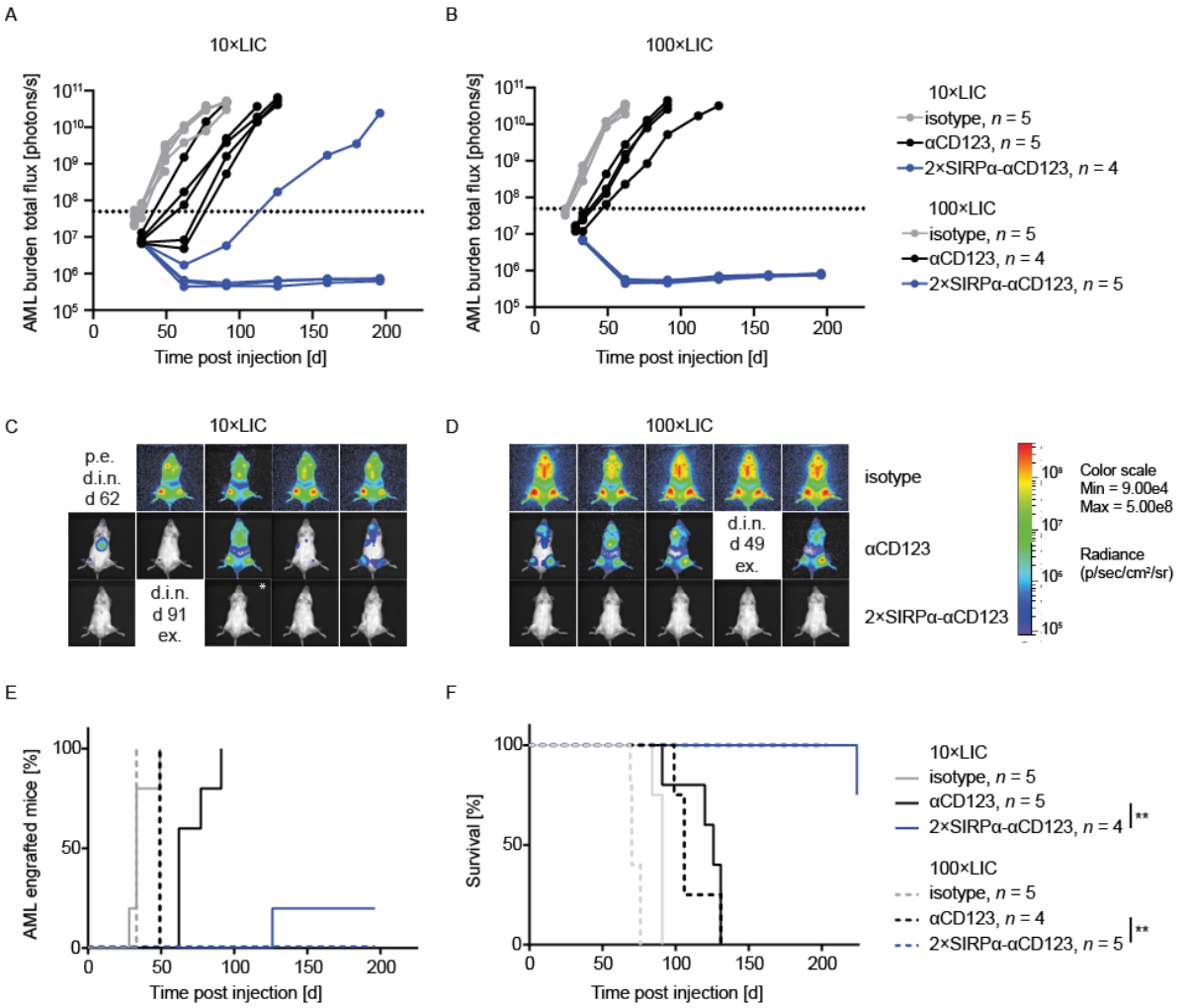

Figure 18. Engraftment of AML-491 PDX samples. (A-B) AML burden in individual mice of the 10×LIC and 100×LIC groups was measured by quantifying the BLI signal. Dotted line indicates total flux of 5×107 photons/s as cut-off for evaluating positive AML engraftment. 10×LIC (C) and 100×LIC (D) engraftment visualized on day (d) 62. Mice that died in narcosis during imaging (d. i. n.) were counted as positive if the last imaging signal showed positive engraftment (p. e.) or were excluded from analysis (ex.) if not engrafted. (E) Positive engraftment analysis. (F) Survival analysis.

For AML-579, 4 mice were injected with 14×LIC and 2 mice with 140×LIC dose of the isotype control treated cells. Same number of mice were injected with respective volumes of αCD123 and 2×SIRPα-αCD123 antibody treated cells. Similar results as for AML-491 were observed (Figure 19A-B, Table 10). Mice who received 14×LIC dose of the isotype treated cells showed early engraftment and most of the mice receiving αCD123 antibody treated cells engrafted soon after. All mice that were injected with the 14×LIC dose of the residual cells from 2×SIRPα-αCD123 cultures did not engraft and both animals in the 100×LIC group demonstrated delayed engraftment. Figures 19C-D contain representative images of the BLI analysis from day 63. A significantly reduced engraftment probability could be demonstrated between the αCD123 and 2×SIRPα-αCD123 treatments in the 14×LIC cohort (Figure 19E). All mice with positive engraftment reached end stage leukemia fast (Figure 19F).

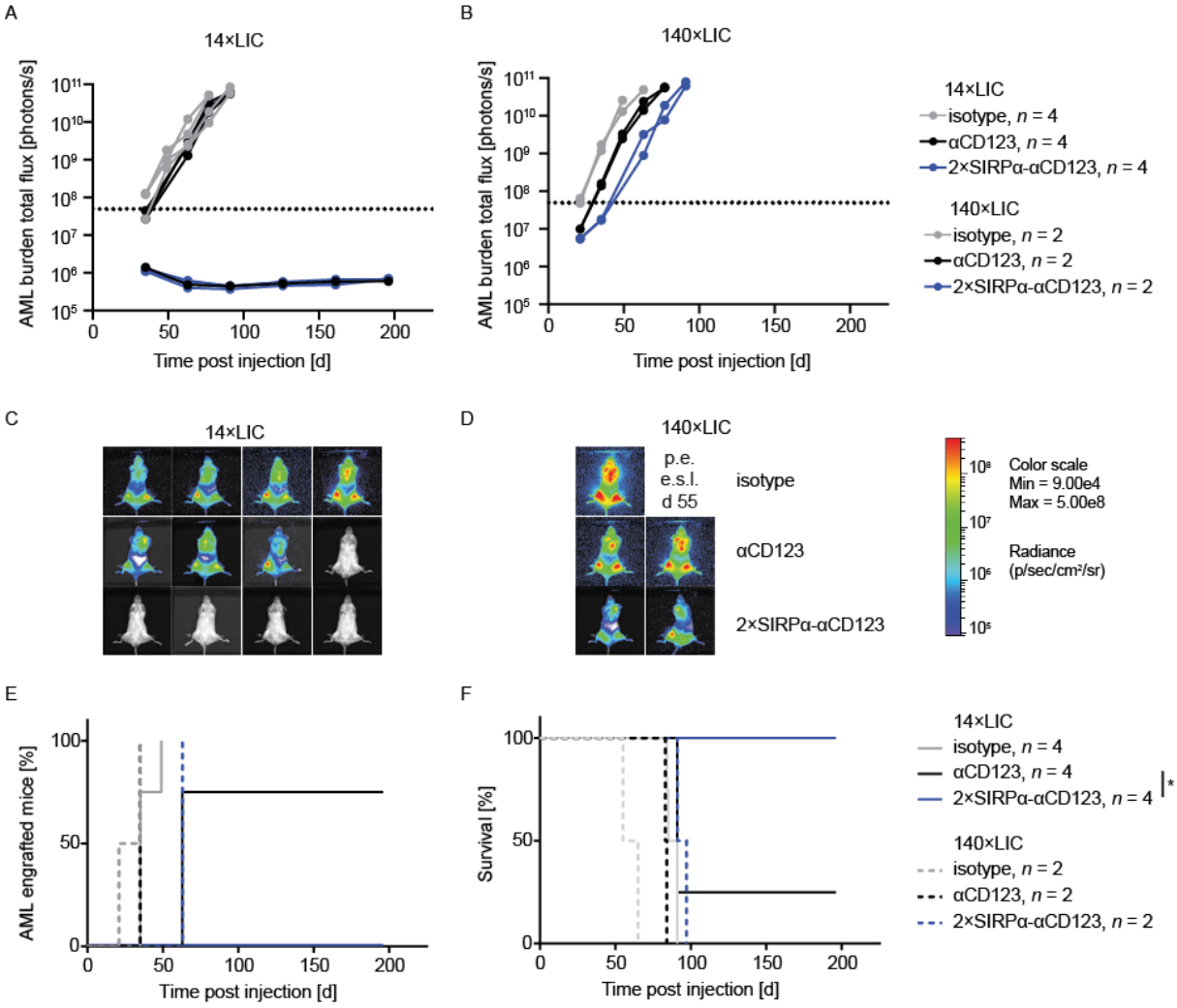

Figure 19. Engraftment of AML-579 PDX samples. (A, B) AML burden in individual mice of the 14×LIC and 140×LIC groups was measured by quantifying the BLI signal. Dotted line indicates total flux of 5×107 photons/s as cut-off for evaluating positive engraftment. AML-5791 14×LIC (C) and 140×LIC (D) engraftment visualized on day (d) 63. Mice that died in narcosis during imaging (d. i. n.) were counted as positive if the last imaging signal showed positive engraftment (p. e.) or were excluded (ex.) if not engrafted. End stage leukemia (e. s. l.). (E) Positive engraftment analysis. (F) Survival analysis.

Overall, the AML-579 showed a slightly earlier engraftment, which is expected due to a higher LIC cell dose the mice receive compared to the AML-491 (Table 10). Nevertheless, 2×SIRPα-αCD123 could target LICs in both patient samples significantly more than αCD123.

Table 10. Engraftment days. Number of mice/mice injected in parenthesis.

		Isotype control	**αCD123**	**2×SIRPα-αCD123**
AML-491	10×LIC	28 – 49 (5/5)	62-91 (5/5)	no engraftment (3/4)
				114 (1/4)
	100×LIC	33 (5/5)	49 (4/4)	no engraftment (5/5)
AML-579	14×LIC	35 – 49 (4/4)	no engraftment (1/4)	no engraftment (4/4)
			63 (3/4)	
	140×LIC	21 and 35 (2/2)	35 (2/2)	63 (2/2)

To determine whether the nearly absent engraftment in the 2×SIRPα-αCD123 condition was due to specific LIC targeting or as a result of lower number of residual cells injected, LIC frequencies were analyzed by ELDA algorithm [272]. Even though all mice in the isotype and αCD123 treatment groups showed engraftment, ELDA can give estimations of LIC frequencies even in cases with 0% or 100% responses [272]. A significant difference in the estimated LIC frequencies was detected between αCD123 and 2×SIRPα-αCD123 treatments, concluding that although 2×SIRPα-αCD123 markedly reduces the numbers of bulk AML, it targets leukemic stem cells with even higher preference (Table 11, Figure 20).

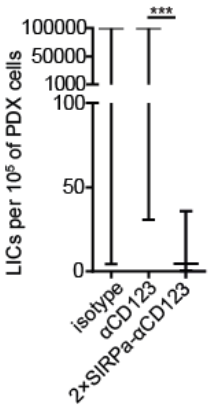

Figure 20. Leukemia-initiating cell (LIC) frequencies. Estimations of LIC frequencies with 95% confidence intervals were calculated with the ELDA software [272] (related to Table 11).

Taken together, the results of the first part of the thesis demonstrate that the bifunctional SIRPα-αCD123 antibodies selectively target AML cells and efficiently recruit macrophages to overcome the CD47 induced inhibition of phagocytosis of primary AML patient blasts *in vitro.* In addition, 2×SIRPα-αCD123 also effectively targets LSCs as demonstrated by the *in vivo* engraftment assay.

Table 11. Estimated LIC frequencies of AML PDX samples after NK cell-mediated lysis with the SIRPα-αCD123 fusion antibodies

Sample	Number of injected cells	Number of mice injected / engrafted	Estimated LIC frequency (95% confidence interval)
AML-491, isotype	180 000	5 / 5	1/1 (1/1 - 1/22 575)
	1800	5 / 5	
AML-491, αCD123	26 000	4 / 4	1/1 (1/1 - 1/3 261)
	2600	5 / 5	
AML-491, 2×SIRPα-αCD123	4 000	5 / 0	1/21 399(1/2 786 - 1/164 397)
	400	4 / 1	
AML-579, isotype	50 000	2 / 2	1/1 (1/1 - 1/7 800)
	5 000	4 / 4	
AML-579, αCD123	20 000	2 / 2	1/1 443 (1/424 – 1/4 908)
	2 000	4 / 3	
AML-579, 2×SIRPα-αCD123	3 000	2 / 2	1/1 674 (1/410 - 1/6 842)
	300	4 / 0	
Historic AML-491 [267]			1/1 799 (1/945 - 1/3 426)
Historic AML-579 [267]			1/351 (1/776-1/1 590)

Residual patient-derived xenograft cells were counted before injection during cell sorting and LIC frequencies were estimated using the ELDA software [272]. LIC frequencies of historic untreated AML-491 and AML-579 were previously determined by Ebinger et al. [267].

4.2. αGD2-SIRPα fusion antibodies targeting neuroblastoma

4.2.1. Generation and purification of αGD2-SIRPα fusion antibodies

To enhance the antitumor response of tumor associated macrophages in NBS, human SIRPα-αGD2 antibodies, that carry one SIRPα domain at the N-terminus of the LC, were generated (Figure 21). Initial screening of SIRPα-αGD2 revealed a decreased binding of these antibodies to human NBS cell line IMR-32 (data not shown). The proposed structure of GD2 and 14G2a antibody interaction indicates that the binding occurs close to the cell membrane [278]. The binding to the antigen could potentially be influenced by the fusion of the SIRPα domain to the N-terminal region of the αGD2 antibody LC by a $(Gly_4Ser)_4$ linker. The αGD2-SIRPα was thus generated by fusing the SIRPα domain to the C-terminal region of the αGD2 antibody HC with a longer $(Gly_4Ser)_8$ linker (Figure 21). Both SIRPα-αGD2 and αGD2-SIRPα and the αGD2 antibody were generated in human IgG1 and mouse IgG2a formats carrying the respective human or mouse SIRPα domains.

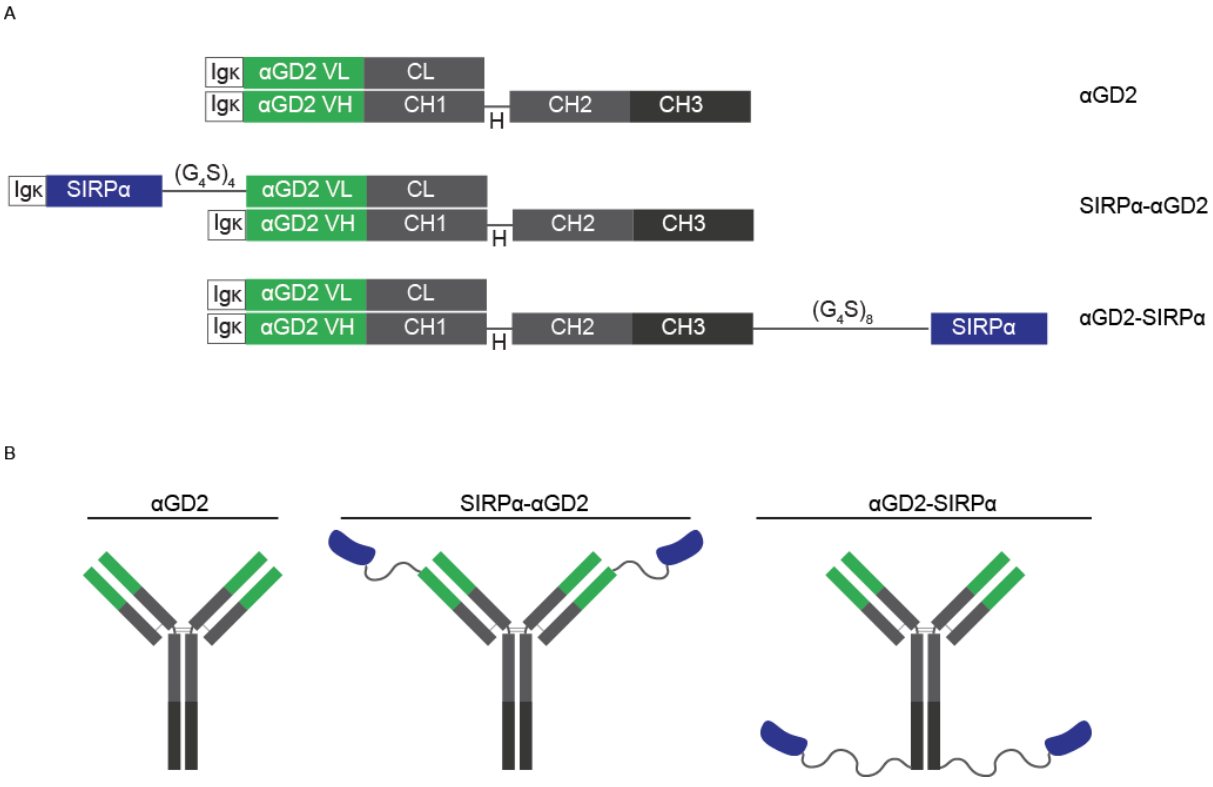

Figure 21. General schematic representation of the structure of the human and mouse αGD2 and SIRPα-fusion antibodies. (A) The encoding DNA constructs. Igκ is cleaved from the protein chain. The molecules were generated with regions of either human IgG1 or mouse IgG2a antibodies. VL – variable light, CL – constant light, VH – variable heavy, CH1 – constant heavy 1, CH2 – constant heavy 2, CH3 – constant heavy 3, H – hinge region. The N-terminal human or mouse SIRPα immunoglobulin V-like domain is fused to the αGD2 via a $(G_4S)_4$ linker. The C-terminal human or mouse SIRPα immunoglobulin V-like domain is fused to the αGD2 via a $(G_4S)_8$ linker. (B) Schematic drawings of the antibodies.

Protein A affinity chromatography followed by preparative SEC were used to purify the antibodies from Expi293F cell supernatant. A single peak was observed in the SEC chromatogram for the αGD2 and SIRPα-αGD2 antibodies whereas the αGD2-SIRPα showed a small additional aggregation peak, which was excluded from final protein preparation (Figure 22A, B). Purified proteins were analyzed by SDS-PAGE where the LCs and HCs corresponded to the computed masses with no detectable unspecific protein bands (Figure 22C, D).

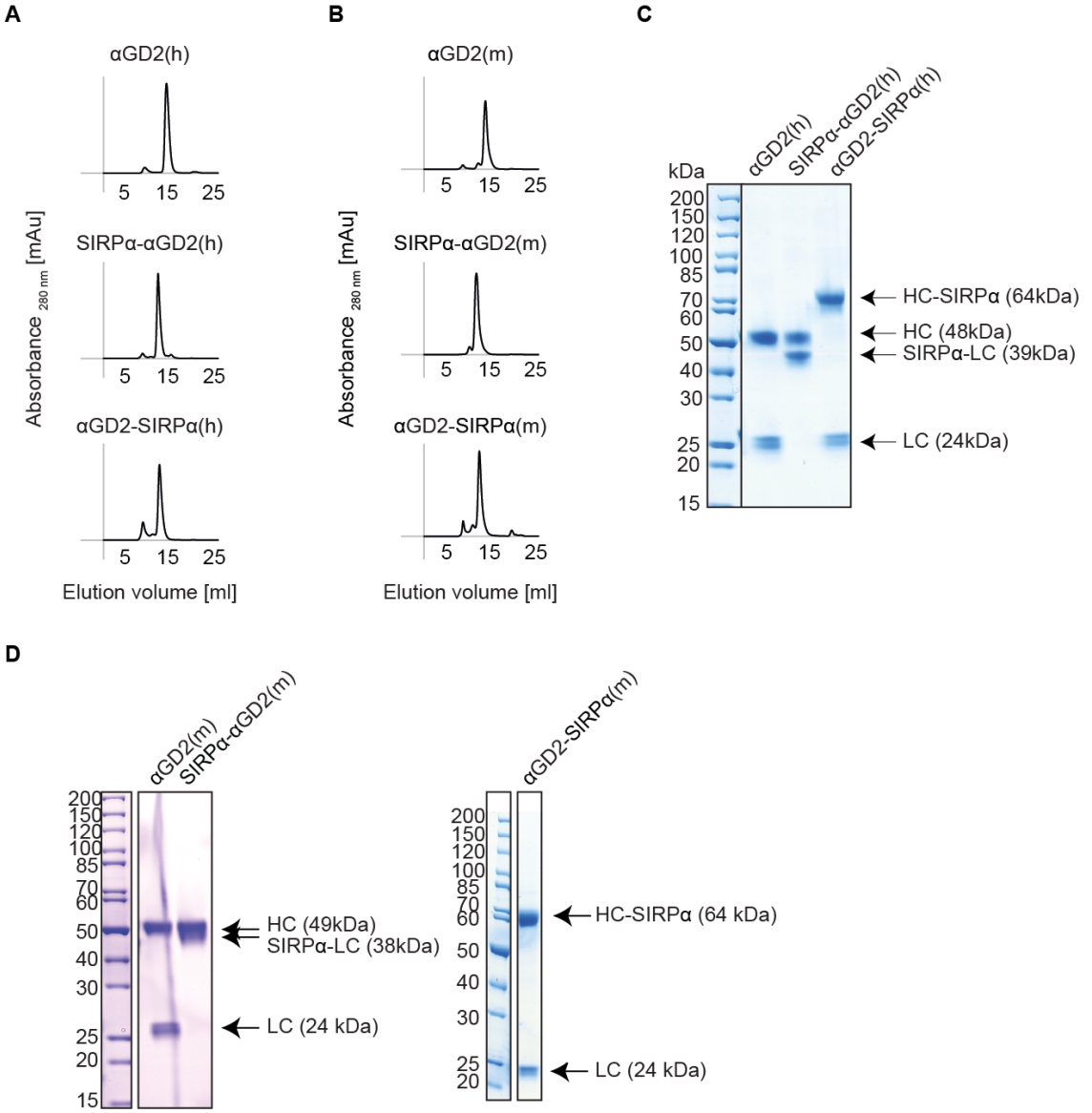

Figure 22. Purification of αGD2-SIRPα fusion antibodies. SEC Chromatograms of preparative purifications of (A) human and (B) mouse antibodies. SDS-PAGE of the purified (C) human and (D) mouse antibodies under reducing conditions. Computed masses of antibody chains are indicated.

Thermal stability of the antibodies was assessed by nanoDSF. The thermal unfolding profiles with T_i representing unfolding showed that the N- or C-terminal SIRPα fusion did not change the thermal stability of the antibodies compared to αGD2. (Figure 23).

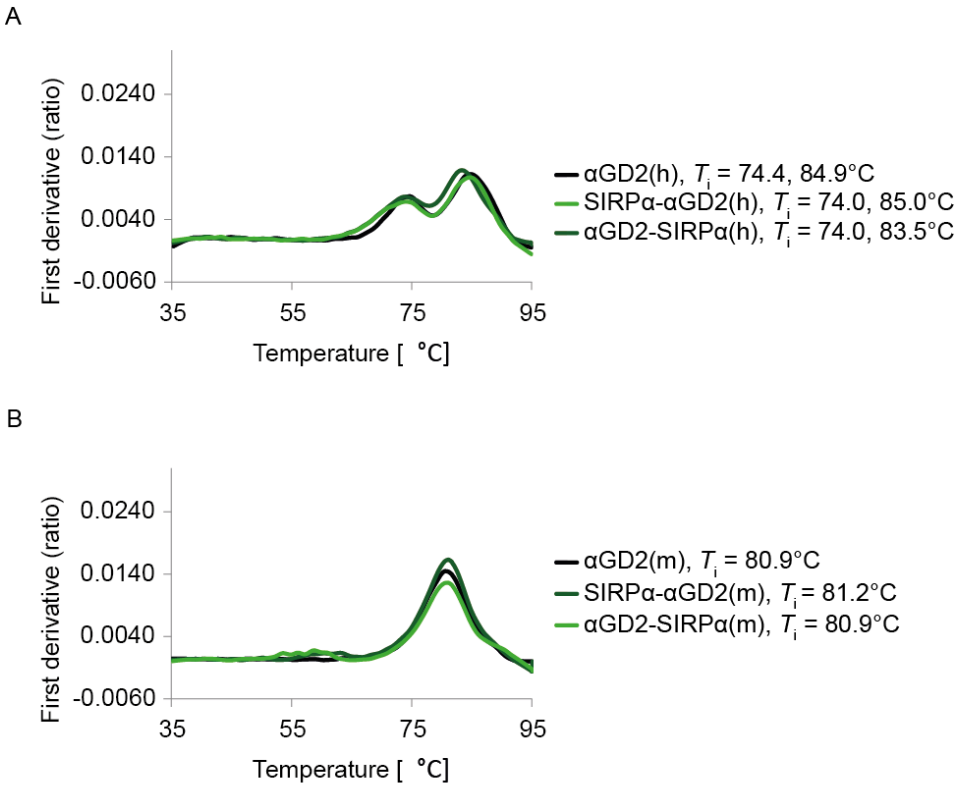

Figure 23. Thermal stability of αGD2-SIRPα fusion antibodies. Thermal stability of (A) human and (B) mouse antibodies was determined by Tycho NT.6. The measured inflection temperatures (*T*i) are indicated, *n*=2.

4.2.2. Binding of -SIRPα fusion antibodies to mouse and human cells

4.2.2.1. Binding to neuroblastoma cells

The expression of GD2 and CD47 on human and mouse cell lines was characterized to analyze the binding of bifunctional antibodies to these cell lines. Three human (SK-N-AS, IMR32 and Shep2) and four mouse cell lines (Neuro2a, 9464D, 9464D-OVA, 9464D-GFP) were included in the analysis. The human cell line phenotype and binding was kindly analyzed and data provided by Anja Wittner. All experiments performed with mouse cell lines were performed with Renske van den Bijgaart in the laboratory of ROI.

The surface expression of GD2 was determined using a QIFIKIT quantitative analysis assay and flow cytometry-based analysis of antibody binding. All cell lines showed different levels of GD2 surface antigens (Table 13) that corresponded to the binding of αGD2 measured by flow cytometry (Figure 24A and C). Overall, the human NBS cells expressed higher levels of GD2 than mouse cells and the mouse NBS cell line Neuro2a did not express any GD2 (Table 13, Figure 24A and C). Human cell lines varied in CD47 expression with the lowest levels measured on IMR-32 and highest on Shep2 cells (Table 13, Figure 24A). Surprisingly, in comparison to CD47, higher levels of GD2 were estimated from the QIFIKIT measurement than by using the αGD2 antibody (Table 13, Figure 24A). All mouse cell lines expressed high levels of CD47 but the highest expression was observed on Neuro2a cells (Figure 24C).

Table 13. Average surface antigen expression levels per cell.

Organism	Cell line	GD2	CD47
Human	SK-N-AS	17 880 ± 5 102	99 614 ± 14 542
Human	IMR-32	63 092 ± 17 513	29 098 ± 5 123
Human	Shep2	183 394 ± 64 591	126 769 ± 24 584
Mouse	Neuro2a	162 ± 146	n. d.
Mouse	9464D	966 ± 372	n. d.
Mouse	9464D-OVA	12 359 ± 2 741	n. d.
Mouse	9464D-GFP	64 094± 18 197	n. d.

Determined by QIFIKIT. Data are means ± SEM (*n*=2-3). Not determined (n. d.).

The binding of αGD2, SIRPα-αGD2 and αGD2-SIRPα antibodies to NBS cells was analyzed next. As expected, the binding of the αGD2 antibody correlated to the amount of GD2 on human NBS cells with SK-N-AS showing the lowest and Shep2 the highest binding. The αGD2-SIRPα bound similar to αGD2 but the SIRPα-αGD2 demonstrated less binding (Figure 24B). In the mouse setting, αGD2 did not bind to $GD2^-$ Neuro2a cells but the αGD2-SIRPα and SIRPα-αGD2 antibodies bound to these cells (Figure 24D). Likewise, αGD2 targeted the 9464D cell line minimally while a considerable binding of the αGD2-SIRPα and SIRPα-αGD2 antibodies was detected (Figure 24D). αGD2 bound well to 9464D-OVA cells, but αGD2-SIRPα and SIRPα-αGD2 still bound slightly better. The 9464D-GFP cell showed the highest αGD2 binding and differences compared to αGD2-SIRPα and SIRPα-αGD2 were not pronounced. Interestingly, although 9464D-OVA and SK-N-AS cells as well as 9464D-GFP and IMR-32 cells had similar GD2 levels based on QIFIKIT (Table 13), mouse cell lines bound the αGD2 antibody less (Figure 24B and D). At the same time, an extensive increase in αGD2-SIRPα and SIRPα-αGD2 binding compared to αGD2 was observed for mouse and not for human cell lines, indicating a possible difference between the species in the autonomous binding of the SIRPα domains.

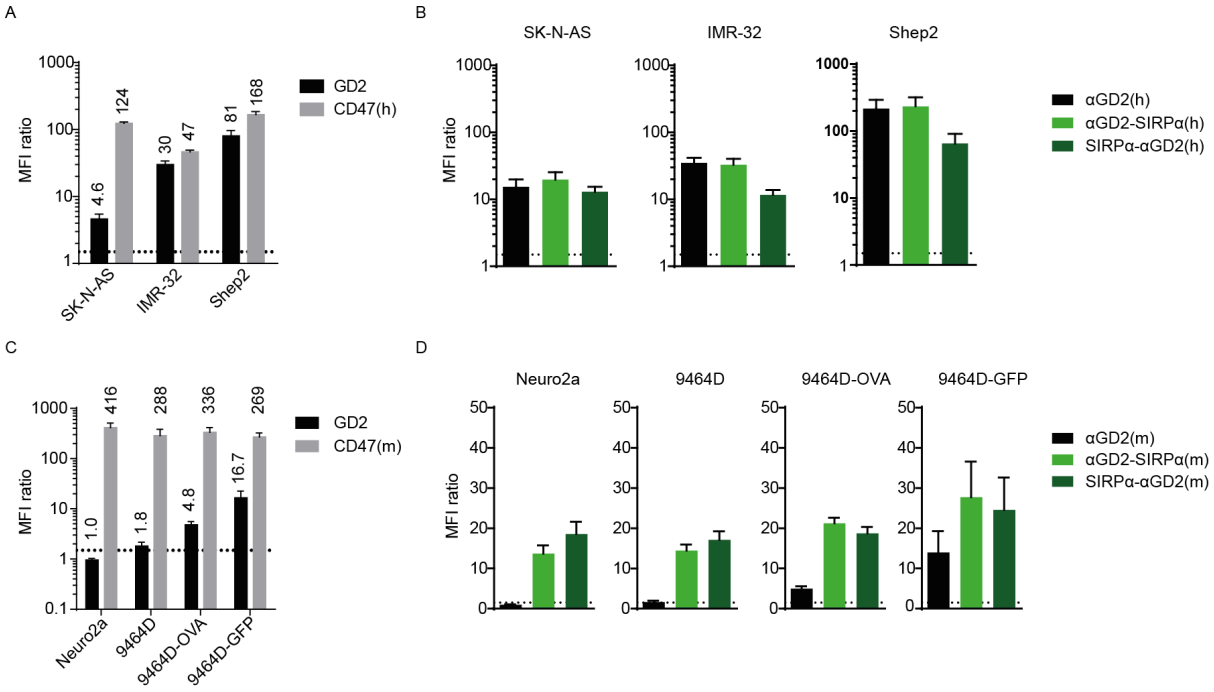

Figure 24. αGD2-SIRPα fusion antibodies binding to human and mouse neuroblastoma cell lines. (A) Phenotype of human NBS cell lines SK-N-AS, IMR-32 and Shep2 measured by flow cytometry. Shown are mean values from *n*=6-11 experiments ± SEM. (B) Binding of 100 nM αGD2(h), SIRPα-αGD2(h) and αGD2-SIRPα(h) antibodies to NBS cells was measured by flow cytometry. Shown are mean values from *n*=9-10 experiments ± SEM. (C) Phenotype of mouse NBS cell lines Neuro2a, 94654D, 94654D-OVA and 94654D-GFP measured by flow cytometry. Shown are mean values from 4 experiments ± SEM. (D) Binding of 100 nM mouse antibodies to NBS cells measured by flow cytometry. Dotted line indicates MFI ratio of 1.5 as cut-off for positive expression. Shown are mean values of *n*=5 experiments ± SEM.

4.2.2.2. Unspecific binding to healthy cells

Healthy cells, such as RBCs, also express CD47 and the on-target off-cancer binding of αCD47 antibodies has been shown to induce severe anemia due to RBCs targeting (Table 9) [149, 150, 167]. Besides phagocytic clearance, αCD47 antibodies can also induce aggregation of RBCs, known as hemagglutination. To analyze the unspecific targeting of CD47 by αGD2-SIRPα and SIRPα-αGD2, hemagglutination of human and mouse RBCs was investigated. The SIRPα-αGD2 induced human RBC hemagglutination starting from 50 nM while the αGD2-SIRPα antibody did not show any effect (Figure 25A). αCD47 antibody B6H12 demonstrated hemagglutination at 5 nM concentration but on higher concentrations, the aggregation was not observed. Similar data have been reporter by others [279, 280]. The mouse RBCs hemagglutinated in the presence of SIRPα-αGD2 antibodies at 5 nM concentration whereas the αGD2-SIRPα induced changes at 10-fold higher concentration (Figure 25B). Interestingly, MIAP301 did not induce any hemagglutination unlike the human counterpart B6H12 (Figure 25B).

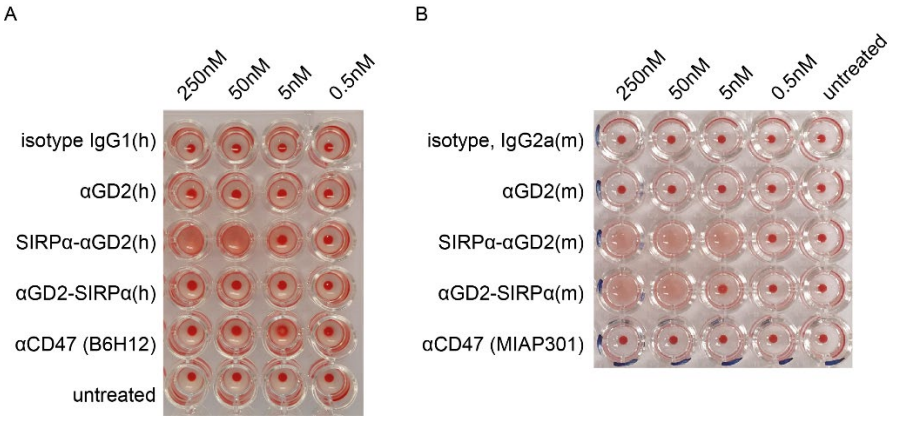

Figure 25. Hemagglutination induced by αGD2-SIRPα antibodies. (A) human or (B) mouse RBCs. Shown are 1 of 3 experiments with similar results.

A major goal of fusing the αGD2 antibodies with the low affinity CD47 blocking SIRPα is to preferentially target $GD2^+$ $CD47^+$ NBS cells over $GD2^-$ $CD47^+$ RBCs. Binding of the αGD2-SIRPα and SIRPα-αGD2 antibodies to NBS target cells was thereby analyzed in the presence of 20-fold excess of RBCs. αGD2, αGD2-SIRPα and SIRPα-αGD2 all preferentially bound to human NBS cells (Figure 26A). Interestingly, SIRPα-αGD2 bound to human NBS cells slightly more than αGD2 and αGD2-SIRPα. The high affinity αCD47 antibody (B6H12) on the other hand primarily bound to human RBCs. In the mouse experiments, the majority of αGD2 and αGD2-SIRPα preferentially targeted mouse NBS cells while, surprisingly, most of the SIRPα-αGD2 bound to mouse RBCs in a similar extent compared to the αCD47 antibody (MIAP301) (Figure 26B).

The results of the hemagglutination and competitive binding assays demonstrate that the fusion antibodies with mouse SIRPα bind more to mouse $GD2^-$ $CD47^+$ cells than the respective human molecules to human $GD2^-$ $CD47^+$ cells. Nevertheless, the αGD2-SIRPα fusion antibody showed favorable NBS targeting over SIRPα-αGD2 and αCD47 in both human and mouse settings.

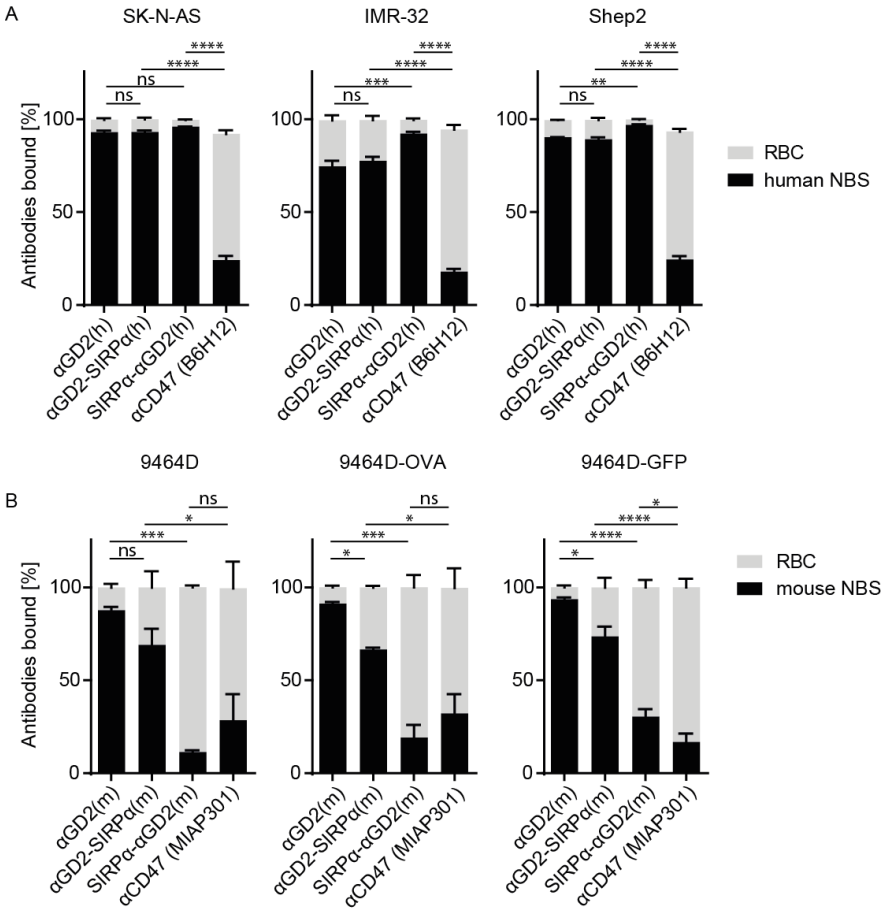

Figure 26. Competitive binding of the αGD2-SIRPα antibodies to neuroblastoma and RBCs. Binding of 100 nM antibodies was measured by flow cytometry in a mixture of either (A) human or (B) mouse NBS cells and human or mouse RBCs at a 20-fold excess, respectively. Shown are results from *n*=3 RBC donors for both human and mouse with mean ± SEM.

4.2.3. Functional characterization of αGD2-SIRPα fusion antibodies

4.2.3.1. αGD2-SIRPα-mediated CD47 blockade on neuroblastoma cells

To analyze the local blockade of CD47 on NBS cells, flow cytometry-based detection of labeled αCD47 antibodies was used to determine unoccupied CD47 sites after αGD2-SIRPα and SIRPα-αGD2 antibody incubation. αCD123 and 1×SIRPα-αCD123 were used as controls in the human setting to determine the effect of SIRPα alone. Both control antibodies did not induce any CD47 blockade (Figure 27A). The αGD2-SIRPα blocked majority of the CD47, while the SIRPα-αGD2 was not as efficient and reached maximum of 50% of blockade only on $GD2^{high}$ IMR-32 and Shep2 cells (Figure 27A). αGD2-SIRPα induced CD47 blockade was highest on Shep2 cells which also have the most abundant levels of GD2. Although the effect of αGD2-SIRPα was almost on a par with the αCD47 antibody B6H12, the maximum blockade of CD47 was seen with the latter (Figure 27A).

αFITC-SIRPα and αhCD33-SIRPα isotype control fusion antibodies both blocked CD47 minimally similar to the αGD2-SIRPα induced CD47 blockade on $GD2^{-}$ Neuro2a cells (Figure

27B). The 9464D cells, which express very low levels of GD2, did not differ much from Neuro2a and isotype control- SIRPα and αGD2-SIRPα demonstrated similar results (Figure 27B). A significantly higher CD47 blockade by αGD2-SIRPα was observed on the 9464D-OVA and 9464D-GFP cells, which express high levels of GD2 (Figure 27B). Similar to human cells, αGD2-SIRPα was superior to SIRPα-αGD2 in blocking CD47 on 9464D-OVA and 9464D-GFP cells. While αCD47 (MIAP301) never reached 100%, it was able to block CD47 on mouse NBS cell lines irrespective of GD2 expression levels (Figure 27B). All together, these results indicate that the αGD2 moiety is needed to facilitate a specific disruption of the CD47/SIRPα axis on $GD2^+$ target cells.

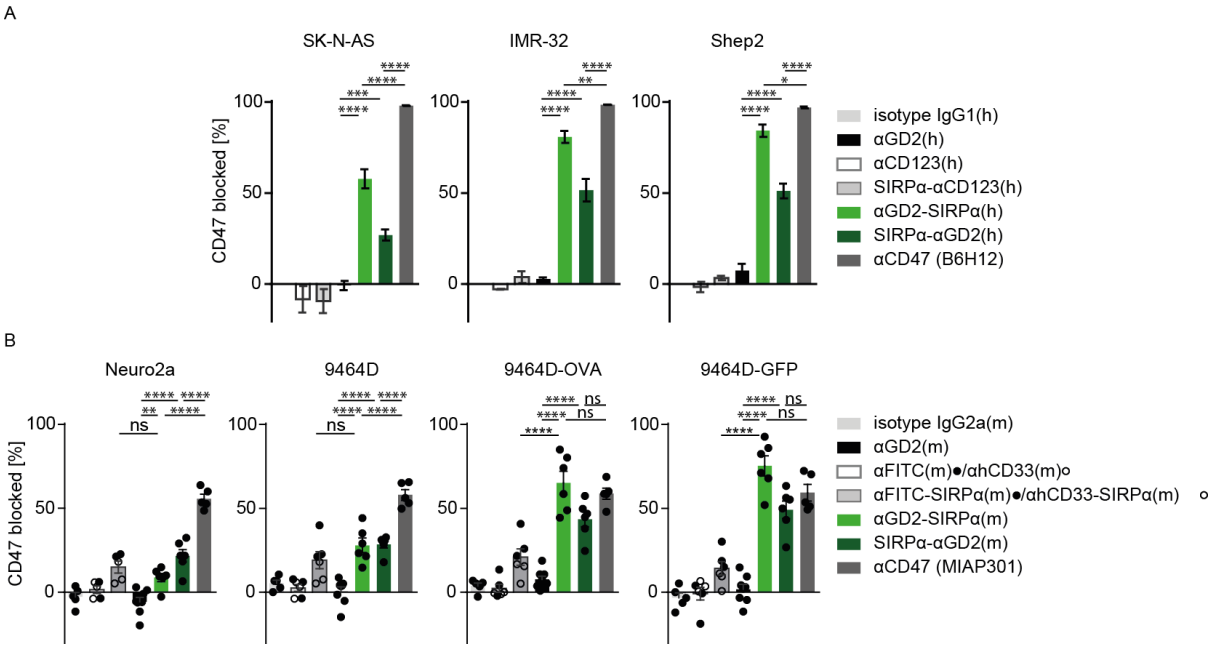

Figure 27. Blockade of CD47 by αGD2-SIRPα antibodies. (A) Human NBS cells were incubated with 100 nM antibodies and CD47 blockade was calculated based on B6H12 binding using flow cytometry. Mean ± SEM of *n*=3 experiments are shown. (B) Mouse NBS cells were incubated with 100 nM antibodies and CD47 blockade was calculated based on MIAP301 binding using flow cytometry. αhumanCD33(m), filled circles, and αFITC(m), empty circles, and the respective antibodies with SIRPα fusions were used as control molecules. Mean ± SEM of *n*=5-8 experiments are shown.

4.2.3.2. CD47 blockade by human or mouse αCD47 antibodies

In the previous assay, αCD47 binding was used to evaluate the percentage of CD47 sites occupied by SIRPα. Here the binding of either mouse or human SIRPα was analyzed after incubation with the respective αCD47 (MIAP301 or B6H12). The monovalent binding affinities of MIAP301 and B6H12 for mouse or human CD47, are similar (K_D values 4 nM and 3.1 nM, respectively) [173, 281]. Human Raji and mouse Panc02 cells were used as they exhibited a similar high CD47 expression and no GD2 expression in a flow cytometry-based measurement (Figure 28A). The accessibility of CD47 after MIAP301 or B6H12 incubation was evaluated by measuring the binding of SIRPα using SIRPα-αGD2 mouse or human constructs. As both cell lines are $GD2^-$, the binding of SIRPα-αGD2 is mediated only by SIRPα.

Surprisingly, in the condition without αCD47 preincubation, a very high binding of mSIRPα to Panc02 was observed in comparison to hSIRPα binding to Raji cells. These results confirm the species-specific difference of SIRPα binding observed in binding, RBC competition and hemagglutination experiments (Figure 28B). Furthermore, 50 nM MIAP301 could not block mSIRPα binding while a 10-fold higher concentration of 500 nM could inhibit approximately 80% of the binding sites (Figure 28B). On the other hand, 50 nM of B6H12 was sufficient to block all binding of hSIRPα.

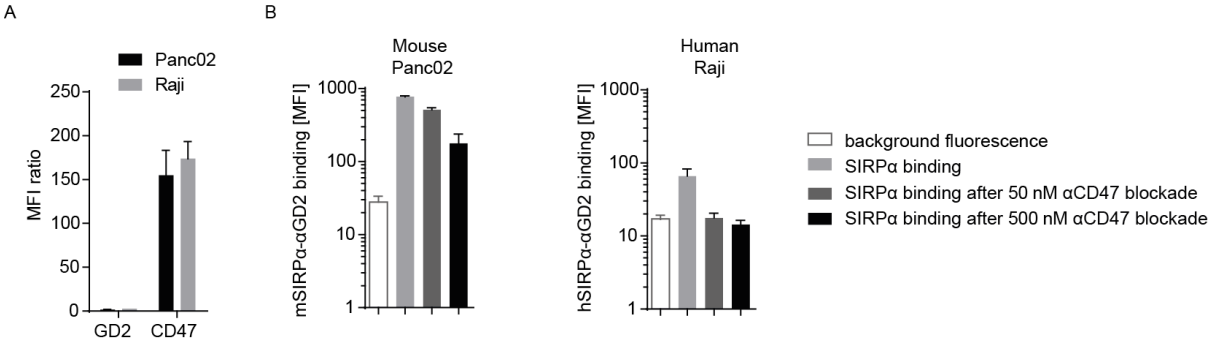

Figure 28. Blockade of SIRPα binding by αCD47 antibodies. (A) Phenotype of Panc02 and Raji cells. MFI ratio was calculated using the unstained control as reference. Panc02 *n*=3-4, Raji GD2 expression *n*=1 and CD47 expression *n*=2. (B) CD47 blockade was calculated based on SIRPα-αGD2 binding using flow cytometry. *n*=2-3.

4.2.3.3. Phagocytosis of human and mouse neuroblastoma cells by αGD2-SIRPα

As the SIRPα-αGD2 and especially the αGD2-SIRPα antibodies demonstrated a high blockade of the inhibitory CD47, the activation of macrophages was analyzed by measuring phagocytosis of NBS cells. ADCP assays with human cell lines were kindly performed and data provided by Anja Wittner. The αGD2 antibody itself was already very potent in inducing phagocytosis of human NBS cells by HD monocyte-derived macrophages (Figure 29A). A slight, but not statistically significant, tendency towards increased phagocytosis of SK-N-AS cells was observed with αGD2-SIRPα and SIRPα-αGD2 antibodies compared to αGD2 (Figure 27A). αGD2 stimulated the phagocytosis of IMR-32 to maximum and no further stimulation could be observed with the αGD2-SIRPα and SIRPα-αGD2 antibodies (Figure 27A). The phagocytosis of Shep2 cells, on the other hand, could be significantly boosted by αGD2-SIRPα and SIRPα-αGD2 antibodies compared to αGD2. Interestingly, the SIRPα-αGD2 seemed to be slightly better than αGD2-SIRPα, but this was not statistically significant. The SIRPα-isotype molecule did not have an effect on IMR-32 or Shep2 cell phagocytosis. The αCD47 antibody alone induced some phagocytosis and in combination with the αGD2 antibody a similar effect as compare with the αGD2-SIRPα and SIRPα-αGD2 antibodies. These results confirm the synergy between CD47 blockade and strong FcγR activation by the fusion antibodies.

Only 9464D-OVA and 9464D-GFP mouse cell lines were included in the ADCP assay based on previous results. The αGD2 antibody efficiently boosted phagocytosis of both cell lines by

BMDMs similar to the human setting (Figure 27B). αGD2-SIRPα induced maximum phagocytosis and unlike in the human setting, the SIRPα-αGD2 was not better than αGD2. The αCD47 did not stimulate phagocytosis of mouse cells and correspondingly the combination with αGD2 was similar to αGD2 treatment alone.

Taken together, experiments performed in this thesis show that differences between the αGD2-SIRPα and SIRPα-αGD2 antibody formats were smaller with human than with mouse cells. This might come from the observed discrepancies of mouse and human SIRPα binding to their respective targets *in vitro*. Overall, αGD2-SIRPα seems to perform better than the SIRPα-αGD2 antibody in both preferential cancer cell targeting and in ADCP assays using NBS target cells.

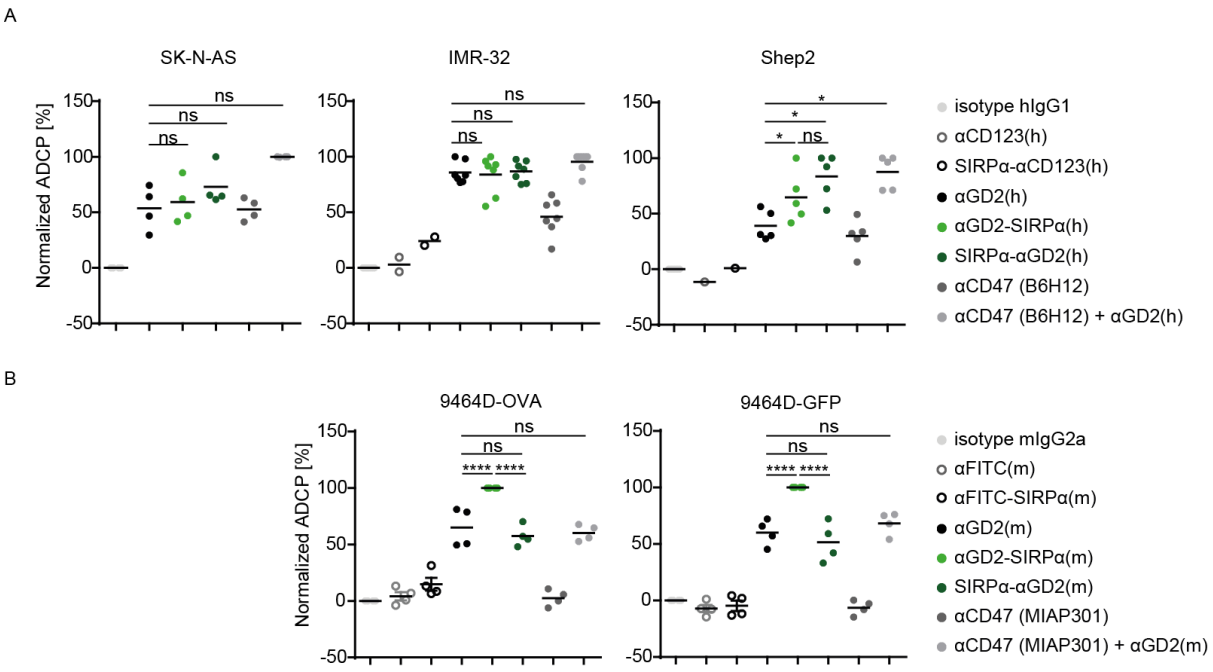

Figure 29. Phagocytosis of neuroblastoma cells by αGD2-SIRPα antibodies. (A) Phagocytosis of human NBS cells by HD macrophages at 50 nM antibody concentration (*n*=4-7, for αCD123 controls *n*=1-2). (B) Phagocytosis of mouse NBS cells by BMDM at 50 nM antibody concentration (*n*=4).

5. Discussion

5.1. Rationale for the bifunctional SIRPα-antibody fusion molecules

The most advanced immunotherapeutic strategies to date enhance the immune response of T cells. CTLA4 and PD1/PDL1 checkpoint inhibitors together with CD19-directed chimeric antigen receptor (CAR) T cell therapies (Kymriah and Yescarta) have dramatically changed the treatment options for many patients [84-86, 282, 283]. In spite of this huge step forward, the issue of cancer treatment is not resolved in all cases. The inhibitory CD47 "don't eat me" signal is overexpressed on several malignancies, which has prompted the development of therapeutic agents targeting the myeloid specific CD47/SIRPα checkpoint [73, 75, 76]. Indeed, in combination with a pro-phagocytic signal, effective anticancer responses have been observed upon CD47 blockade [158]. CD47 blockade with the αCD47 antibody magrolimab has been clinically successful in combination with an anticancer antibody rituximab in NHL patients or with calreticulin-inducing AZA in patients with AML and MDS [167, 206]. However, the ubiquitous expression of CD47 on healthy cells, such as RBCs, creates a so-called "antigen sink" for αCD47 therapies and causes severe anemia [149, 167, 274]. Moreover, unspecific targeting of CD47 can cause unexpected toxicities to healthy cells besides RBCs, as CD47 has various roles in physiological tissue homeostasis [144, 284]. The SIRPα-antibody fusion molecules targeting CD123 on AML LSCs or GD2 on human NBS generated in this thesis aim to overcome the unspecific targeting of healthy cells and combine CD47 blockade with a strong activating signal from human IgG1.

5.2. SIRPα-antibody fusion constructs target AML and NBS but spare healthy cells

The K_D values of αCD123 for CD123ex measured here (1.2-2.9 nM) were orders of magnitude lower than the affinity of SIRPα for CD47 (500-1200 nM) [146, 148]. Similarly, a much lower K_D value of 50 nM has been reported for the αGD2 antibody [285]. This indicates that the SIRPα-antibody fusion molecules are likely to target the cancer antigen primarily and the fused SIRPα binds to CD47 subsequently. The 1×SIRPα-αCD123 antibody studied here preferentially binds to AML cell line MOLM-13 in the presence of 20-fold excess of $CD123^-$ $CD47^+$ RBCs indicating an αCD123 directed binding. The 2×SIRPα-αCD123 antibody carries an extra SIRPα domain on the LC and as a result, targets more RBCs than the fusion antibodies with a single SIRPα. Nevertheless, the 2×SIRPα-αCD123 bound RBCs with low intensity. Similarly, the human SIRPα-αGD2 and αGD2-SIRPα antibodies target human NBS cell lines and not RBCs. These results agree with previous reports where similar constructs targeting CD33 and CD20 avoid the CD47 sink generated by RBCs [176, 177].

In contrast to the SIRPα-antibody fusion molecules, the majority of the high-affinity αCD47 antibody B6H12 targeted RBCs. These results agree with previous data from others and indicate major on-target off-leukemia side effects for αCD47-based therapies [176, 177]. In preclinical studies with αCD47 magrolimab, cynomolgus monkeys developed a dose-dependent anemia [274]. This was suggested to be due to erythrophagocytosis and not hemolysis as no free plasma hemoglobin was detected [274]. The increase in blood bilirubin seen in human clinical trials nevertheless suggest that hemolysis is at least one of the causes for anemia [206, 286]. A dosing strategy to mitigate anemia has been developed comprising of a 1 mg/kg priming followed by a 30 mg/kg maintenance therapy [274]. Similar dosing has been used later in clinical trials [167, 206, 286]. It has been proposed that the priming dose leads to elimination of older RBCs that have accumulated pro-phagocytic signals accompanied with a compensatory reticulocytosis generating younger RBC that do not express significant pro-phagocytic signals [158]. A phenomenon named CD47 pruning has been reported as well, upon which RBCs exposed to the initial priming dose rapidly shed CD47 protein from the cell surface [287]. This CD47 antigen loss was not detected on other healthy cells such as leukocytes nor on AML blasts and the exact molecular mechanism for this process is still under investigation [287]. Thus, on-target off-tumor toxicities beyond RBC targeting are still plausible upon high-affinity αCD47 treatment due to the broad expression of CD47 in healthy tissues. Even with the updated dosing regimen, anemia, along with neutropenia and thrombocytopenia, are the most common severe on-target off-tumor side effect reported in clinical trials with magrolimab as monotherapy or in combination with AZA or rituximab [163, 167, 206]. Using the low affinity SIRPα domain fused to the high affinity αCD123 or αGD2 targeting domain is therefore a compelling alternative to the priming/maintenance dose strategy to mitigate RBC binding and other αCD47 treatment-related toxicities.

5.3. SIRPα-antibody fusion constructs enhance the elimination of cancer cells

In addition to favorable tumor-targeting, bifunctional SIRPα-antibody molecules are able to induce potent immune effector functions. The SIRPα-αCD123 antibodies enhanced the phagocytosis of AML cell line MOLM-13 and primary AML cells by allogenic and autologous macrophages. Likewise, the SIRPα-αGD2 and αGD2-SIRPα antibodies boosted the engulfment of human NBS cell line Shep2 with high GD2 expression. These results agree with other studies that demonstrate a potent synergy between CD47/SIRPα axis disruption and pro-phagocytic signal from the Fc domain of an antibody [75, 149, 158, 162, 167].

Although avidity-dependent binding of SIRPα-αCD123 antibodies increases the targeting of MOLM-13 cells, ADCP does not only correlate with binding. This is indicated by the results obtained with the αCD19-based SIRPα control molecules which bound to MOLM-13 less than αCD123. These controls, however induced a similar ADCP as SIRPα-αCD123 antibodies when

used in high concentrations. With high abundance of antibodies, the low affinity interactions of αCD19-based SIRPα control molecules and CD47 on target cells are probably sufficient to bind target cells and stimulate phagocytosis due to the additional pro-phagocytic signal from the Fc region of the IgG1. Still, when using lower concentrations of antibodies, only the SIRPα-αCD123 induced ADCP of MOLM-13 cells. This demonstrates that binding of the αCD123 moiety to the target cells is needed for an efficient disruption of the CD47/SIRPα axis by the fusion molecules.

Interestingly, when analyzing the phagocytosis of human NBS cell line IMR32, no additional benefit compared to αGD2 was observed with the SIRPα-αGD2 or αGD2-SIRPα fusion antibody. MOLM-13 cells express similar levels of CD47 as IMR32, but have at least 4.5 times less target antigen CD123 compared to GD2 on IMR32 cells. αCD123 is most likely not effective in activating macrophage-mediated phagocytosis of MOLM-13 cells alone due to the low expression of CD123. High GD2 levels lead to an increased αGD2 binding, which might provide enough positive pro-phagocytic signals to counteract the low numbers of the inhibitory CD47. Therefore, the balance of "eat me" and "don't eat me" signals regulates the fate of macrophage-mediated engulfment of target cells. Other signaling pathways beside CD47 also coordinate phagocytosis. For example, MHC class I molecules have been shown to negatively regulate phagocytosis while calreticulin represents a pro-phagocytic signal [160, 288]. Furthermore, GD2 expression has been claimed as a inhibitory macrophage checkpoint and the combination of αGD2 or αCD47 seems to have high level of synergy [289]. Data presented in this thesis confirms these observations. No phagocytosis of $GD2^+$ NBS cell lines was observed with the non-targeting control antibody that contains the SIRPα domain even at high antibody concentration of 50 nM. In the same conditions, the $GD2^-$ AML cell line MOLM-13 was phagocytosed. The αGD2-SIRPα antibodies are thus especially relevant in NBS therapy as they simultaneously address two of the inhibitory checkpoints regulating phagocytosis.

The SIRPα-αCD123 antibodies are developed based on the antigen binding sequence of talacotuzumab, a Fc region modified αCD123 for enhanced ADCC, which has been previously tested in clinical trials [273, 290]. This antibody exhibited limited efficacy alone and in combination with decitabine in two of the phase 2 clinical trials probably due to the compromised NK cell activity reported in AML and MDS [291-293]. Activating macrophage-mediated immune response with αCD47 magrolimab and AZA, on the other hand, has shown to be beneficial in both AML and MDS in a phase 1b clinical trial [155, 206]. The results obtained in this thesis show that αCD123 alone is not sufficient to activate ADCP, which might be needed for an efficient control of AML. The SIRPα-αCD123 fusion antibodies are more potent than αCD123 as they initiate a strong ADCP response and also mediate NK cell-dependent ADCC. In NBS, the αGD2 dinutuximab, which is based on the 14.G2a binding sequence similar to the SIRPα-αGD2 and αGD2-SIRPα antibodies, has been shown to activate NK cells and granulocytes [252-254]. As demonstrated here, the SIRPα-αGD2 and αGD2-

SIRPα can enhance the recruitment of macrophages, which are abundant in NBS [255]. The SIRPα-antibody fusion molecules are thus likely to activate a broader cancer-specific immune response than either the cancer-specific antibody or CD47-blocking IgG4 antibodies and increase the clinical efficacy of the antibody-mediated immunotherapy.

5.4. SIRPα-αCD123 fusion antibodies specifically target LSCs

AML therapy failure and capacity for leukemic regeneration are dependent on the persistence of LSCs [207]. The removal of LSCs is clearly fundamental in AML therapy. LSCs were first described to be enriched in the $CD34^+/CD38^-$ cell population, similar to normal HSCs based on a functional engraftment assay [210]. Using more immunocompromised and thus more permissive mouse models, such as NSG, it has later been demonstrated that cells with LSCs activity can also reside within the $CD34^+/CD38^+$, $CD34^-/CD38^+$ or $CD34^-/CD38^-$ cells [270, 294, 295]. The $CD34^+/CD38^-$ population had nevertheless consistently the highest engraftment potential [270, 294, 295]. Furthermore, only the $CD34^+/CD38^-$ AML cells have high prognostic impact [296-298]. Therefore, the $CD34^+/CD38^-$ LSCs seem to have the highest leukemogenic ability. Unlike the healthy HSCs $CD34^+/CD38^-$ compartment, the LSCs $CD34^+/CD38^-$ cells express high levels of CD123 [221]. The $CD34^+/CD123^+$ cells are competent to establish and maintain leukemia *in vivo* as opposed to the $CD34^-/CD123^{+/-}$ population indicating that all LSCs lay within the $CD123^+$ cells [221].

The role of CD47 on LSCs was established by Jaiswal et al. and Majeti et al. They showed that elevated expression of CD47 on LSCs leads to immune escape due to decreased clearance by macrophages [73, 74]. In addition to their malignant counterparts, CD47 was found to be transiently upregulated on mouse HSPCs [74] where it was associated with increased mobilization from the bone marrow to distant sites [74]. As cancer cells might display signs of cellular “damage” on their cell surface, CD47 upregulation could enable LSCs to have additional protection against phagocytosis [74]. Indeed, CD47 blockade was shown to increase the phagocytosis of AML cells and inhibit engraftment to NSG mice [73].

The high levels of CD123 and CD47 on LSCs makes the combined targeting of these markers by the SIRPα-αCD123 fusion antibodies highly relevant. The expression of both CD47 and CD123 is associated with the capability to recapitulate AML and patients with elevated levels of these markers are more likely to experience poor outcomes [73, 223, 224]. High CD47 and CD123 co-expression has also been shown to correlate with AML chemoresistance [299]. SIRPα-αCD123 antibodies demonstrate an increased targeting efficacy of $CD123^+/CD47^+$ MOLM-13 cells compared to αCD123, which might be due to slower dissociation of the multivalent binder [300]. The 2×SIRPα-αCD123 antibody was highly effective in eliminating the $CD34^+/CD38^-$ population of AML PDX cells by ADCC. Moreover, ADCC with 2×SIRPα-αCD123 but not with the αCD123 antibody resulted in extreme reduction of AML LSCs with *in vivo* engraftment potential. Therefore, the increased avidity of SIRPα-αCD123 antibodies

provides the opportunity to preferentially address AML LSCs for an efficient LSC targeting and elimination.

5.5. GD2-SIRPα fusion antibodies developed for the mouse NBS model

To evaluate the systemic effects mediated by the αGD2-SIRPα fusion antibodies *in vivo*, appropriate immunocompetent mouse NBS models are necessary. The targeted expression of *MYCN* under the control of rat tyrosine hydroxylase promoter (*TH-MYCN*) in mice causes NBS, which recapitulates several biological and histological aspects of the human disease [301-304]. Amplification of the *MYCN* oncogene is found in approximately one third of all human NBS and correlates with advanced stage and poor outcome of the disease [305, 306]. To develop an autologous transplantable NBS model, a cell line named 9464D was established from a spontaneously developed tumor arising in C57BL/6 TH-MYCN mice [307]. While human NBS are highly GD2 positive, mouse NBS cell lines in general do not express significant amounts of GD2. Importantly, the established 9464D cells were GD2 positive [307]. NBL tumors arising in the 9464D based transplantable models were highly infiltrated by myeloid cells including macrophages and MDSC similar to human NBL [307]. The expression of GD2 and high infiltration of macrophages akin to the human disease makes this model ideal for evaluating the bifunctional αGD2-SIRPα antibodies.

Besides the parental cell line, GFP and OVA expressing variants of 9464D have been developed [265]. The *in vitro* characterization of the mouse and human NBS cells performed in this thesis confirms the low expression of GD2 on mouse NBS cell lines compared to the human ones. However, the GFP and OVA expressing variants of 9464D exhibited a slightly higher GD2 expression than the original cell line. Correspondingly, in comparison to αGD2 treatment the αGD2-SIRPα antibody enhanced the phagocytosis in only these two cell lines making them suitable candidates for future *in vivo* studies.

In comparison to human cell lines, mouse cell lines express high levels of CD47. This could be one of the factors contributing to the high autonomous binding of SIRPα-αGD2 and αGD2-SIRPα antibodies to mouse NBS cells. Still, the mouse fusion antibodies also exhibit a strong binding to mouse RBCs while the respective human constructs do not bind human RBCs to that extent. This is not due to higher expression of CD47 on mouse RBCs as it has been reported that the levels are similar on RBCs from both species [308]. Furthermore, the monovalent affinities of SIRPα and CD47 interaction do not differ much for the two species [146]. Our results indicate a species-specific difference in SIRPα and CD47 interaction, which must be depending on other factors. Indeed, variability in CD47 mobility, described as a lack of cytoskeletal connectivity, has been reported for human and mouse. Only about 40% of the CD47 molecules on human RBCs are mobile and can freely diffuse while the mouse CD47 is 100% mobile and can readily cluster [309, 310]. The enhanced mobility of mouse CD47 may strengthen the effective avidity of pre-existing ligand-receptor binding as a result of increased

clustering [308]. The higher binding of mouse SIRPα-αGD2 and αGD2-SIRPα to CD47 compared to the respective human molecules can thus be due to differences in the multivalent association with SIRPα, which are more readily formed in the mouse RBCs. The disparity between mouse and human SIRPα binding could make it harder to clearly evaluate on-target off-tumor side effects of the bifunctional fusion antibodies based on syngeneic mouse studies. This highlights the importance of thorough *in vitro* investigation of the human bifunctional antibodies as animal studies may predict divergent reactions. The αGD2-SIRPα antibody nevertheless showed lower unspecific RBC targeting and boosted phagocytosis of NBS cells in both human and mouse settings. The mouse αGD2-SIRPα antibody is thereby proposed as a promising candidate for *in vivo* studies to evaluate the systemic distribution of the molecules in tumor bearing mice.

The effectiveness of CD47 blockade is well established and our results with the αGD2-SIRPα antibodies in $CD47^{high}$ cells agree with this. Nevertheless, the benefit of the αCD47 antibody MIAP301 was not confirmed in phagocytosis assays with mouse NBS cell lines. This might be due to the fact that MIAP301 is not a good blocking antibody as even 500 nM concentration was not sufficient to disrupt the binding of SIRPα. These results would argue against previous reports where MIAP301 has been demonstrated to successfully induce phagocytosis *in vitro* and control tumor growth *in vivo* [73, 78, 159, 311]. Some studies, however, observe that MIAP301 did not boost phagocytosis alone or in combination with tumor specific antibodies similar to the results described here [281, 312, 313]. Interestingly, the Fab_2 domain of MIAP301, and not the full antibody, enhanced ADCP in a dose-dependent manner in combination with αCD19 [313]. MIAP301 is a rat IgG2a antibody and surprisingly, this isotype binds only the low-affinity mouse FcγRIIb and FcγRIII with K_D of 6.1 µM and 23 µM, respectively [314]. It is therefore conceivable that an inhibitory signal is transmitted to the BMDMs upon MIAP301 binding to FcγRIIb and the pro-phagocytic effects are diminished at least in the experimental setting used here. Using the MIAP301 $F(ab')_2$ domains as controls could help to assess this question in the future. An alternative hypothesis is suggested by Sockolosky et al. by which the MIAP301 facilitates DC acquisition of MIAP301-opsonized cancer cells *in vivo* rather than promotes macrophage phagocytosis [281]. As the αGD2-SIRPα fusion molecules are potent activators of ADCP *in vitro*, future studies should elucidate their role in stimulating both macrophage and DC-mediated NBS tumor control *in vivo*.

5.6. Advantages and limitations of the SIRPα-antibody fusion molecules

It is difficult to find an ideal cancer antigen having an adequate immunogenicity but present only on tumor cells [315]. The surface marker CD33 or sialic acid-binding Ig-like lectin 3 (Siglec-3), is the only clinically approved target in antibody-based therapeutic approaches for AML. The antibody-drug conjugate gemtuzumab ozogamicin (GO, brand name Mylotarg) has been approved for the treatment of newly diagnosed or relapsed/refractory AML by the FDA

and European Medicines Agency (EMA) [316]. Unfortunately, only a subset of patients is likely to benefit from the GO therapy [317, 318]. Based on the sequence of gemtuzumab, Ponce and colleagues created the αCD33 antibody with SIRPα domain fused to the N-terminus of the LC for the first preclinical evaluation of a local inhibition of CD47 checkpoint in AML [177]. CD33 is highly expressed on AML blasts, but it is also a myeloid lineage-specific surface marker well known to be present on myeloid progenitor cells as well as on macrophages [226]. This could have implications in ADCP as the effector cells could be targeted via the αCD33 antibody. Indeed, the CD33 expression on HD and AML patient-derived macrophages analyzed here was similar to the expression on primary AML target cells. Moreover, CD33 on LSCs has been associated with variability [227, 319]. The expression of CD33 was shown to be significantly lower on LSC compared to bulk cells while HD-derived hematopoietic stem/progenitor cells (HSC/HSPC) were positive for CD33 [226]. This emphasizes the difficulties in specifically targeting LSCs with αCD33 constructs.

CD123 is also not exclusively expressed on AML blasts and LSCs but is in addition present on heathy plasmacytoid dendritic cells, basophils and in low levels on monocytes [226, 320]. Here, CD123 expression was not detected on either HD or AML patient-derived macrophages and SIRPα-αCD123 antibodies could spare the effector cells from unspecific targeting. Importantly, high CD123 levels are specific for LSCs and not HSCs/HSPCs. While one publication shows low expression of CD123 on HSCs/HSPCs [226] others report nearly non-detectable levels [221, 321, 322]. Haubner et al. claim that CD123 is highly expressed on normal non-hematopoietic tissues based on public protein expression data repositories [226, 322]. Data on these atlases were obtained by antibody-based immunohistochemistry or protein mass spectrometry. The expression was annotated to be associated with membrane based on Human Protein Atlas database (HPA) or the Jensen Lab's Compartments repository (JLCR) [322]. CD123 has been annotated to be expressed on the membrane by the JLCR but no localization is reported in the HPA [323, 324]. Interestingly, ubiquitous cytoplasmic expression of CD123 was detected in healthy tissues with antibodies used in the HPA whereas the antibody staining was reported not to be consistent with RNA expression data [323]. If the high expression of CD123 was derived from the intracellular staining results, but annotated as membrane expression based on JLCR, it might lead to an overestimation of the surface expression of CD123 on healthy cells. The expression of CD123 on normal non-hematopoietic tissues should thus be reevaluated using validated antibodies.

Several CD123 targeted therapies have reached clinical trials and side effects observed do not confirm the universal expression of the target antigen. CSL360 is a 7G3-derived chimeric human IgG1 antibody which was well tolerated with mild infusion reactions [325]. Tagraxofusp is the first CD123 targeting agent approved in clinics with the most notable toxicity being capillary leak syndrome (CLS) [326, 327]. This has been noted with other bacterial toxin targeted-therapies but could be also associated with the CD123-targeting aspect

due to reported endothelial cell expression [326, 328]. In the study with flotetuzumab, infusion-related reactions and cytokine release syndrome were reported and both are known to be associated with T-cell engagers [232]. Overall, targeting CD123 *per se* might not be related to serious side effects, but nevertheless, the safety and efficacy of SIRPα-αCD123 molecules should be evaluated in regards to the expression of CD123 on healthy tissues.

GD2 is expressed on healthy tissue such as peripheral nerves and brain parenchyma in low amounts [329, 330]. As a result, therapeutic antibodies targeting GD2 have been reported to cause acute neuropathic infusion pain syndrome and infrequently, central neurotoxicity [240, 241, 331]. Novel formats are in development to reduce these side effects [332]. It remains to be investigated whether αGD2-SIRPα fusion antibodies would affect the severity of these side effects.

As described above, the bifunctional SIRPα-antibody fusion molecules developed in this thesis provide an improvement over αCD47 therapeutics regarding the on-target off-tumor profile. A SIRPα-Fc fusion protein TTI-621 without a specific cancer-targeting moiety has also been developed [174]. This molecule binds minimally to human erythrocytes and does not induce any hemagglutination [174]. In clinical trials, however, TTI-621 induced severe thrombocytopenia in 20% of the patients, which is higher than reported in trials with the αCD47 magrolimab [167, 206, 333]. TTI-621 carries the activating Fc domain from human IgG1 isotype, which might be the reason for these side effects. A clinical trial with the TTI-622, which carries the less active Fc region from the hIgG4 isotype, reported approximately five times lower incidence of severe thrombocytopenia [175, 334]. As the SIRPα-antibody fusion molecules are based on the activating IgG1 isotype, platelet binding of the constructs should be tested. The data provided in this thesis indicates that the SIRPα-antibody fusion molecules might, however, improve the anticancer response over the SIRPα-Fc due to the specific targeting of cancer cells via the high affinity antibody domain.

In this thesis, three different formats of SIRPα-antibody molecules were evaluated with either GD2 or CD123 as target antigen. The SIRPα-αCD123 antibodies differed in regards to the autonomous targeting by the SIRPα domains. The 2×SIRPα-αCD123 indicated weak RBC binding and showed unspecific lysis of target antigen negative cells on higher concentrations in comparison to the 1×SIRPα-αCD123. On the other hand, 2×SIRPα-αCD123 was more effective in targeting the $CD34^{+}/CD38^{-}$ LSCs. To further analyze the safety and efficacy of the molecules and to determine whether the 1×- or 2×SIRPα-αCD123 fusion format would be favorable, competitive ADCC experiments with patient-derived AML and healthy cells would be beneficial. Using this material with representative CD123 and CD47 expression would give a clearer picture of healthy tissue targeting by the 2×SIRPα format.

The GD2 targeting antibodies with N-terminal (SIRPα-αGD2) fusion of SIRPα differed substantially in terms of RBC binding from the C-terminal (αGD2-SIRPα) fusion molecule.

This was especially prominent in the mouse antibodies and combined with the data from phagocytosis assay, αGD2-SIRPα was determined as the preferred candidate for future *in vivo* evaluation. The N-terminal fusion format of the SIRPα-antibody caused some hemagglutination of human RBCs, albeit at a 50-fold higher concentration than reported for magrolimab [174], and thus the C-terminal fusion format could have a better safety profile overall.

5.7. Future perspectives

Both GD2 and CD123 are validated cancer antigens with numerous therapeutic agents in clinics or being tested in clinical trials [240, 241, 335]. In addition to AML, CD123 has been shown to be overexpressed on a number of other myeloid and lymphoid malignancies, such as MDS, BPDCN, chronic myeloid leukemia, B-cell acute lymphoblastic leukemia, hairy cell leukemia and Hodgkin's lymphoma [336-340]. For MDS and CML, CD123 overexpression is observed in leukemic stem and progenitor cells [336, 339]. Targeting CD123 in combination with CD47 represents therefore an attractive therapeutic target for these hematological malignancies in addition to AML. GD2 expression is as well found in a subset of melanoma, sarcoma and breast tumors in addition to NBS indicating a possibility to broaden the application of the αGD2-SIRPα fusion molecules in the future [341-343].

Blockade of the CD47/SIRPα interaction does not only promote the direct cancer cell elimination by macrophages, but can further stimulate the adaptive immune response. Either macrophages or dendritic cells have been shown to participate in the antigen presentation upon disruption of the CD47/SIRPα interaction [78, 137, 344, 345]. However, CD47 ligand SIRPγ is expressed on human but not on mouse T cells [346]. SIRPγ regulates cell-cell adhesion, T cell transendothelial migration and cell costimulation with DCs [347, 348]. Targeting CD47 with a mAB has been shown to reduce human T cell activation, proliferation, and transmigration across the human endothelium [172]. Investigating the effect of SIRPα-antibody fusion molecules to human dendritic cells and T cells would be of high interest as the CD47 interaction with SIRPγ would be unaffected and could therefore allow for a potent cancer specific activation of both innate and adaptive immunity.

As the CD47/SIRPα axis blockade contributes to T cell activation, it is not surprising that synergy with T cell immune checkpoint blockade such as αPDL1 has been observed [172, 281, 349, 350]. In humans, however, 56% ovarian cancer patients reached a stable disease as best outcome in a phase 1b study where αPDL1 antibody avelumab and αCD47 antibody magrolimab were combined [165]. Whether this combinatorial treatment would be effective when using a tumor-specific CD47/SIRPα blockade, which would not impair the function of T cells in a way that αCD47 has been shown, remains to be investigated. Experiments with a molecule consisting of human Fc, mouse SIRPα and an αPDL1 single chain variable fragment (scFv) have demonstrated a synergy when addressing the CD47 and PD1 checkpoints together

in mouse models, but indicated that an additional pro-phagocytic signal is needed for a more effective therapy [351]. Further development of the SIRPα-antibodies could include the fusion of a PDL1 checkpoint blocking domain, such as the PD1 extracellular domain, for the local blockade of the two checkpoints [129]. Combining the CD47/SIRPα axis blockade with an APC costimulation through receptors of the tumor necrosis factor receptor (TNFR) family like CD40 and 41BB represent another putative way to boost the antitumor response [172, 352].

Collectively, this work provides evidence that SIRPα-αCD123 antibodies are potent in AML LSCs targeting while sparing healthy cells such as RBSs. The αGD2-SIRPα antibody was similarly effective in targeting of NBS and enhanced ADCP in both human and mouse models. The SIRPα-antibody fusion molecules with a specific and local blockade of CD47 provide many exciting opportunities for research. Future studies evaluating the efficacy of these molecules on different tumors alone or in combination with other immune modulators will hopefully elucidate the therapeutic potential of SIRPα-antibodies in the treatment of cancer patients.

6. References

1. Charles A. Janeway J, Medzhitov R. Innate Immune Recognition. *Annual Review of Immunology*. 2002; **20**: 197-216.
2. Janeway CA. Approaching the Asymptote? Evolution and Revolution in Immunology. *Cold Spring Harbor Symposia on Quantitative Biology*. 1989; **54**: 1-13.
3. Medzhitov R, Preston-Hurlburt P, Janeway CA, Jr. A human homologue of the Drosophila Toll protein signals activation of adaptive immunity. *Nature*. 1997; **388**: 394-7.
4. Medzhitov R. Approaching the Asymptote: 20 Years Later. *Immunity*. 2009; **30**: 766-75.
5. Klose CSN, Artis D. Innate lymphoid cells control signaling circuits to regulate tissue-specific immunity. *Cell Research*. 2020; **30**: 475-91.
6. Janeway CA. The immune system evolved to discriminate infectious nonself from noninfectious self. *Immunology Today*. 1992; **13**: 11-6.
7. Cooper MD, Herrin BR. How did our complex immune system evolve? *Nature Reviews Immunology*. 2010; **10**: 2-3.
8. Waldmann H. Immunological Tolerance. Reference Module in Biomedical Sciences: Elsevier; 2014.
9. Iwasaki A, Medzhitov R. Control of adaptive immunity by the innate immune system. *Nature immunology*. 2015; **16**: 343-53.
10. von Andrian UH, Mackay CR. T-Cell Function and Migration — Two Sides of the Same Coin. *New England Journal of Medicine*. 2000; **343**: 1020-34.
11. Tsai RK, Discher DE. Inhibition of "self" engulfment through deactivation of myosin-II at the phagocytic synapse between human cells. *J Cell Biol*. 2008; **180**: 989-1003.
12. Kärre K, Ljunggren HG, Piontek G, Kiessling R. Selective rejection of H–2-deficient lymphoma variants suggests alternative immune defence strategy. *Nature*. 1986; **319**: 675-8.
13. Hanahan D, Weinberg RA. Hallmarks of cancer: the next generation. *Cell*. 2011; **144**: 646-74.
14. Ehrlich P. Ueber den jetzigen Stand der Karzinomforschung. *Beiträge zur experimentellen Pathologie und Chemotherapie*. 1908: 117–64.
15. Burnet M. Cancer: a biological approach. III. Viruses associated with neoplastic conditions. IV. Practical applications. *Br Med J*. 1957; **1**: 841-7.
16. Thomas L. in Cellular and Humoral Aspects of the Hypersensitive States (ed. Lawrence, H. S.) 529–32 (Hoeber-Harper, New York).
17. Burnet M. Immunological Factors in the Process of Carcinogenesis. *Br Med Bull*. 1964; **20**: 154-8.
18. Burnet FM. The concept of immunological surveillance. *Prog Exp Tumor Res*. 1970; **13**: 1-27.
19. Dunn GP, Bruce AT, Ikeda H, Old LJ, Schreiber RD. Cancer immunoediting: from immunosurveillance to tumor escape. *Nat Immunol*. 2002; **3**: 991-8.
20. Sheil AG. Cancer after transplantation. *World J Surg*. 1986; **10**: 389-96.
21. Penn I. Malignant melanoma in organ allograft recipients. *Transplantation*. 1996; **61**: 274-8.
22. Penn I. Sarcomas in organ allograft recipients. *Transplantation*. 1995; **60**: 1485-91.
23. Pham SM, Kormos RL, Landreneau RJ, Kawai A, Gonzalez-Cancel I, Hardesty RL, et al. Solid tumors after heart transplantation: lethality of lung cancer. *Ann Thorac Surg*. 1995; **60**: 1623-6.
24. Clark WH, Jr., Elder DE, Guerry Dt, Braitman LE, Trock BJ, Schultz D, et al. Model predicting survival in stage I melanoma based on tumor progression. *J Natl Cancer Inst*. 1989; **81**: 1893-904.

25. Clemente CG, Mihm MC, Jr., Bufalino R, Zurrida S, Collini P, Cascinelli N. Prognostic value of tumor infiltrating lymphocytes in the vertical growth phase of primary cutaneous melanoma. *Cancer*. 1996; **77**: 1303-10.
26. Rilke F, Colnaghi MI, Cascinelli N, Andreola S, Baldini MT, Bufalino R, et al. Prognostic significance of HER-2/neu expression in breast cancer and its relationship to other prognostic factors. *Int J Cancer*. 1991; **49**: 44-9.
27. Lipponen PK, Eskelinen MJ, Jauhiainen K, Harju E, Terho R. Tumour infiltrating lymphocytes as an independent prognostic factor in transitional cell bladder cancer. *Eur J Cancer*. 1992; **29a**: 69-75.
28. Nacopoulou L, Azaris P, Papacharalampous N, Davaris P. Prognostic significance of histologic host response in cancer of the large bowel. *Cancer*. 1981; **47**: 930-6.
29. Naito Y, Saito K, Shiiba K, Ohuchi A, Saigenji K, Nagura H, et al. CD8+ T cells infiltrated within cancer cell nests as a prognostic factor in human colorectal cancer. *Cancer Res*. 1998; **58**: 3491-4.
30. Epstein NA, Fatti LP. Prostatic carcinoma: some morphological features affecting prognosis. *Cancer*. 1976; **37**: 2455-65.
31. Deligdisch L, Jacobs AJ, Cohen CJ. Histologic correlates of virulence in ovarian adenocarcinoma. II. Morphologic correlates of host response. *Am J Obstet Gynecol*. 1982; **144**: 885-9.
32. Jass JR. Lymphocytic infiltration and survival in rectal cancer. *J Clin Pathol*. 1986; **39**: 585-9.
33. Palma L, Di Lorenzo N, Guidetti B. Lymphocytic infiltrates in primary glioblastomas and recidivous gliomas. Incidence, fate, and relevance to prognosis in 228 operated cases. *J Neurosurg*. 1978; **49**: 854-61.
34. Diefenbach A, Jensen ER, Jamieson AM, Raulet DH. Rae1 and H60 ligands of the NKG2D receptor stimulate tumour immunity. *Nature*. 2001; **413**: 165-71.
35. Bauer S, Groh V, Wu J, Steinle A, Phillips JH, Lanier LL, et al. Activation of NK cells and T cells by NKG2D, a receptor for stress-inducible MICA. *Science*. 1999; **285**: 727-9.
36. Kärre K, Ljunggren HG, Piontek G, Kiessling R. Selective rejection of H-2-deficient lymphoma variants suggests alternative immune defence strategy. *Nature*. 1986; **319**: 675-8.
37. Piontek GE, Taniguchi K, Ljunggren HG, Grönberg A, Kiessling R, Klein G, et al. YAC-1 MHC class I variants reveal an association between decreased NK sensitivity and increased H-2 expression after interferon treatment or in vivo passage. *The Journal of Immunology*. 1985; **135**: 4281-8.
38. Schumacher TN, Schreiber RD. Neoantigens in cancer immunotherapy. *Science*. 2015; **348**: 69.
39. Boon T, Cerottini JC, Van den Eynde B, van der Bruggen P, Van Pel A. Tumor antigens recognized by T lymphocytes. *Annu Rev Immunol*. 1994; **12**: 337-65.
40. Ferguson TA, Choi J, Green DR. Armed response: how dying cells influence T-cell functions. *Immunological reviews*. 2011; **241**: 77-88.
41. Chen Daniel S, Mellman I. Oncology Meets Immunology: The Cancer-Immunity Cycle. *Immunity*. 2013; **39**: 1-10.
42. Ikeda H, Old LJ, Schreiber RD. The roles of IFNγ in protection against tumor development and cancer immunoediting. *Cytokine & Growth Factor Reviews*. 2002; **13**: 95-109.
43. Sinha P, Clements VK, Miller S, Ostrand-Rosenberg S. Tumor immunity: a balancing act between T cell activation, macrophage activation and tumor-induced immune suppression. *Cancer Immunology, Immunotherapy*. 2005; **54**: 1137-42.

44. Pulaski BA, Smyth MJ, Ostrand-Rosenberg S. Interferon-gamma-dependent phagocytic cells are a critical component of innate immunity against metastatic mammary carcinoma. *Cancer Res*. 2002; **62**: 4406-12.
45. Bancroft GJ, Schreiber RD, Unanue ER. Natural Immunity: A T-Cell-Independent Pathway of Macrophage Activation, Defined in the scid Mouse. *Immunological Reviews*. 1991; **124**: 5-24.
46. Kooi S, Zhang H-Z, Patenia R, Edwards CL, Platsoucas CD, Freedman RS. HLA Class I Expression on Human Ovarian Carcinoma Cells Correlates with T-Cell Infiltrationin Vivoand T-Cell Expansionin Vitroin Low Concentrations of Recombinant Interleukin-2. *Cellular Immunology*. 1996; **174**: 116-28.
47. Zheng P, Sarma S, Guo Y, Liu Y. Two mechanisms for tumor evasion of preexisting cytotoxic T-cell responses: lessons from recurrent tumors. *Cancer Res*. 1999; **59**: 3461-7.
48. Restifo NP, Marincola FM, Kawakami Y, Taubenberger J, Yannelli JR, Rosenberg SA. Loss of functional beta 2-microglobulin in metastatic melanomas from five patients receiving immunotherapy. *J Natl Cancer Inst*. 1996; **88**: 100-8.
49. Cabrera T, Fernandez MA, Sierra A, Garrido A, Herruzo A, Escobedo A, et al. High frequency of altered HLA class I phenotypes in invasive breast carcinomas. *Human Immunology*. 1996; **50**: 127-34.
50. Khong HT, Restifo NP. Natural selection of tumor variants in the generation of "tumor escape" phenotypes. *Nature Immunology*. 2002; **3**: 999-1005.
51. Cornel AM, Mimpen IL, Nierkens S. MHC Class I Downregulation in Cancer: Underlying Mechanisms and Potential Targets for Cancer Immunotherapy. *Cancers*. 2020; **12**: 1760.
52. Vitale M, Cantoni C, Pietra G, Mingari MC, Moretta L. Effect of tumor cells and tumor microenvironment on NK-cell function. *European Journal of Immunology*. 2014; **44**: 1582-92.
53. McGilvray RW, Eagle RA, Watson NFS, Al-Attar A, Ball G, Jafferji I, et al. NKG2D Ligand Expression in Human Colorectal Cancer Reveals Associations with Prognosis and Evidence for Immunoediting. *Clinical Cancer Research*. 2009; **15**: 6993-7002.
54. Munn DH, Mellor AL. IDO and tolerance to tumors. *Trends in Molecular Medicine*. 2004; **10**: 15-8.
55. Frumento G, Rotondo R, Tonetti M, Damonte G, Benatti U, Ferrara GB. Tryptophan-derived catabolites are responsible for inhibition of T and natural killer cell proliferation induced by indoleamine 2,3-dioxygenase. *J Exp Med*. 2002; **196**: 459-68.
56. Della Chiesa M, Carlomagno S, Frumento G, Balsamo M, Cantoni C, Conte R, et al. The tryptophan catabolite L-kynurenine inhibits the surface expression of NKp46- and NKG2D-activating receptors and regulates NK-cell function. *Blood*. 2006; **108**: 4118-25.
57. Gabrilovich DI, Nagaraj S. Myeloid-derived suppressor cells as regulators of the immune system. *Nature reviews Immunology*. 2009; **9**: 162-74.
58. Rodriguez PC, Zea AH, Culotta KS, Zabaleta J, Ochoa JB, Ochoa AC. Regulation of T cell receptor CD3zeta chain expression by L-arginine. *J Biol Chem*. 2002; **277**: 21123-9.
59. Sakaguchi S, Yamaguchi T, Nomura T, Ono M. Regulatory T Cells and Immune Tolerance. *Cell*. 2008; **133**: 775-87.
60. Tanaka A, Sakaguchi S. Regulatory T cells in cancer immunotherapy. *Cell Research*. 2017; **27**: 109-18.
61. Qureshi OS, Zheng Y, Nakamura K, Attridge K, Manzotti C, Schmidt EM, et al. Trans-endocytosis of CD80 and CD86: a molecular basis for the cell-extrinsic function of CTLA-4. *Science*. 2011; **332**: 600-3.
62. Noy R, Pollard JW. Tumor-associated macrophages: from mechanisms to therapy. *Immunity*. 2014; **41**: 49-61.

63. Agata Y, Kawasaki A, Nishimura H, Ishida Y, Tsubata T, Yagita H, et al. Expression of the PD-1 antigen on the surface of stimulated mouse T and B lymphocytes. *Int Immunol*. 1996; **8**: 765-72.
64. Dong H, Strome SE, Salomao DR, Tamura H, Hirano F, Flies DB, et al. Tumor-associated B7-H1 promotes T-cell apoptosis: A potential mechanism of immune evasion. *Nature Medicine*. 2002; **8**: 793-800.
65. Latchman Y, Wood CR, Chernova T, Chaudhary D, Borde M, Chernova I, et al. PD-L2 is a second ligand for PD-1 and inhibits T cell activation. *Nature Immunology*. 2001; **2**: 261-8.
66. Freeman GJ, Long AJ, Iwai Y, Bourque K, Chernova T, Nishimura H, et al. Engagement of the PD-1 immunoinhibitory receptor by a novel B7 family member leads to negative regulation of lymphocyte activation. *J Exp Med*. 2000; **192**: 1027-34.
67. Curiel TJ, Wei S, Dong H, Alvarez X, Cheng P, Mottram P, et al. Blockade of B7-H1 improves myeloid dendritic cell–mediated antitumor immunity. *Nature Medicine*. 2003; **9**: 562-7.
68. Lin H, Wei S, Hurt EM, Green MD, Zhao L, Vatan L, et al. Host expression of PD-L1 determines efficacy of PD-L1 pathway blockade-mediated tumor regression. *J Clin Invest*. 2018; **128**: 805-15.
69. Tang H, Liang Y, Anders RA, Taube JM, Qiu X, Mulgaonkar A, et al. PD-L1 on host cells is essential for PD-L1 blockade-mediated tumor regression. *J Clin Invest*. 2018; **128**: 580-8.
70. Hsu J, Hodgins JJ, Marathe M, Nicolai CJ, Bourgeois-Daigneault MC, Trevino TN, et al. Contribution of NK cells to immunotherapy mediated by PD-1/PD-L1 blockade. *J Clin Invest*. 2018; **128**: 4654-68.
71. Moral JA, Leung J, Rojas LA, Ruan J, Zhao J, Sethna Z, et al. ILC2s amplify PD-1 blockade by activating tissue-specific cancer immunity. *Nature*. 2020; **579**: 130-5.
72. Gordon SR, Maute RL, Dulken BW, Hutter G, George BM, McCracken MN, et al. PD-1 expression by tumour-associated macrophages inhibits phagocytosis and tumour immunity. *Nature*. 2017; **545**: 495-9.
73. Majeti R, Chao MP, Alizadeh AA, Pang WW, Jaiswal S, Gibbs KD, Jr., et al. CD47 is an adverse prognostic factor and therapeutic antibody target on human acute myeloid leukemia stem cells. *Cell*. 2009; **138**: 286-99.
74. Jaiswal S, Jamieson CH, Pang WW, Park CY, Chao MP, Majeti R, et al. CD47 is upregulated on circulating hematopoietic stem cells and leukemia cells to avoid phagocytosis. *Cell*. 2009; **138**: 271-85.
75. Chao MP, Alizadeh AA, Tang C, Myklebust JH, Varghese B, Gill S, et al. Anti-CD47 antibody synergizes with rituximab to promote phagocytosis and eradicate non-Hodgkin lymphoma. *Cell*. 2010; **142**: 699-713.
76. Willingham SB, Volkmer JP, Gentles AJ, Sahoo D, Dalerba P, Mitra SS, et al. The CD47-signal regulatory protein alpha (SIRPa) interaction is a therapeutic target for human solid tumors. *Proc Natl Acad Sci U S A*. 2012; **109**: 6662-7.
77. Tseng D, Volkmer JP, Willingham SB, Contreras-Trujillo H, Fathman JW, Fernhoff NB, et al. Anti-CD47 antibody-mediated phagocytosis of cancer by macrophages primes an effective antitumor T-cell response. *Proc Natl Acad Sci U S A*. 2013; **110**: 11103-8.
78. Liu X, Pu Y, Cron K, Deng L, Kline J, Frazier WA, et al. CD47 blockade triggers T cell-mediated destruction of immunogenic tumors. *Nat Med*. 2015; **21**: 1209-15.
79. Cham LB, Torrez Dulgeroff LB, Tal MC, Adomati T, Li F, Bhat H, et al. Immunotherapeutic Blockade of CD47 Inhibitory Signaling Enhances Innate and Adaptive Immune Responses to Viral Infection. *Cell Reports*. 2020; **31**: 107494.

80. Hoption Cann SA, van Netten JP, van Netten C. Dr William Coley and tumour regression: a place in history or in the future. *Postgraduate Medical Journal*. 2003; **79**: 672-80.
81. Zitvogel L, Galluzzi L, Smyth Mark J, Kroemer G. Mechanism of Action of Conventional and Targeted Anticancer Therapies: Reinstating Immunosurveillance. *Immunity*. 2013; **39**: 74-88.
82. Galluzzi L, Buqué A, Kepp O, Zitvogel L, Kroemer G. Immunological Effects of Conventional Chemotherapy and Targeted Anticancer Agents. *Cancer Cell*. 2015; **28**: 690-714.
83. Brix N, Tiefenthaller A, Anders H, Belka C, Lauber K. Abscopal, immunological effects of radiotherapy: Narrowing the gap between clinical and preclinical experiences. *Immunol Rev*. 2017; **280**: 249-79.
84. Hodi FS, O'Day SJ, McDermott DF, Weber RW, Sosman JA, Haanen JB, et al. Improved Survival with Ipilimumab in Patients with Metastatic Melanoma. *New England Journal of Medicine*. 2010; **363**: 711-23.
85. Brahmer JR, Tykodi SS, Chow LQ, Hwu WJ, Topalian SL, Hwu P, et al. Safety and activity of anti-PD-L1 antibody in patients with advanced cancer. *N Engl J Med*. 2012; **366**: 2455-65.
86. Wei SC, Duffy CR, Allison JP. Fundamental Mechanisms of Immune Checkpoint Blockade Therapy. *Cancer Discov*. 2018; **8**: 1069-86.
87. Janeway C, Travers P, Walport M, et al. . Immunobiology: The Immune System in Health and Disease. 5th edition. . New York: Garland Science; 2001.
88. Silverton EW, Navia MA, Davies DR. Three-dimensional structure of an intact human immunoglobulin. *Proceedings of the National Academy of Sciences of the United States of America*. 1977; **74**: 5140-4.
89. Wu TT, Kabat EA. An analysis of the sequences of the variable regions of Bence Jones proteins and myeloma light chains and their implications for antibody complementarity. *J Exp Med*. 1970; **132**: 211-50.
90. Porter RR. The hydrolysis of rabbit y-globulin and antibodies with crystalline papain. *Biochem J*. 1959; **73**: 119-26.
91. Bruhns P. Properties of mouse and human IgG receptors and their contribution to disease models. *Blood*. 2012; **119**: 5640-9.
92. Bruhns P, Iannascoli B, England P, Mancardi DA, Fernandez N, Jorieux S, et al. Specificity and affinity of human Fcγ receptors and their polymorphic variants for human IgG subclasses. *Blood*. 2009; **113**: 3716-25.
93. Reth M. Antigen receptor tail clue. *Nature*. 1989; **338**: 383-4.
94. Daëron M, Jaeger S, Du Pasquier L, Vivier E. Immunoreceptor tyrosine-based inhibition motifs: a quest in the past and future. *Immunol Rev*. 2008; **224**: 11-43.
95. Nimmerjahn F, Ravetch JV. Fcγ receptors as regulators of immune responses. *Nature Reviews Immunology*. 2008; **8**: 34-47.
96. Lanier LL. NK CELL RECOGNITION. *Annual Review of Immunology*. 2005; **23**: 225-74.
97. May RC, Machesky LM. Phagocytosis and the actin cytoskeleton. *Journal of Cell Science*. 2001; **114**: 1061-77.
98. De Palma M, Lewis Claire E. Macrophage Regulation of Tumor Responses to Anticancer Therapies. *Cancer Cell*. 2013; **23**: 277-86.
99. Gül N, Babes L, Siegmund K, Korthouwer R, Bögels M, Braster R, et al. Macrophages eliminate circulating tumor cells after monoclonal antibody therapy. *The Journal of clinical investigation*. 2014; **124**: 812-23.

100. Boross P, van Montfoort N, Stapels DAC, van der Poel CE, Bertens C, Meeldijk J, et al. FcRγ-Chain ITAM Signaling Is Critically Required for Cross-Presentation of Soluble Antibody–Antigen Complexes by Dendritic Cells. *The Journal of Immunology*. 2014; **193**: 5506-14.
101. Köhler G, Milstein C. Continuous cultures of fused cells secreting antibody of predefined specificity. *Nature*. 1975; **256**: 495-7.
102. Clynes R. Antitumor Antibodies in the Treatment of Cancer: Fc Receptors Link Opsonic Antibody with Cellular Immunity. *Hematology/Oncology Clinics of North America*. 2006; **20**: 585-612.
103. Iannello A, Ahmad A. Role of antibody-dependent cell-mediated cytotoxicity in the efficacy of therapeutic anti-cancer monoclonal antibodies. *Cancer and Metastasis Reviews*. 2005; **24**: 487-99.
104. Lu R-M, Hwang Y-C, Liu IJ, Lee C-C, Tsai H-Z, Li H-J, et al. Development of therapeutic antibodies for the treatment of diseases. *Journal of Biomedical Science*. 2020; **27**: 1.
105. Weng W-K, Levy R. Two Immunoglobulin G Fragment C Receptor Polymorphisms Independently Predict Response to Rituximab in Patients With Follicular Lymphoma. *Journal of Clinical Oncology*. 2003; **21**: 3940-7.
106. Richards JO, Karki S, Lazar GA, Chen H, Dang W, Desjarlais JR. Optimization of antibody binding to FcγRIIa enhances macrophage phagocytosis of tumor cells. *Molecular Cancer Therapeutics*. 2008; **7**: 2517-27.
107. Zhang W, Gordon M, Schultheis AM, Yang DY, Nagashima F, Azuma M, et al. FCGR2A and FCGR3A Polymorphisms Associated With Clinical Outcome of Epidermal Growth Factor Receptor–Expressing Metastatic Colorectal Cancer Patients Treated With Single-Agent Cetuximab. *Journal of Clinical Oncology*. 2007; **25**: 3712-8.
108. Tamura K, Shimizu C, Hojo T, Akashi-Tanaka S, Kinoshita T, Yonemori K, et al. FcγR2A and 3A polymorphisms predict clinical outcome of trastuzumab in both neoadjuvant and metastatic settings in patients with HER2-positive breast cancer. *Ann Oncol*. 2011; **22**: 1302-7.
109. Weiner LM, Surana R, Wang S. Monoclonal antibodies: versatile platforms for cancer immunotherapy. *Nature reviews Immunology*. 2010; **10**: 317-27.
110. Racila E, Link BK, Weng WK, Witzig TE, Ansell S, Maurer MJ, et al. A polymorphism in the complement component C1qA correlates with prolonged response following rituximab therapy of follicular lymphoma. *Clin Cancer Res*. 2008; **14**: 6697-703.
111. Carter PJ, Lazar GA. Next generation antibody drugs: pursuit of the 'high-hanging fruit'. *Nature Reviews Drug Discovery*. 2018; **17**: 197-223.
112. Sharpe AH, Pauken KE. The diverse functions of the PD1 inhibitory pathway. *Nat Rev Immunol*. 2018; **18**: 153-67.
113. Schadendorf D, Hodi FS, Robert C, Weber JS, Margolin K, Hamid O, et al. Pooled Analysis of Long-Term Survival Data From Phase II and Phase III Trials of Ipilimumab in Unresectable or Metastatic Melanoma. *J Clin Oncol*. 2015; **33**: 1889-94.
114. Mellman I, Coukos G, Dranoff G. Cancer immunotherapy comes of age. *Nature*. 2011; **480**: 480-9.
115. Pardoll DM. The blockade of immune checkpoints in cancer immunotherapy. *Nature Reviews Cancer*. 2012; **12**: 252-64.
116. Wei SC, Anang N-AAS, Sharma R, Andrews MC, Reuben A, Levine JH, et al. Combination anti–CTLA-4 plus anti–PD-1 checkpoint blockade utilizes cellular mechanisms partially distinct from monotherapies. *Proceedings of the National Academy of Sciences*. 2019; **116**: 22699-709.

117. Pentcheva-Hoang T, Egen JG, Wojnoonski K, Allison JP. B7-1 and B7-2 Selectively Recruit CTLA-4 and CD28 to the Immunological Synapse. *Immunity*. 2004; **21**: 401-13.
118. Leach DR, Krummel MF, Allison JP. Enhancement of Antitumor Immunity by CTLA-4 Blockade. *Science*. 1996; **271**: 1734-6.
119. Liu Y, Zheng P. Preserving the CTLA-4 Checkpoint for Safer and More Effective Cancer Immunotherapy. *Trends in Pharmacological Sciences*. 2020; **41**: 4-12.
120. Waight JD, Chand D, Dietrich S, Gombos R, Horn T, Gonzalez AM, et al. Selective FcγR Co-engagement on APCs Modulates the Activity of Therapeutic Antibodies Targeting T Cell Antigens. *Cancer Cell*. 2018; **33**: 1033-47.e5.
121. Arce Vargas F, Furness AJS, Litchfield K, Joshi K, Rosenthal R, Ghorani E, et al. Fc Effector Function Contributes to the Activity of Human Anti-CTLA-4 Antibodies. *Cancer Cell*. 2018; **33**: 649-63.e4.
122. Selby MJ, Engelhardt JJ, Quigley M, Henning KA, Chen T, Srinivasan M, et al. Anti-CTLA-4 Antibodies of IgG2a Isotype Enhance Antitumor Activity through Reduction of Intratumoral Regulatory T Cells. *Cancer Immunology Research*. 2013; **1**: 32-42.
123. Fisch H, Laor E, Lipshultz LI. Simplified gonadotropin-releasing hormone (GnRH) stimulation test. *Urology*. 1990; **36**: 260-3.
124. Mayoux M, Roller A, Pulko V, Sammicheli S, Chen S, Sum E, et al. Dendritic cells dictate responses to PD-L1 blockade cancer immunotherapy. *Science Translational Medicine*. 2020; **12**: eaav7431.
125. Garris CS, Arlauckas SP, Kohler RH, Trefny MP, Garren S, Piot C, et al. Successful Anti-PD-1 Cancer Immunotherapy Requires T Cell-Dendritic Cell Crosstalk Involving the Cytokines IFN-γ and IL-12. *Immunity*. 2018; **49**: 1148-61.e7.
126. Oh SA, Wu D-C, Cheung J, Navarro A, Xiong H, Cubas R, et al. PD-L1 expression by dendritic cells is a key regulator of T-cell immunity in cancer. *Nature Cancer*. 2020; **1**: 681-91.
127. Strauss L, Mahmoud MAA, Weaver JD, Tijaro-Ovalle NM, Christofides A, Wang Q, et al. Targeted deletion of PD-1 in myeloid cells induces antitumor immunity. *Science Immunology*. 2020; **5**: eaay1863.
128. June CH, Warshauer JT, Bluestone JA. Is autoimmunity the Achilles' heel of cancer immunotherapy? *Nat Med*. 2017; **23**: 540-7.
129. Herrmann M, Krupka C, Deiser K, Brauchle B, Marcinek A, Ogrinc Wagner A, et al. Bifunctional PD-1 × αCD3 × αCD33 fusion protein reverses adaptive immune escape in acute myeloid leukemia. *Blood*. 2018; **132**: 2484-94.
130. Dammeijer F, van Gulijk M, Mulder EE, Lukkes M, Klaase L, van den Bosch T, et al. The PD-1/PD-L1-Checkpoint Restrains T cell Immunity in Tumor-Draining Lymph Nodes. *Cancer Cell*. 2020; **38**: 685-700.e8.
131. Topalian SL, Hodi FS, Brahmer JR, Gettinger SN, Smith DC, McDermott DF, et al. Safety, Activity, and Immune Correlates of Anti–PD-1 Antibody in Cancer. *New England Journal of Medicine*. 2012; **366**: 2443-54.
132. Brown EJ, Frazier WA. Integrin-associated protein (CD47) and its ligands. *Trends Cell Biol*. 2001; **11**: 130-5.
133. Reinhold MI, Lindberg FP, Plas D, Reynolds S, Peters MG, Brown EJ. In vivo expression of alternatively spliced forms of integrin-associated protein (CD47). *J Cell Sci*. 1995; **108** 3419-25.
134. Brown E, Hooper L, Ho T, Gresham H. Integrin-associated protein: a 50-kD plasma membrane antigen physically and functionally associated with integrins. *J Cell Biol*. 1990; **111**: 2785-94.
135. Oldenborg PA, Zheleznyak A, Fang YF, Lagenaur CF, Gresham HD, Lindberg FP. Role of CD47 as a marker of self on red blood cells. *Science*. 2000; **288**: 2051-4.

136. Olsson M, Bruhns P, Frazier WA, Ravetch JV, Oldenborg P-A. Platelet homeostasis is regulated by platelet expression of CD47 under normal conditions and in passive immune thrombocytopenia. *Blood*. 2005; **105**: 3577-82.
137. Xu MM, Pu Y, Han D, Shi Y, Cao X, Liang H, et al. Dendritic Cells but Not Macrophages Sense Tumor Mitochondrial DNA for Cross-priming through Signal Regulatory Protein alpha Signaling. *Immunity*. 2017; **47**: 363-73 e5.
138. Campbell IG, Freemont PS, Foulkes W, Trowsdale J. An ovarian tumor marker with homology to vaccinia virus contains an IgV-like region and multiple transmembrane domains. *Cancer Res*. 1992; **52**: 5416-20.
139. Barclay AN, Brown MH. The SIRP family of receptors and immune regulation. *Nature Reviews Immunology*. 2006; **6**: 457-64.
140. Matozaki T, Murata Y, Okazawa H, Ohnishi H. Functions and molecular mechanisms of the CD47–SIRPα signalling pathway. *Trends in Cell Biology*. 2009; **19**: 72-80.
141. Barclay AN, Berg TKvd. The Interaction Between Signal Regulatory Protein Alpha (SIRPα) and CD47: Structure, Function, and Therapeutic Target. *Annual Review of Immunology*. 2014; **32**: 25-50.
142. Morrissey MA, Kern N, Vale RD. CD47 Ligation Repositions the Inhibitory Receptor SIRPA to Suppress Integrin Activation and Phagocytosis. *Immunity*. 2020; **53**: 290-302.e6.
143. Okazawa H, Motegi S-i, Ohyama N, Ohnishi H, Tomizawa T, Kaneko Y, et al. Negative Regulation of Phagocytosis in Macrophages by the CD47-SHPS-1 System. *The Journal of Immunology*. 2005; **174**: 2004-11.
144. Soto-Pantoja DR, Kaur S, Roberts DD. CD47 signaling pathways controlling cellular differentiation and responses to stress. *Crit Rev Biochem Mol Biol*. 2015; **50**: 212-30.
145. Subramanian S, Boder ET, Discher DE. Phylogenetic divergence of CD47 interactions with human signal regulatory protein alpha reveals locus of species specificity. Implications for the binding site. *J Biol Chem*. 2007; **282**: 1805-18.
146. Kwong LS, Brown MH, Barclay AN, Hatherley D. Signal-regulatory protein alpha from the NOD mouse binds human CD47 with an exceptionally high affinity-- implications for engraftment of human cells. *Immunology*. 2014; **143**: 61-7.
147. Takenaka K, Prasolava TK, Wang JC, Mortin-Toth SM, Khalouei S, Gan OI, et al. Polymorphism in Sirpa modulates engraftment of human hematopoietic stem cells. *Nat Immunol*. 2007; **8**: 1313-23.
148. Hatherley D, Lea SM, Johnson S, Barclay AN. Polymorphisms in the human inhibitory signal-regulatory protein alpha do not affect binding to its ligand CD47. *J Biol Chem*. 2014; **289**: 10024-8.
149. Weiskopf K, Ring AM, Ho CC, Volkmer JP, Levin AM, Volkmer AK, et al. Engineered SIRPalpha variants as immunotherapeutic adjuvants to anticancer antibodies. *Science*. 2013; **341**: 88-91.
150. Liu J, Wang L, Zhao F, Tseng S, Narayanan C, Shura L, et al. Pre-Clinical Development of a Humanized Anti-CD47 Antibody with Anti-Cancer Therapeutic Potential. *PLoS One*. 2015; **10**: e0137345.
151. Hatherley D, Graham SC, Turner J, Harlos K, Stuart DI, Barclay AN. Paired Receptor Specificity Explained by Structures of Signal Regulatory Proteins Alone and Complexed with CD47. *Molecular Cell*. 2008; **31**: 266-77.
152. Barclay AN, Hatherley D. The Counterbalance Theory for Evolution and Function of Paired Receptors. *Immunity*. 2008; **29**: 675-8.
153. Weiskopf K, Jahchan NS, Schnorr PJ, Cristea S, Ring AM, Maute RL, et al. CD47-blocking immunotherapies stimulate macrophage-mediated destruction of small-cell lung cancer. *J Clin Invest*. 2016; **126**: 2610-20.

154. Ngo M, Han A, Lakatos A, Sahoo D, Hachey SJ, Weiskopf K, et al. Antibody Therapy Targeting CD47 and CD271 Effectively Suppresses Melanoma Metastasis in Patient-Derived Xenografts. *Cell Rep*. 2016; **16**: 1701-16.
155. Sallman DA, Asch AS, Malki MMA, Lee DJ, Donnellan WB, Marcucci G, et al. The First-in-Class Anti-CD47 Antibody Magrolimab (5F9) in Combination with Azacitidine Is Effective in MDS and AML Patients: Ongoing Phase 1b Results. *Blood*. 2019; **134**: (Supplement_1): 569 (*Abstract*).
156. Ring NG, Herndler-Brandstetter D, Weiskopf K, Shan L, Volkmer JP, George BM, et al. Anti-SIRPalpha antibody immunotherapy enhances neutrophil and macrophage antitumor activity. *Proc Natl Acad Sci U S A*. 2017; **114**: E10578-E85.
157. Jain S, Van Scoyk A, Morgan EA, Matthews A, Stevenson K, Newton G, et al. Targeted inhibition of CD47-SIRPalpha requires Fc-FcgammaR interactions to maximize activity in T-cell lymphomas. *Blood*. 2019; **134**: 1430-40.
158. Chao MP, Takimoto CH, Feng DD, McKenna K, Gip P, Liu J, et al. Therapeutic Targeting of the Macrophage Immune Checkpoint CD47 in Myeloid Malignancies. *Front Oncol*. 2019; **9**: 1380.
159. Oldenborg P-A, Gresham HD, Lindberg FP. Cd47-Signal Regulatory Protein α (Sirpα) Regulates Fcγ and Complement Receptor–Mediated Phagocytosis. *Journal of Experimental Medicine*. 2001; **193**: 855-62.
160. Chao MP, Jaiswal S, Weissman-Tsukamoto R, Alizadeh AA, Gentles AJ, Volkmer J, et al. Calreticulin Is the Dominant Pro-Phagocytic Signal on Multiple Human Cancers and Is Counterbalanced by CD47. *Science Translational Medicine*. 2010; **2**: 63ra94-63ra94.
161. Temming AR, Bentlage AEH, de Taeye SW, Bosman GP, Lissenberg-Thunnissen SN, Derksen NIL, et al. Cross-reactivity of mouse IgG subclasses to human Fc gamma receptors: Antibody deglycosylation only eliminates IgG2b binding. *Molecular Immunology*. 2020; **127**: 79-86.
162. Zhao XW, van Beek EM, Schornagel K, Van der Maaden H, Van Houdt M, Otten MA, et al. CD47-signal regulatory protein-alpha (SIRPalpha) interactions form a barrier for antibody-mediated tumor cell destruction. *Proc Natl Acad Sci U S A*. 2011; **108**: 18342-7.
163. Vyas P, Knapper S, Kelly R, Salim R, Lubowiecki M, Royston D, et al. Initial phase 1 results of the first-in-class anti-CD47 antibody Hu5F9-G4 in relapsed/refractory acute myeloid leukemia patients. *European Hematology Association Annual Meeting, Stockholm*. 2018: (*Abstract PF232*).
164. Sikic BI, Lakhani NJ, Patnaik A, Shah S, Chandana SR, Rasco DW, et al. A first-in-class, first-in-human phase 1 pharmacokinetic (PK) and pharmacodynamic (PD) study of Hu5F9-G4, an anti-CD47 monoclonal antibody (mAb), in patients with advanced solid tumors. *Journal of Clinical Oncology*. 2018; **36**: 3002-.
165. Lakhani NJ, Patnaik A, Liao JB, Moroney JW, Miller DS, Fleming GF, et al. A phase Ib study of the anti-CD47 antibody magrolimab with the PD-L1 inhibitor avelumab (A) in solid tumor (ST) and ovarian cancer (OC) patients. *Journal of Clinical Oncology*. 2020; **38**: 18-.
166. Fisher GA, Lakhani NJ, Eng C, Hecht JR, Bendell JC, Philip PA, et al. A phase Ib/II study of the anti-CD47 antibody magrolimab with cetuximab in solid tumor and colorectal cancer patients. *Journal of Clinical Oncology*. 2020; **38**: 114-.
167. Advani R, Flinn I, Popplewell L, Forero A, Bartlett NL, Ghosh N, et al. CD47 Blockade by Hu5F9-G4 and Rituximab in Non-Hodgkin's Lymphoma. *N Engl J Med*. 2018; **379**: 1711-21.
168. Chow LQM, Gainor JF, Lakhani NJ, Lee KW, Chung HC, Lee J, et al. A phase I study of ALX148, a CD47 blocker, in combination with standard anticancer antibodies and chemotherapy regimens in patients with advanced malignancy. *Journal of Clinical Oncology*. 2020; **38**: 3056-.

169. Zhang M, Hutter G, Kahn SA, Azad TD, Gholamin S, Xu CY, et al. Anti-CD47 Treatment Stimulates Phagocytosis of Glioblastoma by M1 and M2 Polarized Macrophages and Promotes M1 Polarized Macrophages In Vivo. *PloS one*. 2016; **11**: e0153550-e.
170. Li Y, Zhang M, Wang X, Liu W, Wang H, Yang YG. Vaccination with CD47 deficient tumor cells elicits an antitumor immune response in mice. *Nat Commun*. 2020; **11**: 581.
171. von Roemeling CA, Wang Y, Qie Y, Yuan H, Zhao H, Liu X, et al. Therapeutic modulation of phagocytosis in glioblastoma can activate both innate and adaptive antitumour immunity. *Nature Communications*. 2020; **11**: 1508.
172. Gauttier V, Pengam S, Durand J, Biteau K, Mary C, Morello A, et al. Selective SIRPα blockade reverses tumor T cell exclusion and overcomes cancer immunotherapy resistance. *The Journal of Clinical Investigation*. 2020; **130**: 6109-23.
173. Piccione EC, Juarez S, Liu J, Tseng S, Ryan CE, Narayanan C, et al. A bispecific antibody targeting CD47 and CD20 selectively binds and eliminates dual antigen expressing lymphoma cells. *MAbs*. 2015; **7**: 946-56.
174. Petrova PS, Viller NN, Wong M, Pang X, Lin GH, Dodge K, et al. TTI-621 (SIRPalphaFc): A CD47-Blocking Innate Immune Checkpoint Inhibitor with Broad Antitumor Activity and Minimal Erythrocyte Binding. *Clin Cancer Res*. 2017; **23**: 1068-79.
175. Patel K, Maris MB, Cheson BD, Zonder JA, Lesokhin AM, Keudell GV, et al. Ongoing, first-in-human, phase I dose escalation study of the investigational CD47-blocker TTI-622 in patients with advanced relapsed or refractory lymphoma. *Journal of Clinical Oncology*. 2020; **38**: 3030-.
176. Piccione EC, Juarez S, Tseng S, Liu J, Stafford M, Narayanan C, et al. SIRPalpha-Antibody Fusion Proteins Selectively Bind and Eliminate Dual Antigen-Expressing Tumor Cells. *Clin Cancer Res*. 2016; **22**: 5109-19.
177. Ponce LP, Fenn NC, Moritz N, Krupka C, Kozik JH, Lauber K, et al. SIRPalpha-antibody fusion proteins stimulate phagocytosis and promote elimination of acute myeloid leukemia cells. *Oncotarget*. 2017; **8**: 11284-301.
178. Dheilly E, Moine V, Broyer L, Salgado-Pires S, Johnson Z, Papaioannou A, et al. Selective Blockade of the Ubiquitous Checkpoint Receptor CD47 Is Enabled by Dual-Targeting Bispecific Antibodies. *Molecular Therapy*. 2017; **25**: 523-33.
179. Qi J, Li J, Jiang B, Jiang B, Liu H, Cao X, et al. A Phase I/IIa Study of Lemzoparlimab, a Monoclonal Antibody Targeting CD47, in Patients with Relapsed and/or Refractory Acute Myeloid Leukemia (AML) and Myelodysplastic Syndrome (MDS): Initial Phase I Results. *Blood*. 2020; **136**: 30-1.
180. Puro RJ, Bouchlaka MN, Hiebsch RR, Capoccia BJ, Donio MJ, Manning PT, et al. Development of AO-176, a Next-Generation Humanized Anti-CD47 Antibody with Novel Anticancer Properties and Negligible Red Blood Cell Binding. *Mol Cancer Ther*. 2020; **19**: 835-46.
181. Voets E, Paradé M, Lutje Hulsik D, Spijkers S, Janssen W, Rens J, et al. Functional characterization of the selective pan-allele anti-SIRPα antibody ADU-1805 that blocks the SIRPα–CD47 innate immune checkpoint. *Journal for ImmunoTherapy of Cancer*. 2019; **7**: 340.
182. Ho CCM, Guo N, Sockolosky JT, Ring AM, Weiskopf K, Özkan E, et al. "Velcro" Engineering of High Affinity CD47 Ectodomain as Signal Regulatory Protein α (SIRPα) Antagonists That Enhance Antibody-dependent Cellular Phagocytosis. *Journal of Biological Chemistry*. 2015; **290**: 12650-63.
183. Döhner H, Weisdorf DJ, Bloomfield CD. Acute Myeloid Leukemia. *New England Journal of Medicine*. 2015; **373**: 1136-52.
184. De Kouchkovsky I, Abdul-Hay M. 'Acute myeloid leukemia: a comprehensive review and 2016 update'. *Blood cancer journal*. 2016; **6**: e441-e.

185. Shlush LI, Zandi S, Mitchell A, Chen WC, Brandwein JM, Gupta V, et al. Identification of pre-leukaemic haematopoietic stem cells in acute leukaemia. *Nature*. 2014; **506**: 328-33.
186. Jan M, Snyder TM, Corces-Zimmerman MR, Vyas P, Weissman IL, Quake SR, et al. Clonal evolution of preleukemic hematopoietic stem cells precedes human acute myeloid leukemia. *Science translational medicine*. 2012; **4**: 149ra18-ra18.
187. Arber DA, Orazi A, Hasserjian R, Thiele J, Borowitz MJ, Le Beau MM, et al. The 2016 revision to the World Health Organization classification of myeloid neoplasms and acute leukemia. *Blood*. 2016; **127**: 2391-405.
188. Papaemmanuil E, Gerstung M, Bullinger L, Gaidzik VI, Paschka P, Roberts ND, et al. Genomic Classification and Prognosis in Acute Myeloid Leukemia. *The New England journal of medicine*. 2016; **374**: 2209-21.
189. Cancer Genome Atlas Research N, Ley TJ, Miller C, Ding L, Raphael BJ, Mungall AJ, et al. Genomic and epigenomic landscapes of adult de novo acute myeloid leukemia. *The New England journal of medicine*. 2013; **368**: 2059-74.
190. Daver N, Schlenk RF, Russell NH, Levis MJ. Targeting FLT3 mutations in AML: review of current knowledge and evidence. *Leukemia*. 2019; **33**: 299-312.
191. Falini B, Brunetti L, Sportoletti P, Martelli MP. NPM1-mutated acute myeloid leukemia: from bench to bedside. *Blood*. 2020; **136**: 1707-21.
192. Béné MC, Nebe T, Bettelheim P, Buldini B, Bumbea H, Kern W, et al. Immunophenotyping of acute leukemia and lymphoproliferative disorders: a consensus proposal of the European LeukemiaNet Work Package 10. *Leukemia*. 2011; **25**: 567-74.
193. Shallis RM, Wang R, Davidoff A, Ma X, Zeidan AM. Epidemiology of acute myeloid leukemia: Recent progress and enduring challenges. *Blood Rev*. 2019; **36**: 70-87.
194. Dohner H, Estey E, Grimwade D, Amadori S, Appelbaum FR, Buchner T, et al. Diagnosis and management of AML in adults: 2017 ELN recommendations from an international expert panel. *Blood*. 2017; **129**: 424-47.
195. Parker WB. Enzymology of purine and pyrimidine antimetabolites used in the treatment of cancer. *Chem Rev*. 2009; **109**: 2880-93.
196. Medeiros BC, Chan SM, Daver NG, Jonas BA, Pollyea DA. Optimizing survival outcomes with post-remission therapy in acute myeloid leukemia. *Am J Hematol*. 2019; **94**: 803-11.
197. Büchner T, Berdel WE, Haferlach C, Haferlach T, Schnittger S, Müller-Tidow C, et al. Age-related risk profile and chemotherapy dose response in acute myeloid leukemia: a study by the German Acute Myeloid Leukemia Cooperative Group. *J Clin Oncol*. 2009; **27**: 61-9.
198. Burnett AK, Milligan D, Prentice AG, Goldstone AH, McMullin MF, Hills RK, et al. A comparison of low-dose cytarabine and hydroxyurea with or without all-trans retinoic acid for acute myeloid leukemia and high-risk myelodysplastic syndrome in patients not considered fit for intensive treatment. *Cancer*. 2007; **109**: 1114-24.
199. Dombret H, Seymour JF, Butrym A, Wierzbowska A, Selleslag D, Jang JH, et al. International phase 3 study of azacitidine vs conventional care regimens in older patients with newly diagnosed AML with >30% blasts. *Blood*. 2015; **126**: 291-9.
200. DiNardo CD, Jonas BA, Pullarkat V, Thirman MJ, Garcia JS, Wei AH, et al. Azacitidine and Venetoclax in Previously Untreated Acute Myeloid Leukemia. *New England Journal of Medicine*. 2020; **383**: 617-29.
201. Ferrara F. Venetoclax plus hypomethylating agents or low-dose cytarabine in acute myeloid leukemia: all that glitters is gold? *Blood cancer journal*. 2020; **10**: 10-.
202. Wei AH, Tiong IS. Midostaurin, enasidenib, CPX-351, gemtuzumab ozogamicin, and venetoclax bring new hope to AML. *Blood*. 2017; **130**: 2469-74.
203. Vago L, Gojo I. Immune escape and immunotherapy of acute myeloid leukemia. *The Journal of Clinical Investigation*. 2020; **130**: 1552-64.

204. Daver NG, Garcia-Manero G, Konopleva MY, Alfayez M, Pemmaraju N, Kadia TM, et al. Azacitidine (AZA) with Nivolumab (Nivo), and AZA with Nivo + Ipilimumab (Ipi) in Relapsed/Refractory Acute Myeloid Leukemia: A Non-Randomized, Prospective, Phase 2 Study. *Blood*. 2019; **134**: 830-.
205. David A. Sallman ASA, , Suman Kambhampati, Monzr M. Al Malki, Joshua F. Zeidner, William Donnellan, Daniel J. Lee, Paresh Vyas, Deepa Jeyakumar, Gabriel N. Mannis, Tiffany N Tanaka, Wanxing Chai-Ho, Richard A. Larson, Andrew R. Whiteley, Guido Marcucci, Rami S. Komrokji, Guillermo Garcia-Manero, Joanna Van Elk, Ming Lin, Roy Maute, Jens-Peter Volkmer, Chris H. Takimoto, Mark P. Chao, and Naval Daver. The First-in-Class Anti-CD47 Antibody Magrolimab Combined with Azacitidine Is Well-Tolerated and Effective in AML Patients: Phase 1b Results. *Blood*. 2020: (Supplement_1): (*Abstract*).
206. Sallman DA, Malki MA, Asch AS, Lee DJ, Kambhampati S, Donnellan WB, et al. Tolerability and efficacy of the first-in-class anti-CD47 antibody magrolimab combined with azacitidine in MDS and AML patients: Phase Ib results. *Journal of Clinical Oncology*. 2020; **38**: 7507-.
207. Shlush LI, Mitchell A, Heisler L, Abelson S, Ng SWK, Trotman-Grant A, et al. Tracing the origins of relapse in acute myeloid leukaemia to stem cells. *Nature*. 2017; **547**: 104-8.
208. Wulf GG, Wang RY, Kuehnle I, Weidner D, Marini F, Brenner MK, et al. A leukemic stem cell with intrinsic drug efflux capacity in acute myeloid leukemia. *Blood*. 2001; **98**: 1166-73.
209. Lapidot T, Sirard C, Vormoor J, Murdoch B, Hoang T, Caceres-Cortes J, et al. A cell initiating human acute myeloid leukaemia after transplantation into SCID mice. *Nature*. 1994; **367**: 645-8.
210. Bonnet D, Dick JE. Human acute myeloid leukemia is organized as a hierarchy that originates from a primitive hematopoietic cell. *Nature Medicine*. 1997; **3**: 730-7.
211. George J, Uyar A, Young K, Kuffler L, Waldron-Francis K, Marquez E, et al. Leukaemia cell of origin identified by chromatin landscape of bulk tumour cells. *Nature communications*. 2016; **7**: 12166-.
212. Krivtsov AV, Figueroa ME, Sinha AU, Stubbs MC, Feng Z, Valk PJ, et al. Cell of origin determines clinically relevant subtypes of MLL-rearranged AML. *Leukemia*. 2013; **27**: 852-60.
213. Kirstetter P, Schuster MB, Bereshchenko O, Moore S, Dvinge H, Kurz E, et al. Modeling of C/EBPalpha mutant acute myeloid leukemia reveals a common expression signature of committed myeloid leukemia-initiating cells. *Cancer Cell*. 2008; **13**: 299-310.
214. Goardon N, Marchi E, Atzberger A, Quek L, Schuh A, Soneji S, et al. Coexistence of LMPP-like and GMP-like leukemia stem cells in acute myeloid leukemia. *Cancer Cell*. 2011; **19**: 138-52.
215. Quek L, Otto GW, Garnett C, Lhermitte L, Karamitros D, Stoilova B, et al. Genetically distinct leukemic stem cells in human CD34− acute myeloid leukemia are arrested at a hemopoietic precursor-like stage. *Journal of Experimental Medicine*. 2016; **213**: 1513-35.
216. Somervaille TC, Cleary ML. Identification and characterization of leukemia stem cells in murine MLL-AF9 acute myeloid leukemia. *Cancer Cell*. 2006; **10**: 257-68.
217. Lu C, Ward PS, Kapoor GS, Rohle D, Turcan S, Abdel-Wahab O, et al. IDH mutation impairs histone demethylation and results in a block to cell differentiation. *Nature*. 2012; **483**: 474-8.
218. Corces MR, Buenrostro JD, Wu B, Greenside PG, Chan SM, Koenig JL, et al. Lineage-specific and single-cell chromatin accessibility charts human hematopoiesis and leukemia evolution. *Nat Genet*. 2016; **48**: 1193-203.

219. Rothenberg-Thurley M, Amler S, Goerlich D, Köhnke T, Konstandin NP, Schneider S, et al. Persistence of pre-leukemic clones during first remission and risk of relapse in acute myeloid leukemia. *Leukemia*. 2018; **32**: 1598-608.
220. Corces-Zimmerman MR, Hong WJ, Weissman IL, Medeiros BC, Majeti R. Preleukemic mutations in human acute myeloid leukemia affect epigenetic regulators and persist in remission. *Proc Natl Acad Sci U S A*. 2014; **111**: 2548-53.
221. Jordan CT, Upchurch D, Szilvassy SJ, Guzman ML, Howard DS, Pettigrew AL, et al. The interleukin-3 receptor alpha chain is a unique marker for human acute myelogenous leukemia stem cells. *Leukemia*. 2000; **14**: 1777-84.
222. Testa U, Riccioni R, Militi S, Coccia E, Stellacci E, Samoggia P, et al. Elevated expression of IL-3Ralpha in acute myelogenous leukemia is associated with enhanced blast proliferation, increased cellularity, and poor prognosis. *Blood*. 2002; **100**: 2980-8.
223. Vergez F, Green AS, Tamburini J, Sarry JE, Gaillard B, Cornillet-Lefebvre P, et al. High levels of CD34+CD38low/-CD123+ blasts are predictive of an adverse outcome in acute myeloid leukemia: a Groupe Ouest-Est des Leucemies Aigues et Maladies du Sang (GOELAMS) study. *Haematologica*. 2011; **96**: 1792-8.
224. Vergez F, Nicolau-Travers ML, Bertoli S, Rieu JB, Tavitian S, Bories P, et al. CD34(+)CD38(-)CD123(+) Leukemic Stem Cell Frequency Predicts Outcome in Older Acute Myeloid Leukemia Patients Treated by Intensive Chemotherapy but Not Hypomethylating Agents. *Cancers (Basel)*. 2020; **12**.
225. Ehninger A, Kramer M, Rollig C, Thiede C, Bornhauser M, von Bonin M, et al. Distribution and levels of cell surface expression of CD33 and CD123 in acute myeloid leukemia. *Blood Cancer J*. 2014; **4**: e218.
226. Haubner S, Perna F, Kohnke T, Schmidt C, Berman S, Augsberger C, et al. Coexpression profile of leukemic stem cell markers for combinatorial targeted therapy in AML. *Leukemia*. 2019; **33**: 64-74.
227. Taussig DC, Pearce DJ, Simpson C, Rohatiner AZ, Lister TA, Kelly G, et al. Hematopoietic stem cells express multiple myeloid markers: implications for the origin and targeted therapy of acute myeloid leukemia. *Blood*. 2005; **106**: 4086-92.
228. Jen EY, Gao X, Li L, Zhuang L, Simpson NE, Aryal B, et al. FDA Approval Summary: Tagraxofusp-erzs For Treatment of Blastic Plasmacytoid Dendritic Cell Neoplasm. *Clin Cancer Res*. 2020; **26**: 532-6.
229. Frankel A, Liu JS, Rizzieri D, Hogge D. Phase I clinical study of diphtheria toxin-interleukin 3 fusion protein in patients with acute myeloid leukemia and myelodysplasia. *Leuk Lymphoma*. 2008; **49**: 543-53.
230. Yalcintepe L, Frankel AE, Hogge DE. Expression of interleukin-3 receptor subunits on defined subpopulations of acute myeloid leukemia blasts predicts the cytotoxicity of diphtheria toxin interleukin-3 fusion protein against malignant progenitors that engraft in immunodeficient mice. *Blood*. 2006; **108**: 3530-7.
231. Feuring-Buske M, Frankel AE, Alexander RL, Gerhard B, Hogge DE. A diphtheria toxin-interleukin 3 fusion protein is cytotoxic to primitive acute myeloid leukemia progenitors but spares normal progenitors. *Cancer Res*. 2002; **62**: 1730-6.
232. Uy GL, Aldoss I, Foster MC, Sayre PH, Wieduwilt MJ, Advani AS, et al. Flotetuzumab as Salvage Immunotherapy for Refractory Acute Myeloid Leukemia. *Blood*. 2020.
233. London WB, Castleberry RP, Matthay KK, Look AT, Seeger RC, Shimada H, et al. Evidence for an age cutoff greater than 365 days for neuroblastoma risk group stratification in the Children's Oncology Group. *J Clin Oncol*. 2005; **23**: 6459-65.
234. Hoehner JC, Gestblom C, Hedborg F, Sandstedt B, Olsen L, Påhlman S. A developmental model of neuroblastoma: differentiating stroma-poor tumors' progress along an extra-adrenal chromaffin lineage. *Lab Invest*. 1996; **75**: 659-75.

235. Maris JM. Recent Advances in Neuroblastoma. *New England Journal of Medicine*. 2010; **362**: 2202-11.
236. Howlader N, Noone AM, Krapcho M, D.Miller, A.Brest, Yu M, et al. SEER Cancer Statistics Review, 1975-2017. National Cancer Institute. Bethesda, MD2020. Available from: https://seer.cancer.gov/csr/1975_2017/.
237. Pinto NR, Applebaum MA, Volchenboum SL, Matthay KK, London WB, Ambros PF, et al. Advances in Risk Classification and Treatment Strategies for Neuroblastoma. *J Clin Oncol*. 2015; **33**: 3008-17.
238. Speleman F, Park JR, Henderson TO. Neuroblastoma: A Tough Nut to Crack. *American Society of Clinical Oncology Educational Book*. 2016: e548-e57.
239. Park JA, Cheung N-KV. Targets and Antibody Formats for Immunotherapy of Neuroblastoma. *Journal of Clinical Oncology*. 2020; **38**: 1836-48.
240. Yu AL, Gilman AL, Ozkaynak MF, London WB, Kreissman SG, Chen HX, et al. Anti-GD2 Antibody with GM-CSF, Interleukin-2, and Isotretinoin for Neuroblastoma. *New England Journal of Medicine*. 2010; **363**: 1324-34.
241. Ladenstein R, Pötschger U, Valteau-Couanet D, Luksch R, Castel V, Yaniv I, et al. Interleukin 2 with anti-GD2 antibody ch14.18/CHO (dinutuximab beta) in patients with high-risk neuroblastoma (HR-NBL1/SIOPEN): a multicentre, randomised, phase 3 trial. *The Lancet Oncology*. 2018; **19**: 1617-29.
242. Shochat SJ, Abt AB, Schengrund C-L. VCN-Releasable sialic acid and gangliosides in human neuroblastomas. *Journal of Pediatric Surgery*. 1977; **12**: 413-8.
243. Schulz G, Cheresh DA, Varki NM, Yu A, Staffileno LK, Reisfeld RA. Detection of Ganglioside G_{D2} in Tumor Tissues and Sera of Neuroblastoma Patients. *Cancer Research*. 1984; **44**: 5914-20.
244. Wu ZL, Schwartz E, Seeger R, Ladisch S. Expression of GD2 ganglioside by untreated primary human neuroblastomas. *Cancer Res*. 1986; **46**: 440-3.
245. Svennerholm L, Boström K, Fredman P, Jungbjer B, Lekman A, Månsson J-E, et al. Gangliosides and allied glycosphingolipids in human peripheral nerve and spinal cord. *Biochimica et Biophysica Acta (BBA) - Lipids and Lipid Metabolism*. 1994; **1214**: 115-23.
246. Suzuki M, Cheung NK. Disialoganglioside GD2 as a therapeutic target for human diseases. *Expert Opin Ther Targets*. 2015; **19**: 349-62.
247. Sait S, Modak S. Anti-GD2 immunotherapy for neuroblastoma. *Expert Rev Anticancer Ther*. 2017; **17**: 889-904.
248. Olshefski R, Ladisch S. Intercellular transfer of shed tumor cell gangliosides. *FEBS Lett*. 1996; **386**: 11-4.
249. Li RX, Ladisch S. Shedding of human neuroblastoma gangliosides. *Biochim Biophys Acta*. 1991; **1083**: 57-64.
250. Berois N, Osinaga E. Glycobiology of neuroblastoma: impact on tumor behavior, prognosis, and therapeutic strategies. *Frontiers in oncology*. 2014; **4**: 114-.
251. Dhillon S. Dinutuximab: First Global Approval. *Drugs*. 2015; **75**: 923-7.
252. Cheung N-KV, Dyer MA. Neuroblastoma: developmental biology, cancer genomics and immunotherapy. *Nat Rev Cancer*. 2013; **13**: 397-411.
253. Albertini MR, Gan J, Jaeger P, Hank JA, Storer B, Schell K, et al. Systemic interleukin-2 modulates the anti-idiotypic response to chimeric anti-GD2 antibody in patients with melanoma. *J Immunother Emphasis Tumor Immunol*. 1996; **19**: 278-95.
254. Uttenreuther-Fischer MM, Huang CS, Yu AL. Pharmacokinetics of human-mouse chimeric anti-GD2 mAb ch14.18 in a phase I trial in neuroblastoma patients. *Cancer Immunol Immunother*. 1995; **41**: 331-8.

255. Asgharzadeh S, Salo JA, Ji L, Oberthuer A, Fischer M, Berthold F, et al. Clinical significance of tumor-associated inflammatory cells in metastatic neuroblastoma. *J Clin Oncol*. 2012; **30**: 3525-32.
256. Biswas SK, Mantovani A. Macrophage plasticity and interaction with lymphocyte subsets: cancer as a paradigm. *Nature Immunology*. 2010; **11**: 889-96.
257. Liu KX, Joshi S. "Re-educating" Tumor Associated Macrophages as a Novel Immunotherapy Strategy for Neuroblastoma. *Frontiers in immunology*. 2020; **11**: 1947-.
258. Kroesen M, Büll C, Gielen PR, Brok IC, Armandari I, Wassink M, et al. Anti-GD2 mAb and Vorinostat synergize in the treatment of neuroblastoma. *Oncoimmunology*. 2016; **5**: e1164919.
259. Jeanne A, Martiny L, Dedieu S. Thrombospondin-targeting TAX2 peptide impairs tumor growth in preclinical mouse models of childhood neuroblastoma. *Pediatric Research*. 2017; **81**: 480-8.
260. Bakema JE, van Egmond M. Fc receptor-dependent mechanisms of monoclonal antibody therapy of cancer. *Curr Top Microbiol Immunol*. 2014; **382**: 373-92.
261. Broughton SE, Hercus TR, Nero TL, Dhagat U, Owczarek CM, Hardy MP, et al. Crystallization and preliminary X-ray diffraction analysis of the interleukin-3 alpha receptor bound to the Fab fragment of antibody CSL362. *Acta Crystallogr F Struct Biol Commun*. 2014; **70**: 358-61.
262. Gibson DG, Young L, Chuang R-Y, Venter JC, Hutchison CA, Smith HO. Enzymatic assembly of DNA molecules up to several hundred kilobases. *Nature Methods*. 2009; **6**: 343-5.
263. Hanahan D. Studies on transformation of Escherichia coli with plasmids. *Journal of Molecular Biology*. 1983; **166**: 557-80.
264. Haffke M, Rummel G, Boivineau J, Münch A, Jaakola V-P. nanoDSF: Label-free Thermal Unfolding Assay of G Protein-Coupled Receptors for Compound Screening and Buffer Composition Optimization2016.
265. Kroesen M, Brok IC, Reijnen D, van Hout-Kuijer MA, Zeelenberg IS, Den Brok MH, et al. Intra-adrenal murine TH-MYCN neuroblastoma tumors grow more aggressive and exhibit a distinct tumor microenvironment relative to their subcutaneous equivalents. *Cancer Immunol Immunother*. 2015; **64**: 563-72.
266. Vick B, Rothenberg M, Sandhofer N, Carlet M, Finkenzeller C, Krupka C, et al. An advanced preclinical mouse model for acute myeloid leukemia using patients' cells of various genetic subgroups and in vivo bioluminescence imaging. *PLoS One*. 2015; **10**: e0120925.
267. Ebinger S, Zeller C, Carlet M, Senft D, Bagnoli JW, Liu WH, et al. Plasticity in growth behavior of patients' acute myeloid leukemia stem cells growing in mice. *Haematologica*. 2020.
268. Hanson MS, Stephenson AH, Bowles EA, Sridharan M, Adderley S, Sprague RS. Phosphodiesterase 3 is present in rabbit and human erythrocytes and its inhibition potentiates iloprost-induced increases in cAMP. *Am J Physiol Heart Circ Physiol*. 2008; **295**: H786-H93.
269. Bonnet D. In Vivo Evaluation of Leukemic Stem Cells through the Xenotransplantation Model. *Current Protocols in Stem Cell Biology*. 2008; **7**: 3.2.1-3.2.11.
270. Sarry JE, Murphy K, Perry R, Sanchez PV, Secreto A, Keefer C, et al. Human acute myelogenous leukemia stem cells are rare and heterogeneous when assayed in NOD/SCID/IL2Rγc-deficient mice. *J Clin Invest*. 2011; **121**: 384-95.
271. Dick JE. Stem cell concepts renew cancer research. *Blood*. 2008; **112**: 4793-807.
272. Hu Y, Smyth GK. ELDA: extreme limiting dilution analysis for comparing depleted and enriched populations in stem cell and other assays. *J Immunol Methods*. 2009; **347**: 70-8.

273. Busfield SJ, Biondo M, Wong M, Ramshaw HS, Lee EM, Ghosh S, et al. Targeting of acute myeloid leukemia in vitro and in vivo with an anti-CD123 mAb engineered for optimal ADCC. *Leukemia*. 2014; **28**: 2213-21.
274. Liu J, Wang L, Zhao F, Tseng S, Narayanan C, Shura L, et al. Pre-Clinical Development of a Humanized Anti-CD47 Antibody with Anti-Cancer Therapeutic Potential. *PloS one*. 2015; **10**: e0137345-e.
275. Lapidot T, Sirard C, Vormoor J, Murdoch B, Hoang T, Caceres-Cortes J, et al. A cell initiating human acute myeloid leukaemia after transplantation into SCID mice. *Nature*. 1994; **367**: 645-8.
276. Sarry JE, Murphy K, Perry R, Sanchez PV, Secreto A, Keefer C, et al. Human acute myelogenous leukemia stem cells are rare and heterogeneous when assayed in NOD/SCID/IL2Rgammac-deficient mice. *J Clin Invest*. 2011; **121**: 384-95.
277. Krupka C, Kufer P, Kischel R, Zugmaier G, Lichtenegger FS, Kohnke T, et al. Blockade of the PD-1/PD-L1 axis augments lysis of AML cells by the CD33/CD3 BiTE antibody construct AMG 330: reversing a T-cell-induced immune escape mechanism. *Leukemia*. 2016; **30**: 484-91.
278. Horwacik I, Golik P, Grudnik P, Kolinski M, Zdzalik M, Rokita H, et al. Structural Basis of GD2 Ganglioside and Mimetic Peptide Recognition by 14G2a Antibody. *Mol Cell Proteomics*. 2015; **14**: 2577-90.
279. Kauder SE, Kuo TC, Harrabi O, Chen A, Sangalang E, Doyle L, et al. ALX148 blocks CD47 and enhances innate and adaptive antitumor immunity with a favorable safety profile. *PloS one*. 2018; **13**: e0201832-e.
280. Peluso MO, Adam A, Armet CM, Zhang L, O'Connor RW, Lee BH, et al. The Fully human anti-CD47 antibody SRF231 exerts dual-mechanism antitumor activity via engagement of the activating receptor CD32a. *J Immunother Cancer*. 2020; **8**.
281. Sockolosky JT, Dougan M, Ingram JR, Ho CC, Kauke MJ, Almo SC, et al. Durable antitumor responses to CD47 blockade require adaptive immune stimulation. *Proc Natl Acad Sci U S A*. 2016; **113**: E2646-54.
282. Maude SL, Laetsch T, Buechner J, Rives S, Boyer M, Bittencourt H, et al. Tisagenlecleucel in Children and Young Adults with b Cell Lymphoblastic Leukemia. *The New England Journal of Medicine*. 2018; **378**: 43Y 448.
283. Neelapu S, Locke F, Bartlett N, Lekakis L, Miklos D, Jacobson C, et al. Axicabtagene Ciloleucel CAR T Cell Therapy in Refractory Large b Cell Lymphoma. *The New England Journal of Medicine*. 2017; **377**: 253Q 2544.
284. Logtenberg MEW, Scheeren FA, Schumacher TN. The CD47-SIRPalpha Immune Checkpoint. *Immunity*. 2020; **52**: 742-52.
285. Alvarez-Rueda N, Desselle A, Cochonneau D, Chaumette T, Clemenceau B, Leprieur S, et al. A monoclonal antibody to O-acetyl-GD2 ganglioside and not to GD2 shows potent anti-tumor activity without peripheral nervous system cross-reactivity. *PLoS One*. 2011; **6**: e25220.
286. Sikic BI, Lakhani N, Patnaik A, Shah SA, Chandana SR, Rasco D, et al. First-in-Human, First-in-Class Phase I Trial of the Anti-CD47 Antibody Hu5F9-G4 in Patients With Advanced Cancers. *J Clin Oncol*. 2019; **37**: 946-53.
287. Chen JY, McKenna KM, Choi TS, Duan J, Brown L, Stewart JJ, et al. RBC-Specific CD47 Pruning Confers Protection and Underlies the Transient Anemia in Patients Treated with Anti-CD47 Antibody 5F9. *Blood*. 2018; **132**: 2327-.
288. Barkal AA, Weiskopf K, Kao KS, Gordon SR, Rosental B, Yiu YY, et al. Engagement of MHC class I by the inhibitory receptor LILRB1 suppresses macrophages and is a target of cancer immunotherapy. *Nat Immunol*. 2018; **19**: 76-84.

289. Theruvath J, Smith B, Linde MH, Sotillo E, Heitzeneder S, Marjon K, et al. Abstract PR07: GD2 is a macrophage checkpoint molecule and combined GD2/CD47 blockade results in synergistic effects and tumor clearance in xenograft models of neuroblastoma and osteosarcoma. *Cancer Research*. 2020; **80**: PR07-PR.
290. Smith BD, Roboz GJ, Walter RB, Altman JK, Ferguson A, Curcio TJ, et al. First-in Man, Phase 1 Study of CSL362 (Anti-IL3Rα / Anti-CD123 Monoclonal Antibody) in Patients with CD123+ Acute Myeloid Leukemia (AML) in CR at High Risk for Early Relapse. *Blood*. 2014; **124**: 120. (*Abstract*).
291. Kubasch AS, Schulze F, Giagounidis A, Gotze KS, Kronke J, Sockel K, et al. Single agent talacotuzumab demonstrates limited efficacy but considerable toxicity in elderly high-risk MDS or AML patients failing hypomethylating agents. *Leukemia*. 2020; **34**: 1182-6.
292. Montesinos P, Roboz GJ, Bulabois CE, Subklewe M, Platzbecker U, Ofran Y, et al. Safety and efficacy of talacotuzumab plus decitabine or decitabine alone in patients with acute myeloid leukemia not eligible for chemotherapy: results from a multicenter, randomized, phase 2/3 study. *Leukemia*. 2020.
293. Epling-Burnette PK, Bai F, Painter JS, Rollison DE, Salih HR, Krusch M, et al. Reduced natural killer (NK) function associated with high-risk myelodysplastic syndrome (MDS) and reduced expression of activating NK receptors. *Blood*. 2007; **109**: 4816-24.
294. Eppert K, Takenaka K, Lechman ER, Waldron L, Nilsson B, van Galen P, et al. Stem cell gene expression programs influence clinical outcome in human leukemia. *Nature Medicine*. 2011; **17**: 1086-93.
295. Ng SWK, Mitchell A, Kennedy JA, Chen WC, McLeod J, Ibrahimova N, et al. A 17-gene stemness score for rapid determination of risk in acute leukaemia. *Nature*. 2016; **540**: 433-7.
296. Bradbury C, Houlton AE, Akiki S, Gregg R, Rindl M, Khan J, et al. Prognostic value of monitoring a candidate immunophenotypic leukaemic stem/progenitor cell population in patients allografted for acute myeloid leukaemia. *Leukemia*. 2015; **29**: 988-91.
297. Terwijn M, Zeijlemaker W, Kelder A, Rutten AP, Snel AN, Scholten WJ, et al. Leukemic stem cell frequency: a strong biomarker for clinical outcome in acute myeloid leukemia. *PLoS One*. 2014; **9**: e107587.
298. Jentzsch M, Bill M, Nicolet D, Leiblein S, Schubert K, Pless M, et al. Prognostic impact of the CD34+/CD38− cell burden in patients with acute myeloid leukemia receiving allogeneic stem cell transplantation. *American Journal of Hematology*. 2017; **92**: 388-96.
299. Yan B, Chen Q, Shimada K, Tang M, Li H, Gurumurthy A, et al. Histone deacetylase inhibitor targets CD123/CD47-positive cells and reverse chemoresistance phenotype in acute myeloid leukemia. *Leukemia*. 2019; **33**: 931-44.
300. Sengers BG, McGinty S, Nouri FZ, Argungu M, Hawkins E, Hadji A, et al. Modeling bispecific monoclonal antibody interaction with two cell membrane targets indicates the importance of surface diffusion. *mAbs*. 2016; **8**: 905-15.
301. Weiss WA, Aldape K, Mohapatra G, Feuerstein BG, Bishop JM. Targeted expression of MYCN causes neuroblastoma in transgenic mice. *EMBO J*. 1997; **16**: 2985-95.
302. Moore HC, Wood KM, Jackson MS, Lastowska MA, Hall D, Imrie H, et al. Histological profile of tumours from MYCN transgenic mice. *J Clin Pathol*. 2008; **61**: 1098-103.
303. Hackett CS, Hodgson JG, Law ME, Fridlyand J, Osoegawa K, de Jong PJ, et al. Genome-wide array CGH analysis of murine neuroblastoma reveals distinct genomic aberrations which parallel those in human tumors. *Cancer Res*. 2003; **63**: 5266-73.
304. Terrile M, Bryan K, Vaughan L, Hallsworth A, Webber H, Chesler L, et al. miRNA expression profiling of the murine TH-MYCN neuroblastoma model reveals similarities with human tumors and identifies novel candidate miRNAs. *PLoS One*. 2011; **6**: e28356.

305. Brodeur GM, Seeger RC, Schwab M, Varmus HE, Bishop JM. Amplification of N-myc in untreated human neuroblastomas correlates with advanced disease stage. *Science*. 1984; **224**: 1121-4.
306. Brodeur GM. Neuroblastoma: biological insights into a clinical enigma. *Nat Rev Cancer*. 2003; **3**: 203-16.
307. Kroesen M, Nierkens S, Ansems M, Wassink M, Orentas RJ, Boon L, et al. A transplantable TH-MYCN transgenic tumor model in C57Bl/6 mice for preclinical immunological studies in neuroblastoma. *International Journal of Cancer*. 2014; **134**: 1335-45.
308. Subramanian S, Tsai R, Sen S, Dahl KN, Discher DE. Membrane mobility and clustering of Integrin Associated Protein (IAP, CD47)—Major differences between mouse and man and implications for signaling. *Blood Cells, Molecules, and Diseases*. 2006; **36**: 364-72.
309. Dahl KN, Westhoff CM, Discher DE. Fractional attachment of CD47 (IAP) to the erythrocyte cytoskeleton and visual colocalization with Rh protein complexes. *Blood*. 2003; **101**: 1194-9.
310. Mouro-Chanteloup I, Delaunay J, Gane P, Nicolas V, Johansen M, Brown EJ, et al. Evidence that the red cell skeleton protein 4.2 interacts with the Rh membrane complex member CD47: Presented in part at the 43rd Annual Meeting of the American Society of Hematology, Orlando, FL, December 7-11, 2001.46. *Blood*. 2003; **101**: 338-44.
311. Li F, Lv B, Liu Y, Hua T, Han J, Sun C, et al. Blocking the CD47-SIRPα axis by delivery of anti-CD47 antibody induces antitumor effects in glioma and glioma stem cells. *Oncoimmunology*. 2017; **7**: e1391973-e.
312. Liu M, O'Connor RS, Trefely S, Graham K, Snyder NW, Beatty GL. Metabolic rewiring of macrophages by CpG potentiates clearance of cancer cells and overcomes tumor-expressed CD47−mediated 'don't-eat-me' signal. *Nature Immunology*. 2019; **20**: 265-75.
313. Gallagher S, Turman S, Lekstrom K, Wilson S, Herbst R, Wang Y. CD47 limits antibody dependent phagocytosis against non-malignant B cells. *Molecular Immunology*. 2017; **85**: 57-65.
314. Dahan R, Sega E, Engelhardt J, Selby M, Korman Alan J, Ravetch Jeffrey V. FcγRs Modulate the Anti-tumor Activity of Antibodies Targeting the PD-1/PD-L1 Axis. *Cancer Cell*. 2015; **28**: 285-95.
315. Cheever MA, Allison JP, Ferris AS, Finn OJ, Hastings BM, Hecht TT, et al. The prioritization of cancer antigens: a national cancer institute pilot project for the acceleration of translational research. *Clinical cancer research : an official journal of the American Association for Cancer Research*. 2009; **15**: 5323-37.
316. Godwin CD, Gale RP, Walter RB. Gemtuzumab ozogamicin in acute myeloid leukemia. *Leukemia*. 2017; **31**: 1855-68.
317. Fournier E, Duployez N, Ducourneau B, Raffoux E, Turlure P, Caillot D, et al. Mutational profile and benefit of gemtuzumab ozogamicin in acute myeloid leukemia. *Blood*. 2020; **135**: 542-6.
318. Fenwarth L, Fournier E, Cheok M, Boyer T, Gonzales F, Castaigne S, et al. Biomarkers of Gemtuzumab Ozogamicin Response for Acute Myeloid Leukemia Treatment. *Int J Mol Sci*. 2020; **21**: 5626.
319. Walter RB, Appelbaum FR, Estey EH, Bernstein ID. Acute myeloid leukemia stem cells and CD33-targeted immunotherapy. *Blood*. 2012; **119**: 6198-208.
320. Chichili GR, Huang L, Li H, Burke S, He L, Tang Q, et al. A CD3xCD123 bispecific DART for redirecting host T cells to myelogenous leukemia: Preclinical activity and safety in nonhuman primates. *Science Translational Medicine*. 2015; **7**: 289ra82-ra82.

321. Kovtun Y, Jones GE, Adams S, Harvey L, Audette CA, Wilhelm A, et al. A CD123-targeting antibody-drug conjugate, IMGN632, designed to eradicate AML while sparing normal bone marrow cells. *Blood Advances*. 2018; **2**: 848-58.
322. Perna F, Berman SH, Soni RK, Mansilla-Soto J, Eyquem J, Hamieh M, et al. Integrating Proteomics and Transcriptomics for Systematic Combinatorial Chimeric Antigen Receptor Therapy of AML. *Cancer Cell*. 2017; **32**: 506-19.e5.
323. HUMAN PROTEIN ATLAS SUMMARY. Interleukin 3 receptor subunit alpha. [Available from: https://www.proteinatlas.org/ENSG00000185291-IL3RA.
324. IL3RA localizations [Available from: https://compartments.jensenlab.org/Entity?figures=subcell_cell_%&knowledge=10&textmining=10&experiments=10&predictions=10&type1=9606&type2=-22&id1=ENSP00000327890.
325. He SZ, Busfield S, Ritchie DS, Hertzberg MS, Durrant S, Lewis ID, et al. A Phase 1 study of the safety, pharmacokinetics and anti-leukemic activity of the anti-CD123 monoclonal antibody CSL360 in relapsed, refractory or high-risk acute myeloid leukemia. *Leukemia & Lymphoma*. 2015; **56**: 1406-15.
326. Pemmaraju N, Konopleva M. Approval of tagraxofusp-erzs for blastic plasmacytoid dendritic cell neoplasm. *Blood Advances*. 2020; **4**: 4020-7.
327. Frankel AE, Konopleva M, Hogge D, Rizzieri D, Brooks C, Cirrito T, et al. Activity and tolerability of SL-401, a targeted therapy directed to the interleukin-3 receptor on cancer stem cells and tumor bulk, as a single agent in patients with advanced hematologic malignancies. *Journal of Clinical Oncology*. 2013; **31**: 7029-.
328. Brizzi MF, Garbarino G, Rossi PR, Pagliardi GL, Arduino C, Avanzi GC, et al. Interleukin 3 stimulates proliferation and triggers endothelial-leukocyte adhesion molecule 1 gene activation of human endothelial cells. *The Journal of clinical investigation*. 1993; **91**: 2887-92.
329. Lammie G, Cheung N, Gerald W, Rosenblum M, Cordoncardo C. Ganglioside gd(2) expression in the human nervous-system and in neuroblastomas - an immunohistochemical study. *Int J Oncol*. 1993; **3**: 909-15.
330. Suzuki M, Cheung N-KV. Disialoganglioside GD2 as a therapeutic target for human diseases. *Expert Opinion on Therapeutic Targets*. 2015; **19**: 349-62.
331. Ozkaynak MF, Gilman AL, London WB, Naranjo A, Diccianni MB, Tenney SC, et al. A Comprehensive Safety Trial of Chimeric Antibody 14.18 With GM-CSF, IL-2, and Isotretinoin in High-Risk Neuroblastoma Patients Following Myeloablative Therapy: Children's Oncology Group Study ANBL0931. *Frontiers in Immunology*. 2018; **9**.
332. Navid F, Sondel PM, Barfield R, Shulkin BL, Kaufman RA, Allay JA, et al. Phase I trial of a novel anti-GD2 monoclonal antibody, Hu14.18K322A, designed to decrease toxicity in children with refractory or recurrent neuroblastoma. *J Clin Oncol*. 2014; **32**: 1445-52.
333. Ansell SM, Maris M, Lesokhin AM, Chen R, Flinn IW, Sawas A, et al. Phase 1 Study of the CD47 Blocker TTI-621 in Patients with Relapsed or Refractory Hematologic Malignancies. *Clin Cancer Res*. 2021.
334. Patel K, Ramchandren R, Maris M, Lesokhin A, Keudell G, Cheson B, et al. Investigational CD47-Blocker TTI-622 Shows Single-Agent Activity in Patients with Advanced Relapsed or Refractory Lymphoma: Update from the Ongoing First-in-Human Dose Escalation Study. *Blood*. 2020; **136**: 46-7.
335. Testa U, Pelosi E, Castelli G. CD123 as a Therapeutic Target in the Treatment of Hematological Malignancies. *Cancers (Basel)*. 2019; **11**: 1358.
336. Stevens BM, Khan N, D'Alessandro A, Nemkov T, Winters A, Jones CL, et al. Characterization and targeting of malignant stem cells in patients with advanced myelodysplastic syndromes. *Nature Communications*. 2018; **9**: 3694.

337. Muñoz L, Nomdedéu JF, López O, Carnicer MJ, Bellido M, Aventín A, et al. Interleukin-3 receptor alpha chain (CD123) is widely expressed in hematologic malignancies. *Haematologica*. 2001; **86**: 1261-9.
338. Grever MR, Abdel-Wahab O, Andritsos LA, Banerji V, Barrientos J, Blachly JS, et al. Consensus guidelines for the diagnosis and management of patients with classic hairy cell leukemia. *Blood*. 2017; **129**: 553-60.
339. Nievergall E, Ramshaw HS, Yong ASM, Biondo M, Busfield SJ, Vairo G, et al. Monoclonal antibody targeting of IL-3 receptor α with CSL362 effectively depletes CML progenitor and stem cells. *Blood*. 2014; **123**: 1218-28.
340. Fromm JR. Flow cytometric analysis of CD123 is useful for immunophenotyping classical Hodgkin lymphoma. *Cytometry B Clin Cytom*. 2011; **80**: 91-9.
341. Battula VL, Shi Y, Evans KW, Wang RY, Spaeth EL, Jacamo RO, et al. Ganglioside GD2 identifies breast cancer stem cells and promotes tumorigenesis. *The Journal of clinical investigation*. 2012; **122**: 2066-78.
342. Tsuchida T, Saxton RE, Morton DL, Irie RF. Gangliosides of human melanoma. *Journal of the National Cancer Institute*. 1987; **78**: 45-54.
343. Dobrenkov K, Ostrovnaya I, Gu J, Cheung IY, Cheung NK. Oncotargets GD2 and GD3 are highly expressed in sarcomas of children, adolescents, and young adults. *Pediatric blood & cancer*. 2016; **63**: 1780-5.
344. Tseng D, Volkmer J-P, Willingham SB, Contreras-Trujillo H, Fathman JW, Fernhoff NB, et al. Anti-CD47 antibody–mediated phagocytosis of cancer by macrophages primes an effective antitumor T-cell response. *Proceedings of the National Academy of Sciences*. 2013; **110**: 11103-8.
345. Liu Q, Wen W, Tang L, Qin CJ, Lin Y, Zhang HL, et al. Inhibition of SIRPα in dendritic cells potentiates potent antitumor immunity. *Oncoimmunology*. 2016; **5**: e1183850.
346. Brooke G, Holbrook JD, Brown MH, Barclay AN. Human lymphocytes interact directly with CD47 through a novel member of the signal regulatory protein (SIRP) family. *J Immunol*. 2004; **173**: 2562-70.
347. Stefanidakis M, Newton G, Lee WY, Parkos CA, Luscinskas FW. Endothelial CD47 interaction with SIRPγ is required for human T-cell transendothelial migration under shear flow conditions in vitro. *Blood*. 2008; **112**: 1280-9.
348. Piccio L, Vermi W, Boles KS, Fuchs A, Strader CA, Facchetti F, et al. Adhesion of human T cells to antigen-presenting cells through SIRPbeta2-CD47 interaction costimulates T-cell proliferation. *Blood*. 2005; **105**: 2421-7.
349. Lian S, Xie R, Ye Y, Lu Y, Cheng Y, Xie X, et al. Dual blockage of both PD-L1 and CD47 enhances immunotherapy against circulating tumor cells. *Scientific Reports*. 2019; **9**: 4532.
350. Li Y, Zhang M, Wang X, Liu W, Wang H, Yang Y-G. Vaccination with CD47 deficient tumor cells elicits an antitumor immune response in mice. *Nature communications*. 2020; **11**: 581-.
351. Liu X, Liu L, Ren Z, Yang K, Xu H, Luan Y, et al. Dual Targeting of Innate and Adaptive Checkpoints on Tumor Cells Limits Immune Evasion. *Cell Rep*. 2018; **24**: 2101-11.
352. de Silva S, Fromm G, Shuptrine CW, Johannes K, Patel A, Yoo KJ, et al. CD40 Enhances Type I Interferon Responses Downstream of CD47 Blockade, Bridging Innate and Adaptive Immunity. *Cancer Immunology Research*. 2020; **8**: 230-45.

7. List of Abbreviations

ADCC - antibody dependent cellular cytotoxicity

ADCP - antibody dependent cellular phagocytosis

AM - acetoxymethyl

AML - acute myeloid leukemia

ANOVA - analysis of variance

APC - allophycocyanin

APC - antigen presenting cell

ATCC - American Type Culture Collection

AZA – azacitidine

BLI - bioluminescence imaging

BMDM - bone marrow-derived macrophage

BPDCN - blastic plasmacytoid dendritic cell neoplasm

CAR - chimeric antigen receptor

C - constant

CD - cluster of differentiation

cDNA - complementary DNA

CDRs - complementarity-determining regions

cGAS - cyclic GMP-AMP synthase

CHO - Chinese hamster ovary

CLS - capillary leak syndrome

CMV - cytomegalovirus

CR - complete response

Ct - concentration

CTL - cytotoxic T lymphocytes

CTLA4 - CTL associated protein 4

d - day

D - dilution

d. i. n. - died in narcosis

DART - dual-affinity re-targeting

DC - dendritic cells

DMEM - Dulbecco's Modified Eagle Medium

DMSO - dimethyl sulfoxide

DNMT3A - DNA methyltransferase 3A

DPBS - Dulbecco’s PBS

DSMZ - Deutsche Sammlung von Mikroorganismen und Zellkulturen

e. s. l. - end stage leukemia

EC_{50} - 50% effective concentration

EDTA - ethylenediaminetetraacetic acid

ELDA - extreme limiting dilution analysis

ELN - European LeukemiaNet

EMA - European Medicines Agency

ex. - excluded from analysis

F – female

F - fluorochrome

Fab – fragment antigen-binding

FACS - fluorescence-activated cell sorting

FBS - fetal bovine serum

Fc - fragment crystallizable

FcnR - neonatal Fc receptor

FcγRs - Fc gamma receptors

FDA - Food and Drug Administration

FITC - fluorescein isothiocyanate

FLT3 - FMS-like tyrosine kinase 3

GFP - green fluorescent protein

GM-CSF - granulocyte-macrophage colony stimulating factor

H - heavy

HC – heavy chain

HD - healthy donor

HMA - hypomethylating agent

HPA - Human Protein Atlas

HSC - hematopoietic stem cell

HSCT - hematopoietic stem cell transplantation

IAP - integrin-associated protein

ID - initial diagnosis

IDH1/2 - isocitrate dehydrogenase 1/2

IDO - indoleamine 2,3-dioxygenase

IFNγ - interferon-gamma

Ig - immunoglobulin

IL2 - interleukin-2

IL3Rα - interleukin-3 receptor alpha chain

ITAM - immunoreceptor tyrosine-based activation motif

ITIM - immunoreceptor tyrosine-based inhibition motif

JLCR - Jensen Lab's Compartments repository

K_D - equilibrium binding constant

k_{off} - dissociation rate constant

k_{on} - association rate constant

L - light

LC – light chain

LIC - leukemia-initiating cell

LSC - leukemic stem cells

M - male

M1 - antitumor TAM

M2 - protumor TAM

mAb - monoclonal antibody

MACS - magnetic-activated cell sorting

MDS - myelodysplastic syndrome

MDSC - myeloid-derived suppressor cells

MEM - minimum essential medium

MFI - median fluorescence intensity

MHC - major histocompatibility complex

MICA/B - MHC class I chain-related protein A and B

Mut - mutated

n. a. - not available

n. d. - not determined

nanoDSF - nano differential scanning fluorimetry

NBS - neuroblastoma

NEAA - non-essential amino acids

NHL - non-Hodgkin lymphoma

Ni-NTA - nickel nitrilotriacetic acid

NK - natural killer

NOD - non-obese diabetic

NPM1 - nucleophosmin 1

NSG - NOD scid gamma

ON - overnight

OR - objective response

ORR - overall response rate

OS - overall survival

OVA - chicken ovalbumin

p. e. - positive engraftment

PBMC - peripheral blood mononuclear cell

PBS - phosphate buffered saline

PCR - polymerase chain reaction

PD1 - programmed cell death protein 1

PDX - patient-derived xenograft

PE - phycoerythrin

R - reactivity

RBC - red blood cell

Rh - recombinant human

ROI - Radiotherapy and OncoImmunology

Rpm - revolutions per minute

RPMI - Roswell Park Memorial Institute

RT – room temperature

RU - response units

SCF - stem cell factor

SD – standard deviation

SDS-PAGE - sodium dodecyl sulfate polyacrylamide gel electrophoresis

SEC - size exclusion chromatography

SEER - Surveillance, Epidemiology, and End Results

SEM – standard error of the mean

SHP - Src homology region 2 domain-containing phosphatase

Siglec-3 - sialic acid-binding Ig-like lectin 3

SIRPα - signal regulatory protein alpha

SPR - surface plasmon resonance

STING - stimulator of interferon genes

T_a - annealing temperature

TAM - tumor-associated macrophage

TCR - T cell receptors

TET2 - ten-eleven translocation 2

TH - tyrosine hydroxylase

T_i - inflection temperature

TNFR - tumor necrosis factor receptor

TPO - thrombopoietin

Treg - regulatory T cells

V - variable

VEN – venetoclax

Wt - wild type

WT1 - Wilms' tumor protein

κ - kappa

λ - lambda

8. Acknowledgements

First of all, I would like to thank my supervisor Prof. Karl-Peter Hopfner for a chance to fulfil my aspirations and work in the field of cancer immunotherapy and protein engineering. I am deeply grateful for the scientific support during my PhD and appreciate the opportunity to manage my research projects. This enabled me to grow as a scientist and develop my own views and ideas.

I am also very grateful for the chance to take part in the IMMUTRAIN training network. This opportunity introduced me to amazing scientists all over Europe and greatly widened my professional perspective. I want to express my special gratitude to Prof. Gosse Adema, who welcomed me in his laboratory to work on an exciting collaboration within the IMMUTRAIN network. Moreover, I want to thank Renske van den Bijgaart for the support and great teamwork in the project we shared. I definitely learnt a lot from this and enjoyed the experience.

I thank Prof. Marion Subklewe for great collaboration and helpful scientific input. Further, I highly appreciate the help from Prof. Irmela Jeremias and Binje Vick. I am sincerely grateful for their interest in my work and enthusiasm in the project. Our collaborative investigations were crucial for the successful accomplishment of my PhD project.

I truly value the opportunity to work with the creative and intelligent people from the Hopfner lab and antibody subgroup. My special thanks are addressed to Nadja for all her valuable advice and input during the PhD. I am especially grateful for the time and effort she put into the writing process of the manuscript and my thesis. I also want to express my gratitude to Laia who took care of me at the beginning of my PhD and taught me all the basics in the lab. Alongside, many thanks go to Saskia, Anja, Alex, Moni, Anna K, Björn, Enrico, Markus, Anna R, Szilvia, Claudia and Lorenza for the support in the lab and great working atmosphere.

Viimaks, ma tänan oma pere ja sõpru sellel imelisel teekonnal. Minu kallis Ott, aitäh et oled minu kõrval, motiveerides ja minu püüdlusi toetades. Ma olen nii õnnelik, et sina ja Endla olete minuga koos! Olen tohutult tänulik oma vanematele nende toe eest, eriti viimasel doktorantuuriaastal. Ilma teieta, poleks see töö võimalik olnud.